Vibration Measurement Based Damage Identification for Structural Health Monitoring

Saurabh S. Bisht

Dissertation submitted to the Faculty of the
Virginia Polytechnic Institute and State University
in partial fulfillment of the requirements for the degree of

Doctor of Philosophy
in
Engineering Mechanics

Mahendra P. Singh, Chair
Surot Thangjitham, Co-chair
Muhammad R. Hajj
Romesh C. Batra
Scott L. Hendricks

December, 13^{th} 2010
Blacksburg, Virginia

Keywords: damage identification, flexibility, Gibb's phenomenon, unscented Kalman filter

Vibration Measurement Based Damage Identification for Structural Health Monitoring

Saurabh S. Bisht

ABSTRACT

The focus of this research is on the development of vibration response-based damage detection in civil engineering structures. Modal parameter-based and model identification-based approaches have been considered. In the modal parameter-based approach, the flexibility and curvature flexibility matrices of the structure are used to identify the damage. It is shown that changes in these matrices can be related to changes in stiffness values of individual structural members. Using this relationship, a method is proposed to solve for the change in stiffness values. The application of this approach is demonstrated on the benchmark problem developed by the joint International Association of Structural Control and American Society of Civil Engineers Structural Health Monitoring task group. The proposed approach is found to be effective in identifying various damage scenarios of this benchmark problem. The effect of missing modes on the damage identification scheme is also studied.

The second method for damage identification aims at identifying sudden changes in stiffness for real time applications. It is shown that the high-frequency content of the response acceleration can be used to identify the instant at which a structure suffers a sudden reduction in its stiffness value. Using the Gibb's phenomenon, it is shown why a high-pass filter can be used for identifying such damages. The application of high-pass filters is then shown in identifying sudden stiffness changes in a linear multi-degree-of-freedom system and a bilinear single degree of freedom system. The impact of measurement noise on the identification approach is also studied. The noise characteristics under which damage identification can or cannot be made are clearly identified. The issue of quantification of the stiffness reduction by this approach is also examined.

It is noted that even if the time at which the reduction in stiffness happens can be identified, the quantification of damage requires the knowledge of system displacement values. In principle, such displacements can be calculated by numerical integration of the acceleration response, but the numerical integrations are known to suffer from the low frequency drift error problems. To avoid the errors introduced due to numerical integration of the acceleration response, an approach utilizing the unscented Kalman filter is developed to track the sudden changes in stiffness values. This approach is referred to as the adaptive unscented Kalman filter (AUKF) approach. The successful application of the proposed AUKF approach is shown on two multi-degree of freedom systems that experience sudden loss of stiffness values while subjected to earthquake induced base excitation.

Acknowledgment

First and foremost I would like to thank my advisors Dr. Mahendra P. Singh and Dr. Surot Thangjitham. Without their continued encouragement, guidance and support, this work would not have been possible.

I would also like to thank Dr. Romesh C. Batra, Dr. Scott L. Hendricks and Dr. Muhammad R. Hajj for serving on my graduate committee, and for the inputs and suggestions they provided.

I was fortunate enough to make many new friends during the course of my graduate studies. I'm grateful to all of them for their support. Special thanks are due to my friend Satyavarta for, among other things, the numerous discussions which we had on various topics related to my field of study. Also, I would like to thank Dr. Apoorva Shende, Bharath Ramesh, Harsh Nandan, Dr. Karthik Channakeshava and Dr. Rakesh Pathak, for their help in research related and other matters. Special thanks are also due to Sapna Kaul for all her support and encouraging talks.

Finally, I would like to extend my thanks to my father, Dr. Sher S. Bisht, my mother, the late Mrs. Asia Bisht, and my sister Deepti, for their unconditional love and support.

This research was supported by National Science Foundation through grant nos. CMMI-0700558 and 0533223 with Dr. S. C. Liu and Dr. D. Foutch as the Program Directors. This support is gratefully acknowledged. Any opinion, findings, and conclusions or recommendations expressed in this study are those of the writers and do not necessarily reflect the views of the National Science Foundation.

Contents

List of Figures

List of Tables

Chapter 1

Introduction

1.1 Structural Health Monitoring

The field of structural health monitoring (SHM) addressing numerous engineering problems of current interest has evolved over the past several years. The literature on this subject is abundant and continues to grow. Where as on one hand a variety of methods for detecting and quantifying damage in structural systems have been proposed in the literature, practical implementations of these approaches are yet to be shown. Thus continued efforts are being made to refine the available methods and relax the assumptions on which these methods are based to develop better and more robust techniques.

In this chapter, to begin with, the motivation for implementing SHM techniques and further exploration of this topic are reviewed. It is noted that implementation of the SHM techniques can result in effective and economical repair and maintenance plan with enhanced safety of civil structures. A brief literature survey of the available methods for SHM of civil structures related to the proposed study is presented. Following the literature survey the organization of the work is outlined.

1.2 Motivation for Structural Health Monitoring

Civil engineering structures such as buildings, bridges, roads etc. are designed to provide satisfactory service continuously for the entire period of their long service lives.

During their lifetime, these structures are inspected to ensure that their strengths have not degraded to a point that their serviceability is compromised. This degradation might happen due to the continued use of a structure and due to the fact that all structures lose strength over time due to natural aging. This can also happen because of unexpected exposure to extreme events such as the occurrence of a strong earthquake or wind storm. To ensure proper functionality of an important structure, regular as well as special inspections by trained and experienced professionals are carried out. Such manual inspections demand high resources, are time consuming, and in some cases may not be quite reliable.

Pines and Aktan (2002) indicate that the visual inspection of the Brooklyn Bridge in New York, which is done biennially, lasts for about three months and costs about $ 1 million. According to the economic census data, the cost for inspection, routine maintenance and repair of structural systems runs into billions of dollars (Atalla and Orisamolu (2001), USDoC (2002)). Besides the time and cost involved, the practice of visual inspection has an additional limitation. Damage and the resulting changes in structural characteristics generally become visually apparent only at an advanced stage. Considering the large number of civil structures which need regular inspections, it is of interest to find feasible alternatives to manual inspections to detect damages at an early stage. These alternative approaches are being called as the structural health monitoring (SHM) methods. The implementation of a proper SHM approach can lead to timely repairs and a reduction in the total cost with enhanced safety of use. The cost-benefit analyses of implementing SHM techniques have also been carried out (Alampalli *et al.* (2005)) to examine their economic viability; it is shown that even a simple SHM method (e.g. the use of closed-circuit television) can lead to financial savings over the years in bridge deck maintenance costs. Similar or higher cost savings are possible for other structures with the use of more sophisticated SHM techniques.

With the need and advantages of SHM techniques in mind, currently methods are being sought that do not require much human interaction but rather make use of some measured responses of the structure to some known or unknown excitation to monitor its health. Such measurements can be made by installing sensors that can automat-

ically record, process, and then transmit the processed response for further analysis and interpretation by different health monitoring schemes.

The response of a structural system is mainly affected by the structural stiffness for the static loads and by stiffness, damping and mass properties for the dynamic loads. The damage in one or more structural elements causes a change in these structural properties and, thus, changes in the response. This changed response is used to identify the damage. The damage in a structure primarily causes a decrease in its stiffness, but it can also alter the damping and mass properties of the structure. Among these system properties, especially in civil structures, the change in mass is usually not of much interest as the damage levels that might cause a significant loss of structural mass are usually quite obvious and hardly need any identification procedure. The change in damping is definitely of interest, and it can often be used to identify the damage, but since damping mechanism is hard to model, the identification of change in damping by a SHM system is usually not very crisp. Thus, the main focus of most response-based SHM systems, especially the global damage identification schemes (explained in the next section), is to detect a change in the stiffness to identify the damage. The focus of this study will also be to identify the change in stiffness of structural elements.

Currently, several SHM schemes are being considered with the primary focus on providing a reliable assessment of the condition of a structural system. The main focus of these schemes is to answer four basic questions about a structure: Has any damage occurred? If so where? What is the extent of damage? How does the damage affect the useful life of the structure? Each successive question is harder to answer. The focus of this study will be on answering the first three questions, and we call this as damage identification. Thus, damage identification implies detection, localization, and quantification. The answer to these questions can help in determining the effect of the detected damage on the continued operation of the structures, scheduling timely repairs, and assessing the remaining service life of the structure. Damage, in this study refers to a change in the value of stiffness in one or more structural elements.

With the current development in sensor technology, wireless data transmission, and

advances in the numerical data processing methods, the field implementations of reliable SHM schemes are not very far. The applications of SHM are widespread and not just limited to civil structures. There is abundant literature on its use and benefits in various fields. However in this study, our concern will be with the health monitoring of civil structures such as the building structures. A general literature survey of some methods available for damage identification in civil structures is provided below. Literature specific to methods developed in later chapters is reviewed in those individual chapters.

1.3 Literature Survey

As mentioned in the previous section, the primary objective of any SHM technique is to locate and assess the severity of any damage that occurs. The precise definition of damage is problem specific. But in general terms, any change in the structural system that causes degradation in its ability to reliably serve its intended purpose can be called damage. The problem of SHM can thus be considered as the one in which changes in the structure are to be detected and quantified in some way. Typically the idea is to collect some responses such as accelerations, strains, etc. and use them to infer the state of the structure.

Over the years numerous techniques for damage identification in civil structures have been proposed. A comprehensive list of publications on this topic is given in the two reports by Doebling *et al.*(1996) and by Sohn *et al.* (2003).

The techniques for SHM may be classified in several ways. For the purpose of the current study they are divided into two groups: (a) the local and (b) the global damage identification techniques. The local damage identification techniques are used for a more refined localization and quantification of damage in a structural element. In these techniques, the structural member containing the damage is usually identified by some other method. These techniques often include methods utilizing acoustic emission, reflection and refraction of mechanical waves, electromagnetic field, and radar

and radio frequencies (Chang and Liu (2003)).

The global damage identification techniques utilize the global response measured at several locations of a structure considered as a whole (Chang *et al.* (2003)). These techniques are intended to detect the occurrence of a damage and also identify the structural member that is affected by the damage. They may, however, not be able to pin-point the exact location of damage within the structural member. They generally focus on detecting the changes in the overall stiffness characteristics of the structural elements. In this sense they are less accurate than the local methods, but they are easy to implement and require fewer resources and are more likely to be automated. After initial identification of a damaged structural element, a more thorough inspection by local methods can be pursued. The current study is concerned only with the topic of the global damage identification methods.

In the global damage identification techniques, the common starting point is to record the vibration response of the structure. For civil structures, the measured responses usually consist of acceleration and/or dynamic strain measurements at a few selected locations on the structure. Such responses may be caused by either a known excitation source or an immeasurable natural excitation source such as wind or wave loading. Whether the excitation causing the measured response is known or not, determines the SHM technique that can be used. The offshore oil drilling industry was the pioneer in the implementation of vibration-based health monitoring schemes in 1970s for the offshore platform structures, primarily because a significant part of an offshore platform is inaccessible for visual or other localized inspections.

Depending on how the vibration data is used one can broadly categorize these vibration-data based methods into two categories; (1) the methods that make use of the modal parameters of the system to identify the damage, and (2) the model identification methods that do not use the modal properties but directly attempt to estimate the system characteristics to assess the damage.

The modal parameter based methods first extract the modal parameters (natural

frequencies, damping and mode shapes) from the vibration data and then use them for subsequent damage identification. Out of these parameters, the calculation of natural frequency is the easiest. A direct way to access the condition of a structure then would be to compare the natural frequencies of the structure in the present condition to those obtained previously. Changes in natural frequencies for damage detection have been explored by several researchers (Stubbs and Osegueda (1990a 1999b), Hearn and Testa (1991), Nakris (1994), Choy *et al.* (1995), Messina (1998), Morrasi (2001)). The usefulness of these frequency-only methods in civil engineering structures has, however, been limited primarily because of the following reasons: (1) Local changes in the stiffness of a member due to crack or degradation do not affect much the first few frequencies, and especially the fundamental frequency. The presence of cracks might affect the higher mode frequencies, but such frequencies are hard to extract from measured vibration responses. (2) The environmental influence on structures like bridges can sometime cause large changes in the frequencies to make it difficult to distinguish them from the changes caused by damage in the structure. (3) Detection of damage at multiple locations using the change in the system frequencies is quite difficult.

More information about the system state can be gained if the mode shape values are also known at as many points as is practically possible. Comparisons of mode shapes calculated before and after the damage using the modal assurance criteria (MAC) and coordinate modal assurance criterion (COMAC) have been attempted to locate the damage. See Allemang (2002) for a good review of the indices in damage identification. However, their direct use for damage identification in civil structures has not been very successful. Comparison of the system stiffness matrices calculated from the modes before and after the damage has been considered to identify the damaged structural elements. However, using the measured mode shapes directly to calculate the stiffness matrix is not very reliable unless the higher modes can also be extracted from data. This has prompted researchers to compare the curvature mode shape before and after damage since curvature is more directly related to the flexural strain than the nodal displacements (Pandey *et al.* 1991) and it is thus a more sensitive damage indicator than the MAC or COMAC indices. The numerical calculation of the curvature mode shape from the displacement mode shapes is, however, error prone. The use of Chebyshev

polynomial approximation to smooth out the kinks associated with the finite difference based approach has, thus, been attempted (Wu and Law (2004)). Maeck (2003) has also proposed another method to calculate the curvature mode shape. An alternative to using the stiffness matrix for damage detection is to use the flexibility matrix (Pandey and Biswas (1994)). The flexibility matrix can be constructed more accurately than the stiffness matrix by using only the first few modes since the contribution of a higher mode, being inversely proportional to its squared frequency, decreases quite sharply. For a beam, Pandey and Biswas (1994) showed that the use of the first two modes was quite adequate to identify the damage. Bernal (2002) has developed the concept of damage locating vectors (DLV) for an improved location of a damaged element using the flexibility approach. Gao and Spencer (2002) combine the damage locating vector approach with modal expansion technique to improve the damage localization. Duan *et al.* (2004) present use the concept of a rotational flexibility matrix to detect multiple damages. Wu and Law (2004) use the concept of uniform load surface curvature, which is again related to the curvature mode shape. The approaches described above, fall under the category of modal parameter based methods. The model identification methods on the other hand, use the vibration data directly; they usually minimize a norm of the difference between the measured and estimated responses by adjusting the model parameters to calculate the damage induced changes. It must be noted that once the model parameters have been estimated, a mathematical model describing the system is available. If needed, then the modal parameters may also be calculated.

Pi and Mickleborough (1989) showed that the free and forced vibration response of a multi-degree-of-freedom system can be represented using an autoregressive moving average (ARMA) model. They also showed how the modal parameters of the system can be calculated from the estimated ARMA model. However, instead of calculating the modal parameters, the parameters of the ARMA model may be directly used for damage identification.

Nair *et al.* (2006) suggested a damage identification scheme for linear systems under stationary excitations. They modeled the vibration response collected at different sensor locations using an ARMA model. Making use of the first three auto-regressive

(AR) coefficients, they defined a damage sensitive feature. A change in the mean value of this damage sensitive feature was then used for damage identification. The application of their approach was demonstrated on the ASCE benchmark structure. In a later work (Nair and Kiremidjian (2007)) these parameters were used to define a feature vector which was analyzed using the technique of Gaussian mix models for damage identification.

Lei *et al.* (2003) used an autoregressive exogenous input (ARX) model to represent the vibration data collected from the undamaged structure. The errors in the predicted response of the damaged structure using this model were then used as an indication of damage.

In Kang *et al.* (2005), the authors developed a method for estimating the structural parameter values (damping and stiffness) by minimizing an error function. The error function which they used was based on the squared error between the actual measured and model estimated acceleration values. In effect, by minimizing this error, the assumed mathematical model was refined to give a better representation of the actual structure. A change in the estimated parameter values was then used for damage identification. They showed the application of this approach by using it for damage identification in a simulation (two span truss bridge) and experimental (three story shear beam model) study.

The model identification approach has also attracted much interest because of its application to real-time damage identification. For this, the parameters of the mathematical model describing the structure are recursively estimated as new measurement data becomes available. In Chase *et al.* (2005a and 2005b) the authors expressed the change in stiffness matrix of a multi-degree-of-freedom system as the sum of matrices each of which was directly related to the change in stiffness of individual members. They then identified the parameters related to these matrices using the vibration data. This was done using methods which they suggested based on the adaptive least mean square (LMS) filtering approach (Chase *et al.* 2005a) and the adaptive recursive least squares approach (Chase *et al.* 2005b). The applicability of their technique was demon-

strated by identifying damages in the ASCE benchmark structure.

The methods based on recursive least squares approach have been studied and developed by several researchers for estimating the parameters of structural systems. Wang and Haldar (1994, 1997) developed a method based on least squares approach, for estimating the parameters of structures described by shear beam models. In Smyth *et al.* (1999), the authors developed an adaptive least squares method to identify the parameters of a non-linear model described using Bouc-Wen hysteretic elements. Lin *et al.* (2001) suggested a recursive least squares based scheme to track changes in parameter values. They demonstrated the applicability of their scheme by identifying parameter values in systems described by the Duffing, the Van der Pole oscillator and the Bouc-Wen type hysteretic models. More recently, a technique based on non-linear least-squares estimation has been suggested for tracking sudden and gradual changes in structural parameter values in linear and non-linear systems (Yang and Lin (2004), Yang and Lin (2005), Yang *et al.* (2006a, 2006b, 2007)). One of the chapters in the present study deals with the tracking of sudden changes in stiffness values and these studies are thus mentioned in more details later.

It must be noted that in all these model identification based techniques, the vibration data is directly used to estimate the parameters of a mathematical model. The modal parameters are not estimated, but can be calculated, if needed, once the mathematical model is known. In this study, both these approaches, the modal parameter based approach and the model identification approach, will be considered to develop new damage identification methods.

1.4 Organization of the Work

In general, the approach followed by any SHM technique is as follows. Some response of the structure to be monitored is measured. This response is then used to estimate values of certain parameters which characterize the present state of the structure. In this study, the vibration response (in particular the acceleration response) of the struc-

ture is utilized. New methods for both off-line and on-line damage identification are developed and studied. For the off-line approach the response acceleration is first used to estimate the flexibility matrix of the structure. Following which the new method developed for damage identification is utilized. For the on-line approach utilizing the response acceleration, a new method is suggested to detect the sudden reduction in stiffness and to track its value. A brief description of the contents of the remaining chapters in this dissertation is as follows:

Chapter 2: Flexibility Based Damage Identification

In this chapter a new flexibility-matrix based damage identification approach is presented. The elements of the flexibility matrix are first related to changes in structural element stiffness values and then this relation is used to solve for the changes in stiffness values of the elements iteratively. The flexibility matrix -based framework developed for damage identification is also utilized with the curvature flexibility matrices. The effect of incomplete modal information and error in the estimated flexibility matrices due to measurement noise are studied through numerical simulations. The application of the proposed damage identification scheme is shown on the ASCE-SHM benchmark problem. It is shown that the approach is able to identify and quantify various damage scenarios. The measurement noise and missing modal information, however, are found to degrade the performance of the method. The use of the curvature flexibility matrix for damage identification is suggested using the same basic framework. Its application is illustrated through numerical simulations. The approach for damage identification developed in this chapter is an off-line approach. With the advancement in sensor technology, it is also of interest to detect and quantify damages in real time. This is the topic of presentations in the next two chapters.

Chapter 3: Detection of Sudden Changes in Stiffness Using High-Frequency Components

Detection of sudden changes in stiffness values has been of interest for online health monitoring. For this currently, several studies (Demetriou and Hou (2003), Hou *et al.* (2000), Hera and Hou (2004)) have focused on the use of the discrete wavelet transform where these sudden changes have been shown to manifest themselves as significant non-

zero value(s) or spikes in the details of the discrete wavelet transforms. In this chapter, we provide a formal explanation for this observation through the Gibbs' phenomenon. More specifically, it is shown that a *spike* which identifies the occurrence of the sudden change in stiffness is due to the step response of the high-pass filter. The theoretical relationship between the change in stiffness and the spike magnitude is derived. The chapter provides an analysis of how the measurement error affects the detection of spikes and why the damage cannot be identified in the presence of measurement noise. Using this insight the application of high-pass filters for the identification of damage instant is proposed and illustrated by numerical examples. It is noted that for damage quantification, the displacement response should be known or be available through measurements. In the absence of such information the damage instant can be identified but the value of change in stiffness cannot be calculated. A method to estimate and track (sudden changes in) stiffness and damping values is then explored in the next chapter.

Chapter 4: An Adaptive Unscented Kalman Filter for Tracking Sudden Stiffness Changes

In this chapter a new scheme is suggested which allows the tracking of sudden changes in stiffness values of a structure subjected to earthquake induced base excitations. For this the unscented Kalman filter (UKF) approach is utilized. The application of the UKF in the area of target tracking and control has been explored by other researchers (Duan *et al.* (2005a), Khairnar *et al.* (2007), Leven and Lanterman (2009), Meuter *et al.* (2008), Rao and Basu (2008), Sadeghi and Moshiri (2007), Zhan and Wan (2007), Zhang and Hu (2006), Zhang *et al.* (2006)). With respect to civil engineering the application of UKF in estimating structural parameter values has also been investigated by other researchers.. It is, however, found that the UKF cannot track sudden changes in parameter values. In order to do this, the usual UKF approaches need to be modified. With this objective in mind, a scheme is developed which is used along with the basic UKF algorithm to track sudden changes in stiffness. The UKF utilizing this scheme is referred to as the adaptive unscented Kalman filter (AUKF) in this study. The applicability of the AUKF is illustrated through various numerical simulations of structures experiencing sudden reduction in stiffness for the cases of earthquake

induced base excitations. The effect of measurement noise on the performance of the AUKF is also studied. The AUKF is found to be effective in tracking sudden changes in stiffness for low levels of measurement noise. Like any other system identification technique the performance of the suggested AUKF degrades with the increase in noise level.

Chapter 5: Summary and Concluding Remarks

In this final chapter the major findings and conclusions drawn from this study are provided and some possible topics for future studies are suggested.

Chapter 2

Flexibility Based Damage Identification

2.1 Introduction

In this chapter, we describe the development of a flexibility-based damage identification approach for civil engineering structure such as buildings. Damage in a civil structure could occur in many different ways. It may be caused by natural degradation of the structure due to corrosion or loss of material strength. It could also be caused by, for example, loosening of a connection or development of a crack in a joint or a structural element due to overloads or fatigue. All these damages generally reduce the stiffness of structural elements as well as the entire structure. Herein, and in subsequent chapters, therefore, we refer to damage as a reduction in the stiffness value of one or more structural elements and not go into the details as to how it occurred. Our objective in this study will be to identify the damage causing a reduction in the structural stiffness, if it occurs. We will attempt to detect the occurrence of a damage followed by its quantification (that is, how much it is) and localization (that is, where it is) in the structure.

Several approaches have been considered by researchers for the identification of such damages. As briefly discussed in Chapter 1, these approaches can be classified as the global and local approaches. The approach described in this chapter is a global approach where we plan to use some measured response of a structure to identify the

damage. Again as mentioned earlier, the global approaches can also be divided into two categories: modal parameter-based approach and the model identification approach. In this chapter we will focus on the modal parameter based damage identification approach. The model identification approaches will be the subject of the following chapters.

In the modal parameter-based approaches, one attempts to identify the damage or change in the system stiffness from the observed changes in the modal properties of the system. Since this method depends upon the use of the modal properties, a basic assumption of this method is that the undamaged as well as the damaged structures behave linearly and, thus, can be represented by the modal properties. However, since a damage such as the presence of a crack in a structure will render it nonlinear, this approach only aims to identify an approximate smeared effect of such damages on the structural stiffness.

In this approach, one first extracts modal properties such as mode shapes and frequencies from the measured response. If these modal characteristics can be accurately estimated then, in principle, they can be used to calculate the stiffness matrix of the structure. A comparison of these matrices for the damaged and undamaged structures is then expected to lead to the identification of the extent of the damage and the structural element in which it has occurred. (We note that such direct stiffness comparisons will not pinpoint the location of damage such as a crack in a structural element but only give an indication about the element-wise reduction in the parameter value that defines the element stiffness. More refined methods are needed to pinpoint the damages such as cracks.) There are, however, practical difficulties in the calculation of stiffness matrix and, thus, in the implementation of this simple idea. The difficulties are primarily due to the fact that the contributions of the higher modes to the stiffness matrix are much more compared to those of the lower modes, and accurate extraction of the higher modes from the real response data is very difficult (Lin (1990)). This makes it difficult to calculate the stiffness matrix accurately and, thus, the detection of damage very uncertain.

Instead of comparing the whole stiffness matrix, simple comparisons of easily extractable lower modal properties (frequencies and mode shapes) for the damaged and undamaged structure have, thus, been attempted to identify the damage (Adams *et al.* (1978), Wang and Zhang (1987), Stubbs *et al.* (1990), Stubbs and Osegueda (1990a, 1990b), Hearn and Testa (1991), Kam and Lee (1992), Narkis (1994)). It has been possible to detect the damage by such comparison, but the localization and quantification of the damage have been difficult. Pandey *et al.* (1991), thus, suggested the use of changes in the mode shape curvature for damage identification, especially in the beam like structures. This was based on the observation that a reduction in stiffness due to damage would lead to an increase in the curvature. The curvature mode shapes were extracted from displacement mode shapes numerically using a central difference approximation. This idea was somewhat successful for a beam like structure, but because of the problem in numerical calculation of curvature its application to other types of structure such as framed structure is not reliable. Another approach utilizing the modal quantities for damage detection, especially for the 3-D structures, is the modal strain energy approach described by Li *et al.* (2006). Making use of a damage index defined with mode shape entries the authors decompose the modal strain energy into two parts (axial and transverse) and use them for damage identification.

To avoid the problem associated with the calculation of stiffness matrix without higher modes or the calculation of the mode-shape curvatures, researchers have focused on the use of the flexibility matrix as this matrix can be obtained fairly accurately using only a few lower modes. Most likely Pandey and Biswas (1994, 1995) were the first ones to suggest such applications of the flexibility matrix for civil structures. They showed that the change in flexibility matrix between the damaged and undamaged structure can be used for identifying the location of damage. Both numerical and experimental results were presented for a beam like structure to validate the approach. Zhao and DeWolf (1999) numerically studied the sensitivity of the natural frequency, mode shape and flexibility matrix to changes in stiffness. They found the flexibility matrix to be the most sensitive, thus, further justifying the use of the flexibility matrix for stiffness-related damage identification.

Realizing these special attributes of the flexibility matrix, several studies have explored the use of this matrix for damage detection. An issue in using the flexibility matrix is that the mode shapes needed to calculate the matrix must be mass normalized. For this one can use the mass matrix of the analytical model. However, realizing that in some cases a good estimate of the mass matrix may not be available, Bernal and Gunes (2004) presented a method for extracting the flexibility matrix from the measurement data to within a scalar multiple of the actual matrix. For damage localization, Bernal (2002, 2006) has shown that the vectors lying in the null space of the change in the flexibility matrix, called the damage locating vector (DLV), can be used for the identification of damaged structural elements. Duan *et al.* (2005b) have also presented a method for the calculation of a proportional flexibility matrix from measured mode shapes. They used this matrix and the DLV approach for damage localization with just a few modes for a 7-DOF spring mass system and a truss structure. Recently Gao *et al.* (2007) have also provided an experimental verification of the damage localization capability of the DLV method using a scaled model of a truss structure. To further refine the localization of damage in a shear beam structure, Duan *et al.* (2004) proposed the use of a matrix related to the flexibility matrix called the rotational flexibility matrix.

In this study, a new method based on the change in the flexibility matrix is developed for estimating the change in the stiffness values of the structural members. In this method, the difference between the flexibility matrices of the damaged and undamaged structure is defined as the damage index matrix. By expanding the damaged flexibility matrix in a Taylor series about the undamaged state, one can relate this damage index matrix to the changes in the element stiffness values. These changes in the element stiffness values can then be calculated by an iterative procedure using this expansion. To improve the damage localization, the use of curvature flexibility matrix is also examined.

The approach is applied to the simulation data based benchmark problem developed by the joint International Association of Structural Control (IASC) and American Society of Civil Engineers (ASCE) structural health monitoring (SHM) task group

(Johnson *et al.* (2004)). It was found that the proposed scheme performed very well. The damages were identified in various cases (symmetric or asymmetric mass distribution, with or without modeling error) formulated for the benchmark problem. This displacement flexibility matrix concept has also been extended to include the curvature flexibility matrix with specific application to a framed structure where one might be interested in identifying the damaged end of a member. In the framed structure modeling, it is common to condense out the rotational degrees of freedom (which are usually associated with relatively small rotational inertia of the nodal mass) from the dynamic model. The member failure will, however, be associated with flexural over-stressing near the joints in framed structures. Thus, while defining the curvature flexibility, these condensed degrees of freedom are retrieved and introduced back in the analysis in this approach. An example problem of a simple frame was used to illustrate the idea. The numerical results indicate that to identify the damage near the ends of an element in a framed structure or near a connection, more member specific measurements are needed in addition to the acceleration measurements for the condensed degrees of freedom.

This chapter is henceforth organized as follows. In Section 2.2 it is shown how the change in the flexibility matrix can be used to detect damage. The equations relating the change in the elements of the flexibility matrix to the changes in structural stiffness are derived. An approach to solve these equations to obtain the changes in stiffness matrix values is presented in Section 2.3. Often the collected response data may not be adequate to provide extraction of all needed modes. The effect of a missed mode or using a limited number of modes on the damage identification scheme is, thus, examined in Section 2.4. The application of the proposed damage identification approach to the benchmark problem is described in Section 2.5. Motivated by the fact that the curvature can be used to identify the node near which the damage occurs in a framed like structure, in Section 2.6 a curvature flexibility matrix is defined and used for damage identification in a frame model. Finally the chapter summary and conclusions are summarized in Section 2.7.

2.2 Damage Index Matrix

In this section, we introduce the damage index matrix expressed in terms of the flexibility matrix. We describe how it can be used for damage localization and quantification. The equations that need to be solved for damage quantification are developed.

Damage Localization

As mentioned earlier, the damage in structural systems is typically characterized by a reduction of stiffness of one or more structural members. A reduction in stiffness consequently leads to an increase in flexibility. For a N-degree-of-freedom system the flexibility matrix, $\mathbf{F}$, can be written in terms of its natural frequencies and mass normalized mode shapes as follows,

$$\mathbf{F} = \mathbf{\Phi}\mathbf{\Lambda}\mathbf{\Phi}^T \tag{2.1}$$

where $\mathbf{\Phi}$ is the mode shape matrix, of size $N \times N_m$, whose columns consist of mass normalized mode shapes and $\mathbf{\Lambda}$ is a diagonal matrix with entries $1/\omega_i^2$, $i = 1, 2 \ldots N_m$, with ω_i being the i^{th} natural frequency. N_m denotes the number of modes used. The mass matrix used for mass normalization of the mode shapes, is constructed using the masses associated with the degrees of freedom under consideration. Considering the case when all modes are used in constructing the flexibility matrix i.e. $N_m = N$, the individual elements of the matrix can be expressed as,

$$\mathbf{F}_{i,j} = f_{i,j} = \sum_{p=1}^{N} \frac{\phi_{i,p}\phi_{j,p}}{\omega_p^2} \tag{2.2}$$

where $\phi_{i,k}$ is the $(i,k)^{th}$ element of the mode shape matrix $\mathbf{\Phi}$. Since damage in a structural element leads to a reduction in stiffness or consequently an increase in flexibility, for damage identification the difference in the flexibility matrix of the damaged and undamaged structure is used. Denoting the undamaged and damaged flexibility matrix of the structure by $\mathbf{F^u}$ and $\mathbf{F^d}$ respectively, the difference is defined as,

$$\mathbf{D} = \mathbf{F^d} - \mathbf{F^u} \tag{2.3}$$

Henceforth the matrix $\mathbf{D}$ will be referred to as the *damage index matrix*. As an example consider a classical spring mass model or a shear beam model shown in Figure

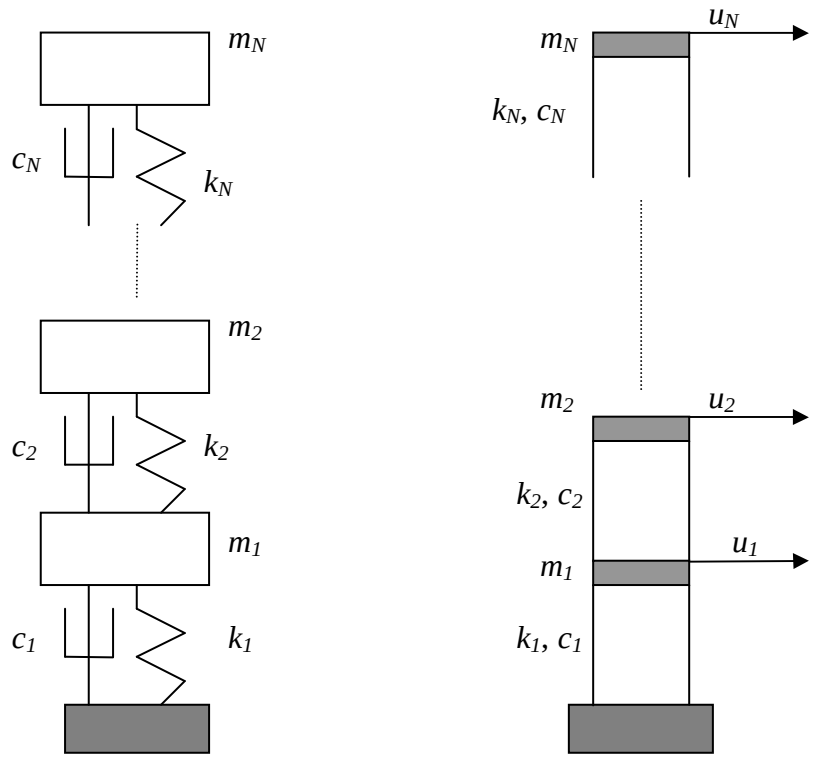

Figure 2.1: The classical spring-mass-damper model (left) and the shear beam model (right) with N degrees-of-freedom. In the shear beam model the N degrees-of-freedom are indicated by u_i (i=1, 2, ...N). m_i, c_i, and k_i are respectively the mass, damping and stiffness coefficients associated with the i^{th} degree of freedom.

2.1 with stiffness terms k_i, for $i = 1, 2 \ldots N$. The stiffness matrix $\mathbf{K^u}$ of this model is given by,

$$\mathbf{K^u} = \begin{bmatrix} k_1 + k_2 & -k_2 & 0 & \ldots & 0 \\ -k_2 & k_2 + k_3 & -k_3 & \vdots & 0 \\ \vdots & \ldots & \ddots & \ldots & -k_N \\ 0 & \ldots & \ldots & -k_N & k_N \end{bmatrix} \tag{2.4}$$

and the flexibility matrix is given by,

$$\mathbf{F^u} = \begin{bmatrix} 1/k_1 & 1/k_1 & \ldots & 1/k_1 \\ 1/k_1 & 1/k_1 + 1/k_2 & \ldots & 1/k_1 + 1/k_2 \\ \vdots & \ldots & \ddots & \vdots \\ 1/k_1 & 1/k_1 + 1/k_2 & \ldots & 1/k_1 + 1/k_2 + \ldots + 1/k_N \end{bmatrix} \tag{2.5}$$

Since damage reduces the stiffness, the term $1/k_i$ would increase due to damage. Let the term $1/k_i$ change to $1/k_i + \Delta_i$ due to a damage in k_i. Assuming that all the stiffness terms change, the damage index matrix would be of the following form,

$$\mathbf{D} = \begin{bmatrix} \Delta_1 & \Delta_1 & \ldots & \Delta_1 \\ \Delta_1 & \Delta_1 + \Delta_2 & \ldots & \Delta_1 + \Delta_2 \\ \vdots & \ldots & \ddots & \vdots \\ \Delta_1 & \Delta_1 + \Delta_2 & \ldots & \Delta_1 + \Delta_2 + \ldots + \Delta_N \end{bmatrix} \tag{2.6}$$

The entries of the damage index matrix are, therefore, expected to be either zero or positive, any non-zero value of the damage index matrix can be used to locate the stiffness term which has suffered a reduction. For example, in Figure 2.2 the diagonal elements of the damage index matrix are shown for the case when all the stiffness elements suffer a reduction. Though this has been illustrated for a shear beam case the same is true for a general structure, i.e. the change in the matrix $\mathbf{D}$ can be related to the actual changes in k_i's. A method to achieve this is presented below.

Damage quantification

In addition to indicating the presence of damage, the numerical value of the entries of the damage index matrix can be used to quantify the stiffness change. For this, we

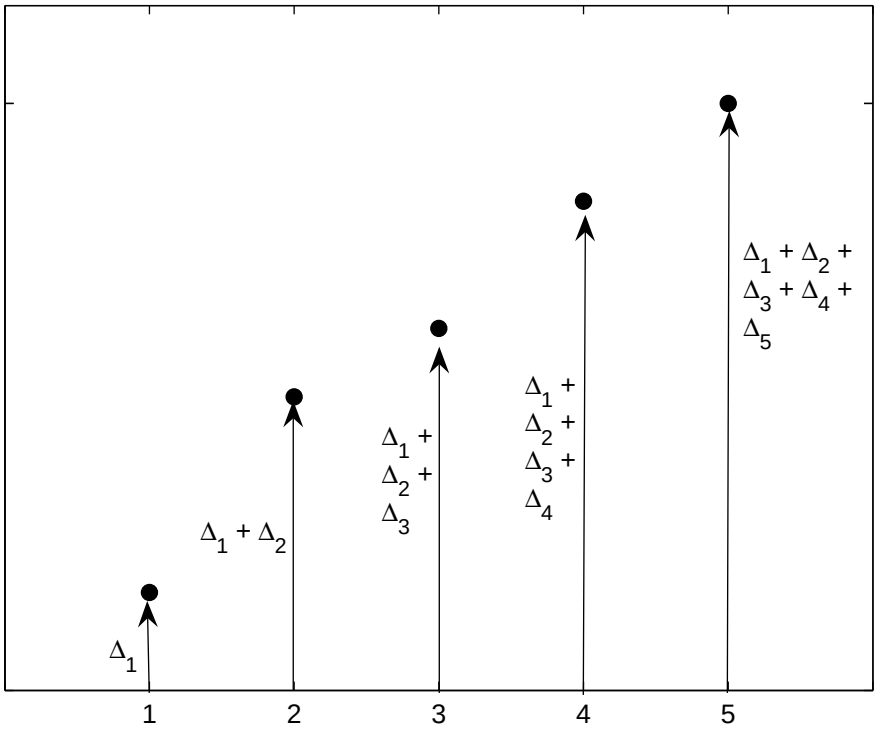

Figure 2.2: Illustration of the step like plot of the diagonal elements of the damage index matrix when all the stiffness elements suffer a change.

expand a typical term of the flexibility matrix in the damaged state, $f^d_{i,j}$, in Taylor series about its undamaged state value, $f^u_{i,j}$, and retain terms up to the second order, to obtain the following,

$$f^d_{i,j} = f^u_{i,j} + \sum_{m=1}^{N_k} \frac{\partial f_{i,j}}{\partial k_m} \Delta k_m + \frac{1}{2} \sum_{m=1}^{N_k} \sum_{n=1}^{N_k} \frac{\partial^2 f_{i,j}}{\partial k_m \partial k_n} \Delta k_m \Delta k_n \tag{2.7}$$

The partial derivatives in the above equation are evaluated at the undamaged state. We note that the number of stiffness terms N_k need not be equal to N, the number of degrees of freedom. The entries in the damage index matrix would then be given by,

$$d_{i,j} = f^d_{i,j} - f^u_{i,j} = \sum_{m=1}^{N_k} \frac{\partial f_{i,j}}{\partial k_m} \Delta k_m + \frac{1}{2} \sum_{m=1}^{N_k} \sum_{n=1}^{N_k} \frac{\partial^2 f_{i,j}}{\partial k_m \partial k_n} \Delta k_m \Delta k_n \tag{2.8}$$

Given the undamaged and damaged flexibility matrices the above equation needs to be solved for the different Δk_i's. This would then give the change in stiffness values for the structural elements.

For a N degree-of-freedom system the damage index matrix would be a square matrix of size N. In order to solve the set of equations as given by Eq. 2.8, we write one equation for each column of the damage index matrix. Denoting $\mathbf{A}(:, j)$ as the j^{th} column vector of $\mathbf{A}$, the equation for the j^{th} column of the damage index matrix may be expressed as:

$$\mathbf{D}(:, j) = \mathbf{F^d}(:, j) - \mathbf{F^u}(:, j) = \mathbf{G^j}_u \Delta k + \begin{bmatrix} \mathbf{H^j_1} \\ \mathbf{H^j_2} \\ \vdots \\ \mathbf{H^j_N} \end{bmatrix} \tag{2.9}$$

where $\mathbf{F^d}(:, j)$ and $\mathbf{F^u}(:, j)$, respectively, are the j^{th} column of the damaged and undamaged flexibility matrices. The elements of the vector Δk contain the unknown stiffness values and the matrix $\mathbf{G^j}_u$ is the gradient matrix and is defined as follows:

$$\mathbf{G^j}_u = \begin{bmatrix} \frac{\partial f_{1,j}}{\partial k_1} & \frac{\partial f_{1,j}}{\partial k_2} & \cdots & \frac{\partial f_{1,j}}{\partial k_{N_k}} \\ \frac{\partial f_{2,j}}{\partial k_1} & \frac{\partial f_{2,j}}{\partial k_2} & \cdots & \frac{\partial f_{2,j}}{\partial k_{N_k}} \\ \cdots & \cdots & \cdots & \cdots \\ \frac{\partial f_{N,j}}{\partial k_1} & \frac{\partial f_{N,j}}{\partial k_2} & \cdots & \frac{\partial f_{N,j}}{\partial k_{N_k}} \end{bmatrix} \tag{2.10}$$

$$\Delta k = \left\{ \begin{array}{c} k_1 \\ k_2 \\ \vdots \\ k_{N_k} \end{array} \right\}$$

The term comprising of $\mathbf{H_q^j}$ $(q = 1 \ldots N)$ can be viewed as the second order or Hessian term. This is defined in terms of the Hessian matrix as follows:

$$\mathbf{H_q^j} = \frac{1}{2}\Delta k^T \left[\begin{array}{cccc} \frac{\partial^2 f_{q,j}}{\partial k_1 \partial k_1} & \frac{\partial^2 f_{q,j}}{\partial k_1 \partial k_2} & \cdots & \frac{\partial^2 f_{q,j}}{\partial k_1 \partial k_{N_k}} \\ \frac{\partial^2 f_{q,j}}{\partial k_2 \partial k_1} & \frac{\partial^2 f_{q,j}}{\partial k_2 \partial k_2} & \cdots & \frac{\partial^2 f_{q,j}}{\partial k_2 \partial k_{N_k}} \\ \cdots & \cdots & \cdots & \cdots \\ \frac{\partial^2 f_{q,j}}{\partial k_{N_k} \partial k_1} & \frac{\partial^2 f_{q,j}}{\partial k_{N_k} \partial k_2} & \cdots & \frac{\partial^2 f_{q,j}}{\partial k_{N_k} \partial k_{N_k}} \end{array} \right] \Delta k \tag{2.11}$$

There are N vector equations of the form shown in Eq. 2.9, one for each column of the damage index matrix, with only N_k unknowns. The method used to solve this redundant set of equation is described in the next section.

The above equation can be simplified in the case of a shear beam model. Due to the structure of the damage index matrix (Eq. 2.6) considering only the diagonal terms we note that:

$$\mathbf{D}_{i,i} - \mathbf{D}_{i-1,i-1} = d_{i,i} - d_{i-1,i-1} = \Delta_i \quad 2 \leq i \leq N \tag{2.12a}$$

$$\mathbf{D}_{1,1} = d_{1,1} = \Delta_1 \quad \text{for} \;\; i = 1 \tag{2.12b}$$

where Δ_i is the change contributed by k_i alone. Thus, the equation relating the change in flexibility to the change in stiffness reduces to,

$$f_{i,i}^d - f_{i,i}^u = \frac{\partial f_{i,i}}{\partial k_i}\Delta k_i + \frac{1}{2}\frac{\partial^2 f_{i,i}}{\partial k_i^2}\Delta k_i^2 \tag{2.13}$$

Hence for a shear beam model we have N uncoupled equations for the $N_k = N$ unknowns. Note that the above relation is possible due to Eq. 2.12 which will not hold for any general structure in which case one will have to solve the set of equations given by Eq. 2.9.

To solve these equations, we assume that at least the mass matrix is known (for mass normalization of mode shapes) and also the structure of the stiffness matrix is known

(used in the evaluation of partial derivatives). The method to be used to solve for the stiffness terms also depends on what information about the system is known that can be used to calculate the partial derivatives. We will consider the two situations: (a) one in which original stiffness matrix of the system is known and other one (b) when stiffness is not known but modal properties of the undamaged structure are available, say, by the analysis of the measured response of the undamaged or baseline structure. The procedures for solving these equations and for calculating the partial derivatives in these two situations are presented next.

2.3 Solution Approach

As discussed in the previous section, the procedure for solving Eq. 2.9 depends on what information is available. This mainly determines the method of calculating the partial derivatives and then the solution for calculating the unknown changes in the stiffness values. The solution approach can also be simplified if a simpler model such as a shear beam model can be used to represent the structure. In the following, we first describe the methods one can use for defining the first and second order partial derivatives that are needed to define the gradient and Hessian matrices of the damage matrix for the two cases of (a) the stiffness matrix being known and (b) the stiffness matrix is not known but the modal properties are available.

Partial Derivatives

To calculate the partial derivatives of the flexibility matrix with respect to a stiffness term k_i, two approaches are considered. In the first case we assume that the initial stiffness of the baseline structure or the undamaged structure is known. In the second case, we will assume that the modal properties of the baseline structure have been determined from the available response data so that they can be used in calculating the sensitivities of the modal parameters needed in Eq. 2.8.

Partials When K is Known

For this consider the equilibrium equation expressed in terms of the stiffness matrix as follows:

$$\mathbf{K}u = f \tag{2.14}$$

where $\mathbf{K}$, u and f are the stiffness matrix, displacement and force vectors respectively. Writing this in terms of the flexibility matrix $\mathbf{F}$, we obtain,

$$u = \mathbf{K}^{-1}f = \mathbf{F}f \tag{2.15}$$

Differentiating Eq. 2.14 with respect to k_m and realizing that the force does not depend on k_m we obtain,

$$\frac{\partial \mathbf{K}}{\partial k_m}u + \mathbf{K}\frac{\partial u}{\partial k_m} = 0 \tag{2.16}$$

or

$$\mathbf{K}\frac{\partial u}{\partial k_m} = -\frac{\partial \mathbf{K}}{\partial k_m}u \tag{2.17}$$

Substituting for u from Eq. 2.14 in Eq. 2.17 we obtain,

$$\mathbf{K}\frac{\partial u}{\partial k_m} = -\frac{\partial \mathbf{K}}{\partial k_m}\mathbf{K}^{-1}f \tag{2.18}$$

or,

$$\frac{\partial u}{\partial k_m} = -\mathbf{K}^{-1}\frac{\partial \mathbf{K}}{\partial k_m}\mathbf{K}^{-1}f \tag{2.19}$$

Differentiating Eq. 2.15 with respect to k_m and realizing again that the force does not depend on k_m we obtain,

$$\frac{\partial u}{\partial k_m} = \frac{\partial \mathbf{F}}{\partial k_m}f \tag{2.20}$$

Comparing Eq. 2.20 with Eq. 2.19 we obtain the equation for the partial derivative of flexibility matrix as,

$$\frac{\partial \mathbf{F}}{\partial k_m} = -\mathbf{K}^{-1}\frac{\partial \mathbf{K}}{\partial k_m}\mathbf{K}^{-1} \tag{2.21}$$

The term $\partial\mathbf{K}/\partial k_m$ is a N by N matrix consisting of ones and zeros. For example, for a 2-degree-of-freedom shear beam model the stiffness matrix would be:

$$\mathbf{K} = \begin{bmatrix} k1+k2 & -k2 \\ -k2 & k2 \end{bmatrix} \tag{2.22}$$

and it partial derivative $\partial\mathbf{K}/\partial k_2$ is given by,

$$\frac{\partial \mathbf{K}}{\partial k_2} = \begin{bmatrix} 1 & -1 \\ -1 & 1 \end{bmatrix} \tag{2.23}$$

which can be calculated by knowing the structure of the stiffness matrix and not its actual values. However, for calculating the partial derivative of the flexibility matrix using Eq. 2.21, we would need to know the complete stiffness matrix and not just its form. Proceeding on similar lines, it can be shown that the second order partial derivatives of the flexibility matrix that is required for the calculation of the Hessian terms, are defined as follows:

$$\frac{\partial^2 \mathbf{F}}{\partial k_m \partial k_n} = \mathbf{K}^{-1}\left[\frac{\partial \mathbf{K}}{\partial k_m}\mathbf{K}^{-1}\frac{\partial \mathbf{K}}{\partial k_n} + \frac{\partial \mathbf{K}}{\partial k_n}\mathbf{K}^{-1}\frac{\partial \mathbf{K}}{\partial k_m} - \frac{\partial^2 \mathbf{K}}{\partial k_m \partial k_n}\right]\mathbf{K}^{-1} \tag{2.24}$$

Partials When K is Unknown

In this case, since $\mathbf{K}^{-1}$ would not be available, the partial derivatives of the elements of the flexibility matrix need to be calculated in terms of the partial derivatives of the modal parameters (mode-shapes and natural frequencies). For example, taking the partial derivative of both sides of Eq. 2.2 with respect to k_q we obtain,

$$\frac{\partial \mathbf{F}_{i,j}}{\partial k_q} = \frac{\partial f_{i,j}}{\partial k_q} = \sum_{p=1}^{N}\left[\frac{\partial \phi_{i,p}}{\partial k_q}\frac{\phi_{j,p}}{\omega_p^2} + \frac{\phi_{i,p}}{\omega_p^2}\frac{\partial \phi_{j,p}}{\partial k_q} - 2\frac{\partial \omega_p}{\partial k_q}\frac{\phi_{i,p}\phi_{j,p}}{\omega_p^3}\right] \tag{2.25}$$

The expressions for these first order rates of change of the modal frequencies and mode shapes, needed in Eq. 2.25, are available in the literature, say, in Fox and Kapoor (1968) for classical eigenvalue problems and in Ashtiany and Singh (1982) for the non-classically damped systems. In the context of structural health monitoring, such rates of change have been utilized in the study of sensitivity of vibration parameters (Zhao and DeWolf (1999)) and also for damage identification by Singh and Bisht (2006). These expressions are given in Appendix B.

To obtain the second order partial derivatives needed in Eq. 2.8, we differentiate Eq. 2.25 again with respect to k_r to obtain the following:

$$\frac{\partial^2 f_{i,j}}{\partial k_r \partial k_q} = S_1 + S_2 + S_3 + S_4 \tag{2.26a}$$

$$S_1 = \sum_{p=1}^{N}\frac{6}{\omega_p^4}\frac{\partial \omega_p}{\partial k_r}\frac{\partial \omega_p}{\partial k_q}\phi_{i,p}\phi_{p,j} \quad S_2 = \sum_{p=1}^{N}\frac{-2}{\omega_p^3}\frac{\partial^2 \omega_p}{\partial k_r \partial k_q}\phi_{i,p}\phi_{p,j} \tag{2.26b}$$

$$S_3 = \frac{-2}{\omega_p^3}\frac{\partial \omega_p}{\partial k_q}\left[\frac{\partial \phi_{i,p}}{\partial k_r}\phi_{p,j} + \phi_{i,p}\frac{\partial \phi_{p,j}}{\partial k_r}\right] + \frac{-2}{\omega_p^3}\frac{\partial \omega_p}{\partial k_r}\left[\frac{\partial \phi_{i,p}}{\partial k_q}\phi_{p,j} + \phi_{i,p}\frac{\partial \phi_{p,j}}{\partial k_q}\right] \tag{2.26c}$$

$$S_4 = \frac{1}{\omega_p^2}\left[\frac{\partial^2 \phi_{i,p}}{\partial k_r \partial k_q}\phi_{p,j} + \frac{\phi_{i,p}}{\partial k_q}\frac{\partial phi_{p,j}}{\partial k_r} + \frac{\phi_{i,p}}{\partial k_r}\frac{\partial phi_{p,j}}{\partial k_q} + \phi_{i,p}\frac{\partial^2 \phi_{p,j}}{\partial k_q \partial k_r}\right] \tag{2.26d}$$

The expressions for the second order partials of the modal parameters needed in Eq. 2.26 can also be obtained following the same approach (Singh and Bisht (2006)) and also shown in Appendix B.

In summary, one can calculate the partial derivative of the flexibility matrix using Eqs. 2.21 and 2.24 if the stiffness matrix of the baseline structure is known. However, when the undamaged stiffness is not known but the modal parameters of the baseline structure can be extracted from its available vibration response, then the partial derivatives are calculated using Eqs. 2.25 and 2.26. The details of these partial derivatives as well as the third order partials needed later are defined in Appendix B.

Iterative Approach

Two solution approaches are described here. One utilizes the complete damage index matrix. The second one, specialized for the simpler case of a shear beam model, utilizes only the modal sensitivities and not the sensitivities calculated using the stiffness matrix.

We need to solve for the N_k unknowns from the N sets of equations, one for each column, of the form given by Eq. 2.9. First, considering only the first order terms and stacking the N equations (Eq. 2.9) one on top of the other we obtain,

$$\begin{Bmatrix} \mathbf{D}(:,1) \\ \mathbf{D}(:,2) \\ \vdots \\ \mathbf{D}(:,N) \end{Bmatrix} = \begin{Bmatrix} \mathbf{G^1}_u \\ \mathbf{G^2}_u \\ \vdots \\ \mathbf{G^N}_u \end{Bmatrix} \Delta k \tag{2.27}$$

In compact form we re-write this equation as:

$$\Delta = \Gamma \Delta k \tag{2.28}$$

where we define

$$\Delta = \left\{ \begin{array}{c} \mathbf{D}(:,1) \\ \mathbf{D}(:,2) \\ \vdots \\ \mathbf{D}(:,N) \end{array} \right\} \text{ and } \Gamma = \left\{ \begin{array}{c} \mathbf{G^1}_u \\ \mathbf{G^2}_u \\ \vdots \\ \mathbf{G^N}_u \end{array} \right\}$$

This equation 2.28 has N_k unknowns and $N \times N$ number of equations. That is, there are more equations than the number of unknowns. To solve this we adopt the pseudo inverse approach which essentially is a least square approach. For this we pre-multiply Eq. 2.28 by Γ^T on both side and solve for Δk to obtain the following:

$$\Delta k = (\Gamma^T \Gamma)^{-1} \Gamma^T \Delta \tag{2.29}$$

This provides the first estimate for Δk which can be iteratively improved. Knowing these first order corrections in the stiffness coefficients, we obtain the new values of the stiffness coefficients and the new stiffness matrix. This new stiffness matrix is used to calculate the new derivative values and the new damage index matrix. These revised matrices are then used in Eq. 2.27 leading to a new Eq. 2.28. A second set of Δk values are then obtained from Eq. 2.29 using the new $\mathbf{D}$ and $\mathbf{G^j}_u$. This process is repeated till the changes in stiffness values are negligible. The total change in stiffness from the undamaged state is then the sum of Δk values at each step.

If desired, one can also consider the second order term in the iteration process. With the second order term included, Eq. 2.27 can be written as,

$$\left\{ \begin{array}{c} \mathbf{D}(:,1) \\ \mathbf{D}(:,2) \\ \vdots \\ \mathbf{D}(:,N) \end{array} \right\} = \left\{ \begin{array}{c} \mathbf{G^1}_u \\ \mathbf{G^2}_u \\ \vdots \\ \mathbf{G^N}_u \end{array} \right\} \Delta k + \left\{ \begin{array}{c} \mathbf{H^1} \\ \mathbf{H^2} \\ \vdots \\ \mathbf{H^N} \end{array} \right\} \tag{2.30}$$

where $\mathbf{G^j}_u$ and $\mathbf{H^j}_i$ are defined earlier by Eqs 2.10 and 2.11. To calculate the contribution of the second order terms $\mathbf{H^j}_i$, the Δk calculated in the previous step can be used. This calculated second order term is then shifted to the left hand side of Eq. 2.30 to

provide the following equation:

$$\left\{\begin{array}{c}\mathbf{D}(:,1)\\ \mathbf{D}(:,2)\\ \vdots\\ \mathbf{D}(:,N)\end{array}\right\}-\left\{\begin{array}{c}\mathbf{H^1}\\ \mathbf{H^2}\\ \vdots\\ \mathbf{H^N}\end{array}\right\}=\left\{\begin{array}{c}\mathbf{G^1}_u\\ \mathbf{G^2}_u\\ \vdots\\ \mathbf{G^N}_u\end{array}\right\}\Delta k \tag{2.31}$$

With only Δk unknown, this can again be solved for the next iteration value. The above steps are enumerated as follows:

1. Begin with $q = 1$.
2. Iteration step q
3. Set $k_i^u = k_i^u + \Delta k_i^{q-1}$. If $q = 1$ then $\Delta k_i^{q-1} = 0$.
4. Using these set of stiffness values, calculate the stiffness matrix and the flexibility matrix.
5. Calculate the partial derivatives of the flexibility matrix using Eq. 2.21.
6. Calculate the second order partial derivatives using Eq. 2.24.
7. Calculate the values of the terms involving $\mathbf{D}(:,j)$, $\mathbf{H^j}$ and $\mathbf{G^j}_u$ which appear in Eq. 2.31.
8. Solve Eq. 2.31 for Δk. Set $\Delta k_i^q = i^{th}$ element of Δk.
9. Set $q = q + 1$. Go to step 2.
10. The total change in the i^{th} stiffness value is given by $\sum_q \Delta k_i^q$.

Numerical Example

The application of these steps is illustrated on an example problem of a six degree of freedom shear structure. The mass, stiffness and the undamped natural frequency values of this model are listed in Table 2.1. For the damaged structure, a 10% reduction in the value of k_1 was used. Assuming that the initial stiffness values are known,

Table 2.1: Parameters for the 6-DOF shear beam model

	Degree-of-freedom					
	1	2	3	4	5	6
m (kg)	4.8×10^4	4.8×10^4	4.32×10^4	4.32×10^4	3.84×10^4	3.84×10^4
k (N/m)	8.34×10^7	8.34×10^7	5.34×10^7	5.34×10^7	3.34×10^7	3.34×10^7
ω (rad/sec)	9.4994	23.899	38.237	49.402	60.358	72.172

Table 2.2: True and estimated change in stiffness values for the 6-DOF example problem. The estimated values are listed for two cases, one where the initial stiffness matrix is assumed to be known and the second when it is assumed to be unknown.

	True	Initial **K** known	Initial **K** unknown
(1)	(2)	(3)	(4)
k_1	-8.34×10^6	-8.34×10^6	-8.34×10^6
k_2	0	1.11×10^{-7}	1.57×10^{-7}
k_3	0	7.55×10^{-8}	-5.85×10^{-8}
k_4	0	1.15×10^{-7}	1.88×10^{-8}
k_5	0	8.49×10^{-9}	4.52×10^{-9}
k_6	0	5.74×10^{-11}	-3.93×10^{-8}

the iteration steps listed above were carried out. The total estimated change in various stiffness values are plotted in Figure 2.4 for the first 5 iterations. The estimated changes can be seen to converge right after the second iteration. In Table 2.2 the correct values of the change in stiffness coefficients are listed in column 2. In column 3, the estimated changes in stiffness are shown for the present case where the initial stiffness matrix is known. The change in the value of k_1 is estimated accurately. The estimated changes in other stiffness values are too small and these can be taken to be zero.

The same problem was also solved for the unknown stiffness case. Only difference in this case was that the partial derivatives were calculated using the frequencies and mode shapes which were assumed to be known. For this Eq. 2.25 and Eq. 2.26 were used which only make use of the modal parameter values. With this change the steps outlined at the end of the previous subsection can be used to calculate the changes in

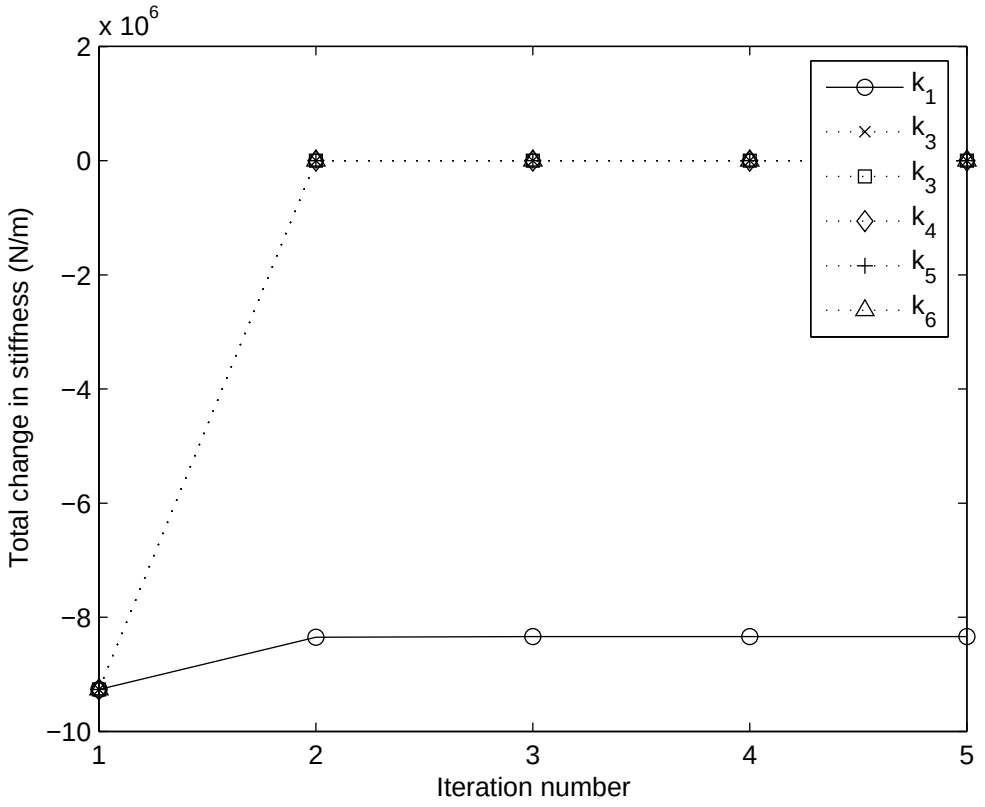

Figure 2.3: Estimated change in stiffness for the 6-DOF example problem, assuming knowledge of the initial stiffness matrix.

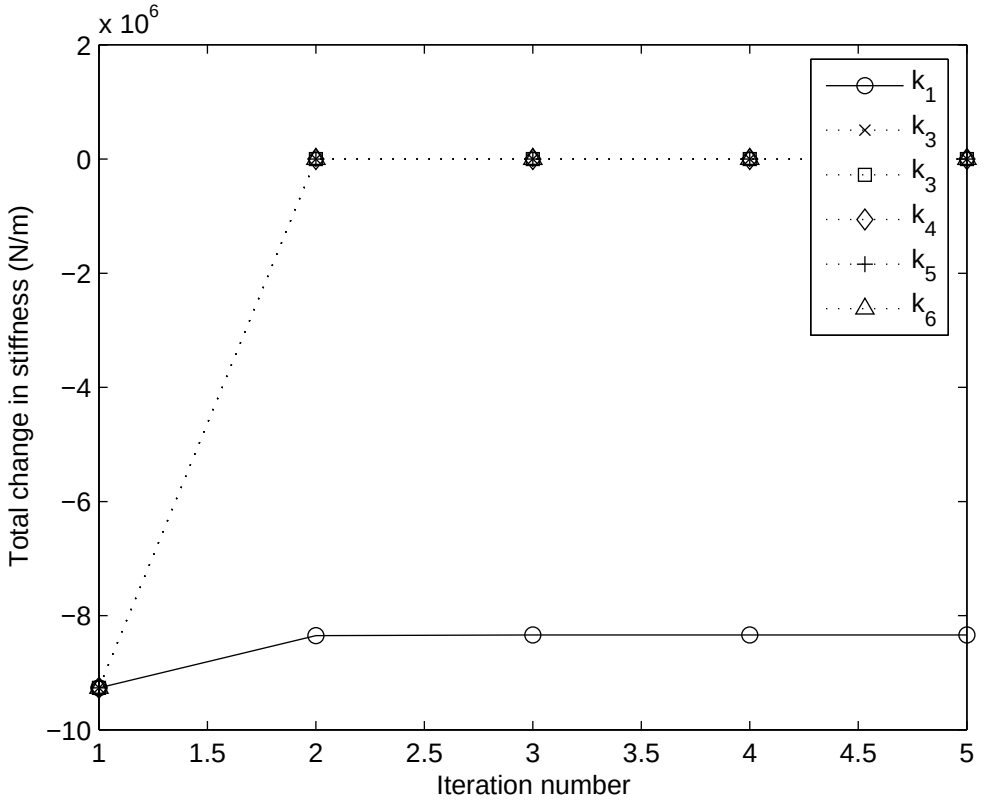

Figure 2.4: Estimated change in stiffness for the 6-DOF example problem, assuming initial stiffness matrix is unknown.

the stiffness parameters. The results for the first five iterations are shown in Figure 2.4. The convergence to the final results was almost identical to that shown in Figure 2.3. The numerical values of the estimated changes in stiffness are listed in Table 2.2 in column 4. Comparing these values with the true ones, listed in column 2, it can be seen that the change in k_1 is accurately calculated by this approach as well.

In the examples considered above the complete flexibility matrix was used for damage identification and, Eq. 2.30 was solved at each iteration step. Given the change in the flexibility matrix, the Newton-Raphson scheme can also be used to iteratively solve for the change in stiffness.

Some simplifications in the solution approach can be achieved if a shear beam model

of the structure is considered. Because of the structure of the flexibility matrix, the diagonal elements of the damage index matrix can be used to define the story damage which is just a function of the story stiffness, as seen in Eq. 2.12. That is, there is a separate equation for each story, where in each equation the damage index is just the function of the stiffness of that story. These separate uncoupled equations can be solved much easily than the coupled equations represented by the set in Eq. 2.30.

The solution of each uncoupled equation is obtained as follows. Eq. 2.13 describes the story damage in quadratic terms where the third and higher order terms have been dropped. The solution for this quadratic equation for a given value of damage index, thus, only provides an approximate estimate of the change in story stiffness. This, however, can be successively improved through an iterative procedure. For this, one first utilizes the eigenvalues of the undamaged structure to calculate the partial derivative need in Eq. 2.13. The solution of the quadratic equation obtained for Δk_i provides the first estimate of the change in the stiffness values. For this change, one estimates the new eigen properties (frequencies and mode shapes) using the third order expansion of these quantities (the required expressions are given in Appendix B). These new estimated eigen properties are then used to calculate the new flexibility matrix. This revised flexibility matrix is used to calculate the revised damage index value. The revised damage index values are then used to calculate the new Δk_i. The process is repeated till a convergence in the Δk_i values is reached.

These steps are graphically shown in Figure 2.5 for a numerical example. The first story of the shear beam was damaged such that its first story stiffness was reduced by 10%. Corresponding to this reduction in the stiffness, the value of the damage index in the first story was 2.36×10^{-8}. This is denoted by the point "Given damage index" on the damage index axis in this figure. For this value of the damage index, the quadratic Eq. 2.13 was solved, giving the first estimate for change in story stiffness of $\Delta k_1 = 5.2 \times 10^7$. Assuming that the stiffness indeed had reduced by Δk_1, changes in natural frequencies and mode shapes were obtained; using which the flexibility matrix was calculated. With this new flexibility matrix the damage index value, indicated by point $d_1 = 4.36 \times 10^{-8}$ was obtained. A straight line is drawn which passes through the

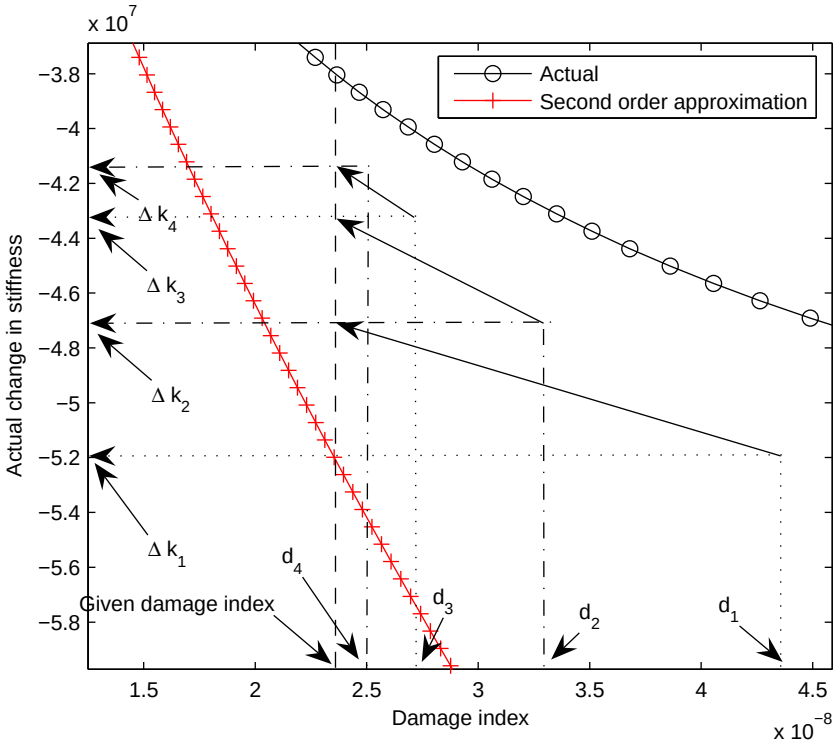

Figure 2.5: Iterative solution scheme, when solving using the diagonal elements

point $(d_1, \Delta k_1)$ and has the slope of $1/(\partial f/\partial k)$. The point where this line intercepts the vertical line corresponding to the given damage index value provides the next estimate of the value of the change in stiffness, i.e., Δk_2. The process is then repeated to obtain Δk_3, Δk_4 etc.

2.4 Missing Mode Effect

In a practical situation it might not be possible to extract all the modes of the structure from the dynamic response. It can happen because the excitation acting on the structure may not excite some modes. As a result they may not appear in the measured response, and the analysis of such a response will not provide these modes. This will most likely be the case when considering ambient vibration data. In the presence of such incomplete modal information, errors will be introduced in the estimated flexibility matrix. In this section, we examine the effects of such missing mode on damage identification. A numerical study with a 6 degree-of-freedom shear building model is carried out to illustrate the effect of missing modes on the damage identification procedure. These results are similar to those presented in Bisht and Singh (2006a, 2006b). The parameters of the 6-degrees of freedom model considered in this illustration are listed in Table 2.1.

To simulate single and multiple damage scenarios in this model, the stiffness values in one or more stories are reduced. To study the effect of missing modes on the damage quantification scheme, the damage identification and quantification is then attempted and compared by successively reducing the number of modes used. A knowledge of all the modes of the undamaged structure from which the level of damage is measured is assumed.

In Figures 2.6 and 2.7 the estimated changes in stiffness using different number of modes for two different scenarios of single damage introduced at two different locations are shown. In both these, and subsequent figures in this section, the legend "n modes" implies that the first n modes were used to form the flexibility matrix. Figure 2.6 is for

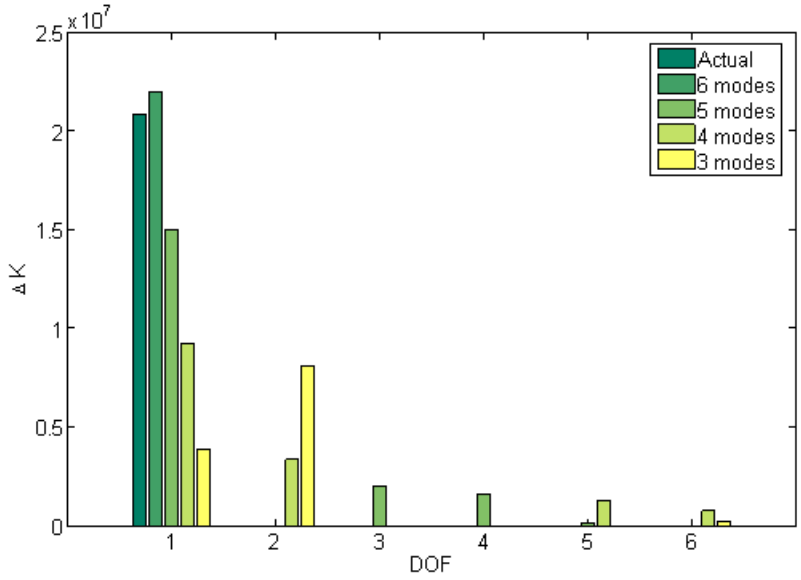

Figure 2.6: The estimated change in stiffness obtained by using different number of modes to form the flexibility matrix. The legends "n modes" implies that the first n modes were used to estimate the flexibility matrix. Damage in this case corresponds to a 25% reduction in stiffness at DOF 1.

the case of 25% stiffness reduction in only the first story, and Figure 2.7 for the case of 25% stiffness reduction in third story only. In Figure 2.8 the damage quantification results are presented for the case of multiple damages (30%, 20% and 5% reduction in stories 2, 4 and 6 respectively). Based on these results the following observations can be made. First, the damage can be identified in all three scenarios using as few as the first three modes, but the damage quantification error increases with the decrease in the number of modes used. There are also some false indications of damages in the stories higher than the story with actual damage when less than the complete set of modes is used. This is shown by the indication of some changes in stiffness values in stories 2-6 in Figure 2.6 and stories 4-6 in Figure 2.7.

The first observation is explained by the fact that the flexibility matrix estimated with fewer modes will have some error which in turn will introduce error in the calculated damage index and in the estimated change in the stiffness values as well. The false indications in the higher stories of the shear beam model also result due to this

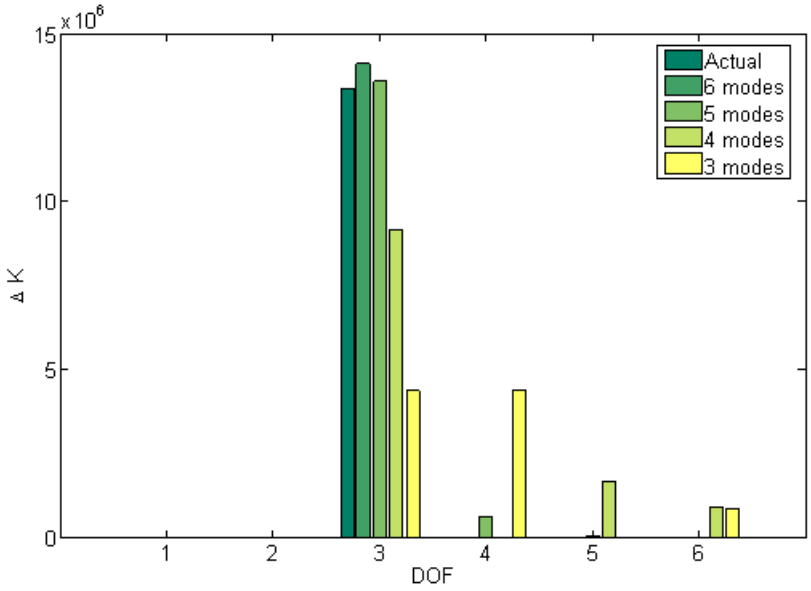

Figure 2.7: The estimated change in stiffness obtained by using different number of modes to form the flexibility matrix. The legends "n modes" implies that the first n modes were used to estimate the flexibility matrix. Damage in this case corresponds to a 25% reduction in stiffness at DOF 3.

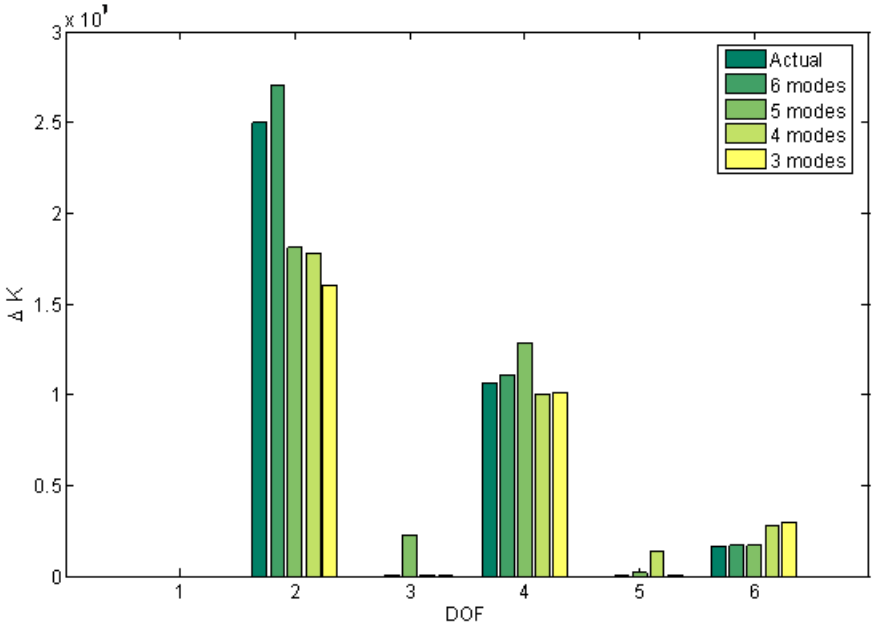

Figure 2.8: The estimated change in stiffness obtained by using different number of modes to form the flexibility matrix. The legends "n modes" implies that the first n modes were used to estimate the flexibility matrix. Damage in this case corresponds to a 30%, 20% and 5% reduction in stiffness at DOF 2, 4 and 6 respectively.

error in the estimated flexibility of the damaged structure. In a shear beam structure, the change in the flexibility in a lower story will also change the flexibility at all higher stories, but it will remain constant if no higher story is damaged. However, because of using lesser number of modes which affect different stories differently there is an additional change in the flexibility at the higher level indicating a change in the story stiffness, and thus false damage indications. This is shown in Figure 2.9 where the estimates of the damage index at various degrees of freedom calculated with increasing number of modes are plotted, and it corresponds to the case of 25% reduction in the third story stiffness shown earlier in Figure 2.7. In the plot drawn with all six modes, it can be noted that there is a large increase in the damage index from second to the third degree of freedom and the curve remains at the same level after that. This clearly indicates damage in the third story and no damage thereafter as the damage index remains constant. However, when the number of modes used is decreased we note that the damage index value changes from one story to another; in some cases the damage index values even become negative when the incomplete set of modes is used. The negative index value can be clearly discarded as being impossible, but the increase in the damage index from lower level to next will imply damage in the story as it appears in Figure 2.7.

Another important effect of missing modes is that if the damage index is smaller than the combined contribution of the missing modes, then it cannot even be detected. This is shown in Figure 2.10 where the damage quantification results for the case with 10% reduction in the stiffness of the stories 1, 2 and 6 are shown. It can be seen that we can detect damage in stories 2 and 6 even with just 2 modes whereas we cannot detect this in story 1 even when we use five modes. Such a situation can arise when the combined contribution of the missing modes of a damaged structure to the flexibility coefficient associated with the story stiffness is more than the contribution due to the damage. To explain this, in Table 2.3, the percent contributions of different modes of the damaged structure to the diagonal elements of the flexibility matrix are shown. We note that the 6th mode contributes about 11% to the flexibility coefficient of the first degree of freedom associated with the first story. Since this is more than the change in the stiffness of the first story in Figure 2.10, we cannot detect the damage

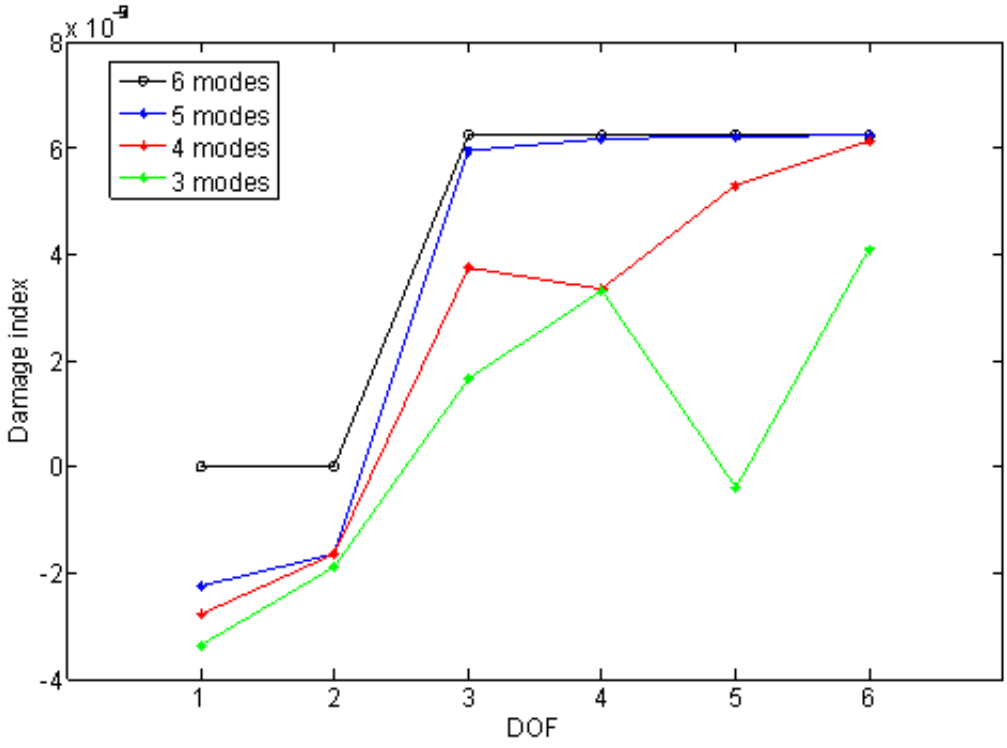

Figure 2.9: Damage index plot based on flexibility matrix for a 25% reduction in stiffness at DOF 3 for different number of modes. The legends "n modes" implies that the first n modes were used to estimate the flexibility matrix.

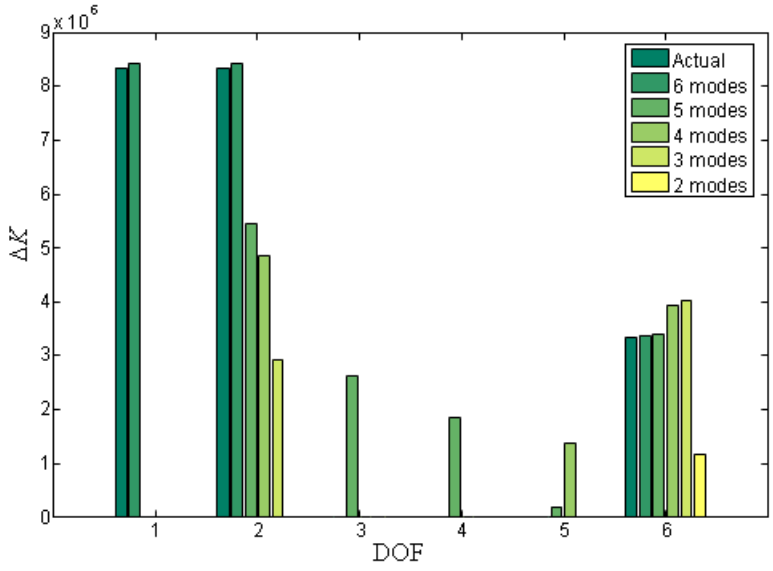

Figure 2.10: The estimated change in stiffness obtained by using different number of modes to form the flexibility matrix. The legends "n modes" implies that the first n modes were used to estimate the flexibility matrix. Damage in this case corresponds to a 10% reduction in stiffness at DOF 1, 2 and 6

if we do not include this mode in the analysis. On the other hand, since the combined contributions of the modes 3, 4, 5, and 6 to the 6^{th} degree of freedom coefficient is less than 10%, omitting them from the analysis still allows the detection of the damage. Similar reasoning applies to the detection of damage in story 2 where the combined contribution of modes 4, 5, and 6 is less than 10%, and as such the damage can still be identified if these modes are not available. In summary, the accuracy of damage quantification deteriorates as the available number of modes decrease. Also, the effect of a missing mode depends on where the damage is and what is its magnitude. If the missing mode contributes to the damage index more than the contribution of the damage to the index, then the damage can not be detected. Finally, as the number of modes used in estimating the flexibility matrix is reduced, the error in the damage identification procedure increases.

Table 2.3: Percentage contributions of different modes to the diagonal elements of the flexibility matrix of the damaged structure. Damage: 10% stiffness reductions in stories 1, 2 and 6.

		Mode number					
Diagonal element	Total %	1	2	3	4	5	6
1	100	23.68	23.9	22.6	8.29	10.27	11.26
2	100	44.8	32.76	14.09	1.12	0.37	6.87
3	100	67.83	22.15	0.07	3.73	4.32	1.9
4	100	82.12	6.27	6.88	0.79	3.64	0.3
5	100	89.6	1.67	2.12	5.92	0.67	0.02
6	100	83.5	12.64	2.67	1.14	0.04	0

2.5 Numerical Results: ASCE SHM Benchmark Problem

In this section we test the proposed damage identification algorithm on a benchmark problem. This benchmark problem was primarily created by the International Association of Structural Control (IASC) and American Society of Civil Engineers (ASCE) Structural Health Monitoring task group for testing of different damage identification techniques that are being proposed by different researchers. A detailed description of the ASCE-SHM benchmark problem using simulated data can be found in Johnson *et al.* (2004). In the following we provide the details of the benchmark problem, followed by the numerical results on damage identification.

Benchmark Problem

Figure 2.11 shows the schematic of the model of the benchmark problem structure with all columns, braces and floor slabs. It is a 2-bay by 2-bay 4-story framed structure with diagonal braces in each bay in all the stories. The computer codes are provided by the IASC-ASCE SHM task group to the research community to generate the simulated response of the structure for use in the damage identification algorithms. The

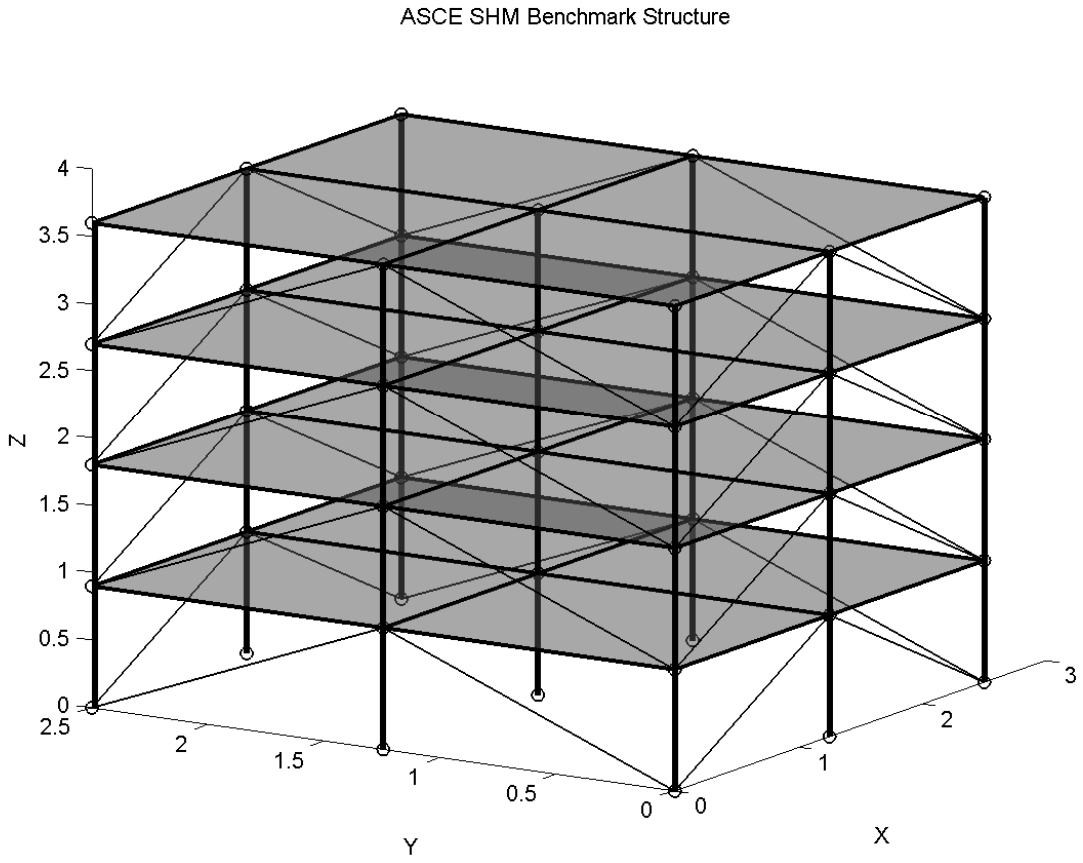

Figure 2.11: The ASCE-SHM benchmark structure. The x, y and z direction dimensions are in meters.

Table 2.4: Description of various cases for the benchmark problem using simulated data

Case number	Data generation model	Mass distribution	Excitation
(1)	(2)	(3)	(4)
1	12 DOF	Symmetric	ambient on all floors
2	120 DOF	Symmetric	ambient on all floors
3	12 DOF	Symmetric	shaker on top floor
4	12 DOF	Asymmetric	shaker on top floor
5	120 DOF	Asymmetric	shaker on top floor
6	120 DOF	Asymmetric	shaker on top floor

Table 2.5: Description of various damage patterns for the benchmark problem using simulated data

Damage pattern	Description (elements removed)
1	All braces in first story
2	All braces in first and third story
3	One brace in first story
4	One brace in first and third story
5	As in #4 and loosen floor beam at first story
6	Reduce stiffness in one brace in first story

analytical model used in generating the response for this benchmark problem is based on an actual 2-bay by 2-bay scaled steel frame structure fabricated and now located at the University of British Columbia, Canada.

In this problem, six different cases are defined based on the model used to generate the vibration response (12 or 120 degrees-of-freedom), mass distribution (symmetric or asymmetric), the loading type (wind loading on all floors or shaker excitation applied at the top floor) and the number of measurement points available (on all floors or at only two floors). These cases are listed in Table 2.4. Column 2 indicates the model that was used to generate the simulation data. Two different models, one with 12 DOF

Table 2.6: Damage patterns to be considered for different cases

	Damage patterns to be considered
Case 1	1, 2
Case 2	1, 2
Case 3	1, 2
Case 4	1, 2, 3, 4, 6
Case 5	1, 2, 3, 4, 5, 6
Case 6	1, 2, 3, 4, 5, 6

model and the other a more detailed 120 DOF model, were employed. The latter one allows for more realistic scenarios (response is generated using a much detailed model but damage identification is carried out using a lower order model). In column 3, the type of mass distribution for the structure is listed. Asymmetric mass distribution introduces torsional effects. Two different types of excitations considered are listed in column 4. For cases 1 and 2, ambient excitation in the form of filtered white noise is applied on all the floors. For cases 3 4 5 and 6, the excitation is provided along the diagonal direction by a shaker on the top floor. In this study, the first five cases are considered; the last case which considers availability of limited sensor information has not been explored.

A total of six different damage patterns are defined for the problem. These damage patterns are described in Table 2.5. In damage pattern 1, all the braces of the first story are removed. Damage pattern 2 considers the removal of all the braces from both the first and the third story. Damage pattern 3 corresponds to the removal of one brace in the first story, and in damage pattern 4 in addition to this another brace from the third story is removed. Damage pattern 5 is similar to damage pattern 4 but it also includes the loosening of the floor beam joint at the first story. Finally, damage pattern 6 considers the reduction of stiffness by a factor of 2/3 in one brace in the first story. The different damage patterns to be considered for various cases described in Table 2.4 are listed in Table 2.6. For the six damage patterns mentioned above, the percentage change in the stiffness of each story (indicated by Column 1 of the table) and in each direction (indicated by Column 2 of the table) as given by Johnson *et al.* (2004) are

Table 2.7: Percentage change in stiffness for various damage patterns for the 12-DOF model.

		Damage pattern					
Story	Direction	1	2	3	4	5	6
(1)	(2)	(3)	(4)	(5)	(6)	(7)	(8)
1	x	45.24	45.24	0	0	0	0
1	y	71.03	71.03	17.76	17.76	17.76	5.92
1	θ	64.96	64.96	9.87	9.87	9.87	2.88
2	x	0	0	0	0	0	0
2	y	0	0	0	0	0	0
2	θ	0	0	0	0	0	0
3	x	0	45.24	0	11.31	11.31	0
3	y	0	71.03	0	0	0	0
3	θ	0	64.96	0	9.16	9.16	0
4	x	0	0	0	0	0	0
4	y	0	0	0	0	0	0
4	θ	0	0	0	0	0	0

listed in Table 2.7 for the 12-DOF model, and in Table 2.8 for the 120-DOF model. The "equivalent" stiffness for the 120-DOF model was calculated by a least-squares optimization method, Johnson *et al.* (2004).

The noise corrupted vibration response of the structure at four different locations on each floor (2 in the x direction and 2 in the y direction) is provided. The objective is to identify the location of damage and the magnitude of the change in story stiffness values. In the following, we use the proposed damage identification technique based on the damage index values defined earlier.

Numerical Results

The steps involved in the proposed damage quantification approach can be outlined as follows: (1) Form the undamaged and damaged structures flexibility matrix,

Table 2.8: Percentage change in "equivalent" stiffness for various damage patterns for the 120-DOF model.

		Damage pattern					
Story	Direction	1	2	3	4	5	6
(1)	(2)	(3)	(4)	(5)	(6)	(7)	(8)
1	x	54.50	54.13	0	-0.11	-0.11	0
1	y	74.99	74.79	19.14	19.15	20.38	6.29
1	θ	71.60	71.12	9.12	9.08	9.08	3
2	x	14.52	24.44	0	2.13	2.13	0
2	y	13.21	20.06	1.32	1.34	2.75	0.35
2	θ	17.00	26.51	1.02	1.73	1.73	0.27
3	x	0.04	59.61	0.01	15.20	15.20	0
3	y	-0.19	76.00	-0.02	0.02	-0.08	0
3	θ	-2.27	76.57	-0.11	10.37	10.36	-0.03
4	x	0.76	20.10	0.01	3.23	3.23	0
4	y	0.95	15.23	0.08	0.14	0.17	0.02
4	θ	0.28	22.87	0.01	1.19	1.20	0

(2) Form the damage index matrix, (3) Apply any correction to the damage index matrix if needed (i.e., disregard any damage index value which indicates an increase in stiffness), (4) Solve the system of equations given by Eq. 2.9 or Eq. 2.13 using the method outlined in the previous sections.

In all the simulation cases, the natural excitation technique (NeXT) (Beck *et al.* (1994)) and the eigensystem realization algorithm (ERA) (Juang and Pappa (1985)) methods were used to estimate a state-space model from the noise corrupted acceleration responses. The basic elements of the NeXT and ERA are given in Appendix A. Since measurement noise also introduces spurious modes, to identify the structural modes, modal frequency, and damping ratio, the modal phase collinearity (MPC) (Pappa and Elliott (1993)) conditions were applied. From the calculated system matrix of the state-space model, the modes which had a frequency < 100 Hz, damping $< 5\%$, and MPC value $> 90\%$ were taken to be structural modes and the flexibility matrix was formed from them.

Since the eccentricity between the system mass and stiffness centers were rather small, the motion in the two horizontal directions was considered uncoupled. In other words, although the building model has 12 degrees of freedom (two horizontal and one rotation about vertical axis for each floor) because of low eccentricity the coupling in the two horizontal models was neglected and for damage identification two 4-DOF shear beam models, one for each horizontal direction, were utilized in all the cases.

In Case 1 the structure is symmetric and ambient excitation is applied in the y direction on all the floors. Damage patterns 1 and 2 are to be considered in this case. These involve the removal of all braces from the first story and from the first and the third stories. The structure remains symmetric in both these damage patterns. Therefore a 4-DOF shear beam model in the y direction was used. The estimated percentage changes in stiffness calculated using the proposed method are presented in the top two plots in Figure 2.12. The left plot is for damage pattern 1 and the right plot is for damage pattern 2. In this and the subsequent figures the black bars are the true values as given in Johnson *et al.* (2004) and listed in Table 2.7 for the 12-DOF model and in

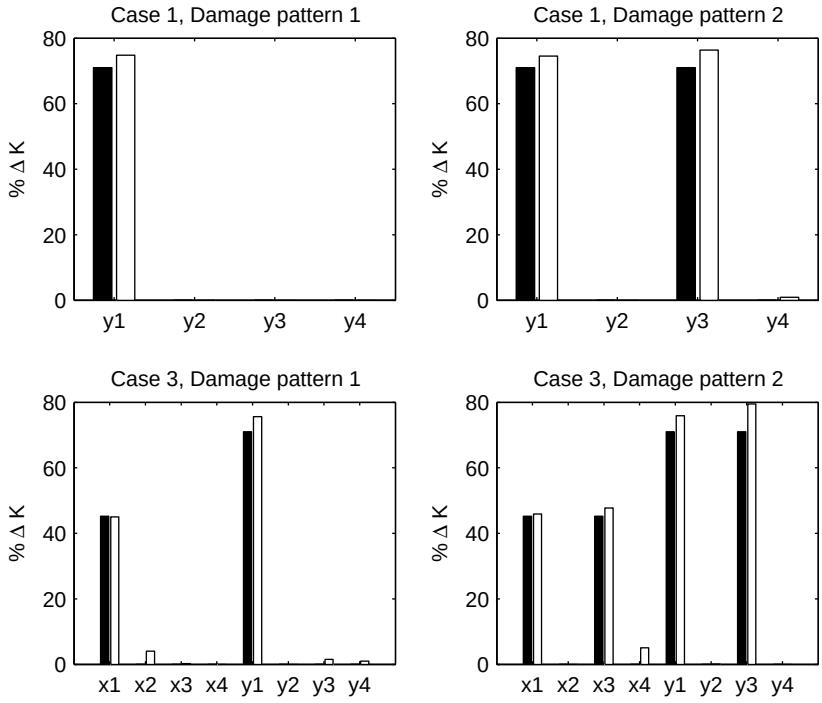

Figure 2.12: Percentage change in stiffness for Case 1 and 3. The black bars represent the true values and the white represent the estimated values.

Table 2.8 for the 120-DOF model. Also, the labels xi and yi for $i = 1, 2, 3, 4$ on the x-axis in these figures refer to the x or y direction value for the i^{th} floor. It can be seen that damage in both the patterns is correctly identified and quantified. Note that even though a change in stiffness results in the x direction but since the excitation is applied only in the y direction and the structure is symmetric the structure was analyzed only in the y direction.

The lower two plots in Figure 2.12 show the results for Case 3. Similar to Case 1 the model used to generate the response in Case 3 is a 12-DOF model with symmetric mass distribution. The same damage patterns i.e. 1 and 2 are to be examined in this case also. However Case 3 differs from Case 1 in terms of the excitation. In Case 3 excitation is applied at the top floor along the diagonal. Due to this, significant response is obtained in both the x and y directions. From the results presented in Figure 2.12 for Case 3, it can be seen that in both damage patterns, the damage was correctly identified. The estimated change in stiffness is slightly more than the true value, for example in damage pattern 2 for $y3$ direction. Also, small changes in stiffness are also indicated in floors (e.g. in damage pattern 2 for $x4$ direction) where the actual change in stiffness is zero. Such false damage indications can be attributed to the error in the estimated modal properties which arise due to measurement noise.

In Case 4, the response is generated using a 12 DOF model with the excitation being applied at the roof along the diagonal element. In this respect, Case 4 is similar to Case 3. However the mass distribution in Case 4 is asymmetric. The asymmetric mass distribution causes coupling in the response in the two horizontal directions. However it was decided that the coupling was not significant and that the shear beam models could be used to identify the story and direction in which the damage occurs. Thus similar to the previous cases discussed, two 4-DOF shear beam models were utilized. The results are presented in Figure 2.13 for the damage patterns 1, 2, 3, 4, and 6, as prescribed in Table 2.6. Major damages like those in damage pattern 1 and 2 as well as minor damages like a 5% reduction in damage pattern 6, all are correctly identified. The estimated changes in stiffness are also close to the true values for all the damage patterns. There are however certain false damage indications, for example in damage

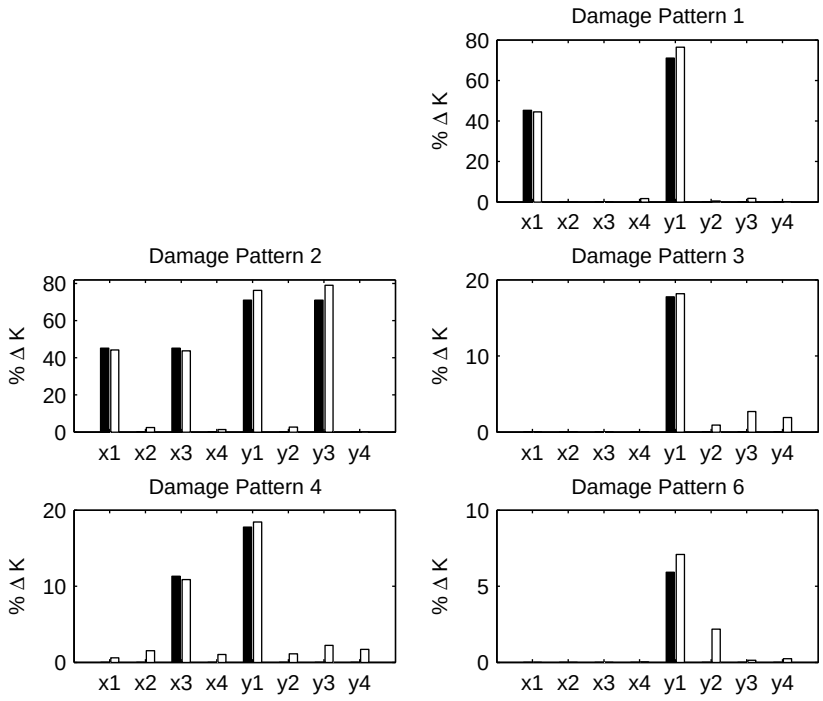

Figure 2.13: Percentage change in stiffness for case 4. The black bars represent the true values and the white represent the estimated values.

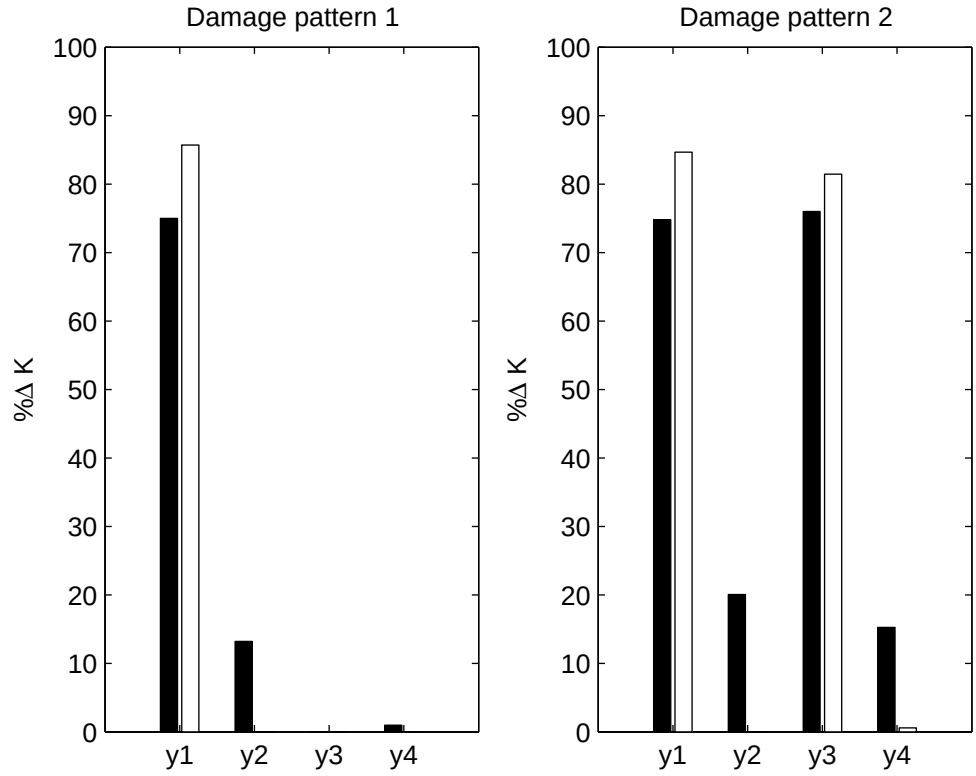

Figure 2.14: Percentage change in stiffness for case 2. The black bars represent the true values and the white represent the estimated values.

along $y2$ direction in damage pattern 6. These can be attributed to the noise in the measurement data.

In cases 1, 3 and 4 the response was generated using a 12-DOF model. In comparison, in cases 2 and 5, the response is generated using a 120 DOF model, but the damage estimation is to be made with a 12 DOF model. Thus, in these cases we will have modeling error also. The damage identification results for Case 2 are shown in Figure 2.14. In this case only damage patterns 1 and 2 need to be considered, and the mass distribution and excitation are similar to Case 1. It can be seen that the damage in the first story (in damage pattern 1) and in the first and third stories (in damage pattern 2) is identified correctly. The estimated change in stiffness is slightly more that the true value. Also, some minor damages are missed. This can be attributed to the

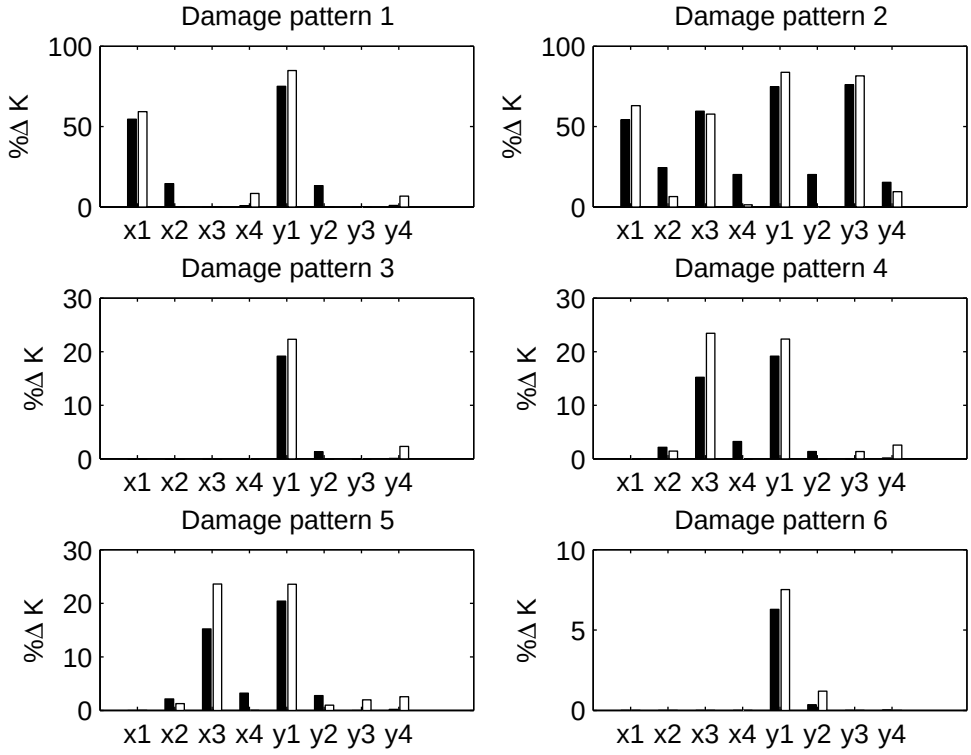

Figure 2.15: Percentage change in stiffness for case 5. The black bars represent the true values and the white represent the estimated values.

use of a shear beam model in which change in a particular story stiffness will not affect the adjacent story stiffness values.

Finally, Figure 2.15 shows the change in stiffness results for Case 5. In addition to the response being generated by the 120 DOF model (like in Case 2), the mass distribution in this case is asymmetric and the ambient excitation is considered. From Figure 2.15, we note that the method is able to identify the major damages correctly. Similar to the observation in Case 2 above, minor damages are missed. This can be attributed to the use of a shear beam model. Thus, in an overall sense, the method can in-fact identify the damaged story and give an accurate enough change in stiffness value.

2.6 Curvature Flexibility for Damage Identification

In using the flexibility matrix for damage identification only the translational degrees of freedom were used. This is because, in dynamic analysis, the rotational degrees-of-freedom are condensed out and only the translational degrees-of-freedom are retained. Therefore the idea of incorporating the rotational degrees-of-freedom into the analysis for damage identification was explored. For this a matrix referred to as the curvature flexibility matrix was defined and utilized for damage identification.

Consider a general n degree-of-freedom (DOF) system for which the force-displacement equation can be written as,

$$\mathbf{K}x = f \tag{2.32}$$

where $\mathbf{K}$ is the $n \times n$ stiffness matrix, x is a n dimension displacement vector, and f the corresponding force vector of length n. Taking into account the rotational DOF's which are condensed out, this matrix equation can be written as follows,

$$\begin{bmatrix} \mathbf{K_{rr}} & \mathbf{K_{rc}} \\ \mathbf{K_{cr}} & \mathbf{K_{cc}} \end{bmatrix} \begin{Bmatrix} x_r \\ x_c \end{Bmatrix} = \begin{Bmatrix} f \\ 0 \end{Bmatrix} \tag{2.33}$$

where the subscript r and c represent the DOF's (and their numbers) which are finally retained and condensed respectively. The lower partition of this matrix equation gives

the relationship between the condensed DOF's and the retained DOF's,

$$x_c = -\mathbf{K_{cc}}^{-1}\mathbf{K_{cr}}x_r \tag{2.34}$$

Using this relation, the static equation, Eq. 2.32, for the system, considering just the retained DOF's becomes,

$$\mathbf{K}^* x_r = f \tag{2.35}$$

where the condensed stiffness matrix $\mathbf{K}^*$ is given by,

$$\mathbf{K}^* = \mathbf{K_{rr}} - \mathbf{K_{rc}}\mathbf{K_{cc}}^{-1}\mathbf{K_{cr}} \tag{2.36}$$

From the measured translational DOF's the flexibility matrix of the system can be estimated by (Eq. 2.1),

$$\mathbf{F_r} = \mathbf{\Phi\Lambda\Phi}^T \tag{2.37}$$

Note that the dimension of this flexibility matrix would be $r \times r$. Using Eq. 2.34 a $c \times r$ flexibility matrix for the condensed DOF's can be defined as,

$$\mathbf{F_c} = -\mathbf{K_{cc}}^{-1}\mathbf{K_{cr}}\mathbf{F_r} \tag{2.38}$$

Using the two flexibility matrices defined above in Eqs. 2.37 and 2.38, the complete flexibility matrix for the system is then formed, the size of which is $(r + c) \times r$, (note that $r + c = n$) this is given by

$$\mathbf{F_{str}} = \begin{bmatrix} \mathbf{F_r} \\ \mathbf{F_c} \end{bmatrix} \tag{2.39}$$

Next, for each beam like element in the structure, curvature (ρ) is calculated at both ends. Therefore for a structure with n_e beam elements there will be $2n_e$ curvature values. Assembling all the curvatures in vector form, an equation relating the curvature vector to the displacement vector can be written as

$$\rho = \mathbf{T}x \tag{2.40}$$

where ρ is a vector of length $2n_e$, $\mathbf{T}$ is a matrix of size $2n_e \times n$ consisting of constants which relate the different displacements to the curvature. Substituting for x we have,

$$\rho = \mathbf{TF_{str}}f \tag{2.41}$$

Using this expression a curvature flexibility matrix $\mathbf{F}_\rho$ is defined as,

$$\mathbf{F}_\rho = \mathbf{T}\mathbf{F}_{\mathbf{str}} \tag{2.42}$$

Using the same idea which was used previously for damage identification using flexibility matrix, the damaged curvature flexibility matrix is expressed in terms of the undamaged matrix using the Taylor's series expansion. Denoting the j^{th} column of the damaged and undamaged curvature flexibility matrices by $\mathbf{F}_\rho(:,\mathbf{j})_D$ and $\mathbf{F}_\rho(:,\mathbf{j})_U$ respectively, we have

$$\mathbf{F}_\rho(:,\mathbf{j})_D - \mathbf{F}_\rho(:,\mathbf{j})_U = \left[\frac{\partial[\mathbf{F}_\rho(:,\mathbf{j})]}{\partial k}\right]\Delta k + \begin{bmatrix} \mathbf{H_1^j} \\ \mathbf{H_2^j} \\ \vdots \\ \mathbf{H_N^j} \end{bmatrix} \tag{2.43}$$

where $\left[\frac{\partial[\mathbf{F}_\rho(:,\mathbf{j})]}{\partial k}\right]$ and $\mathbf{H_i^j}$ are the gradient and second order term (involving the Hessian matrices) respectively and Δk is the vector of changes in the element stiffness values. The gradient and second order terms are defined similar to the case when using the flexibility matrix (Eq. 2.10 and Eq. 2.11). The first and second partial derivatives needed in the definition of the gradient and Hessian matrices are calculated as follows. Using the definition given in Eqs. 2.38 2.39 and 2.42 we have,

$$\mathbf{F}_\rho = \mathbf{T}\begin{bmatrix} \mathbf{F_r} \\ \mathbf{F_c} \end{bmatrix} = \mathbf{T}\begin{bmatrix} \mathbf{F_r} \\ -\mathbf{K_{cc}}^{-1}\mathbf{K_{cr}}\mathbf{F_r} \end{bmatrix}$$

Taking the partial derivative of the above equation with respect to k_i,

$$\frac{\partial \mathbf{F}_\rho}{\partial k_i} = \mathbf{T}\begin{bmatrix} \frac{\partial \mathbf{F_r}}{\partial k_i} \\ -\frac{\partial \mathbf{K_{cc}}^{-1}}{\partial k_i}\mathbf{K_{cr}}\mathbf{F_r} + \mathbf{K_{cc}}^{-1}\frac{\partial \mathbf{K_{cr}}}{\partial k_i}\mathbf{F_r} + \mathbf{K_{cc}}^{-1}\mathbf{K_{cr}}\frac{\partial \mathbf{F_r}}{\partial k_i} \end{bmatrix} \tag{2.44}$$

Taking the partial derivative once again with respect to k_j we obtain,

$$\frac{\partial^2 \mathbf{F}_\rho}{\partial k_j \partial k_i} = \mathbf{T}\begin{bmatrix} \frac{\partial^2 \mathbf{F_r}}{\partial k_j \partial k_i} \\ \mathbf{S_1} + \mathbf{S_2} + \mathbf{S_3} \end{bmatrix} \tag{2.45}$$

where

$$\mathbf{S_1} = -\frac{\partial^2 \mathbf{K_{cc}}^{-1}}{\partial k_j \partial k_i}\mathbf{K_{cr}}\mathbf{F_r} - \frac{\partial \mathbf{K_{cc}}^{-1}}{\partial k_i}\frac{\partial \mathbf{K_{cr}}}{\partial k_j}\mathbf{F_r} - \frac{\partial \mathbf{K_{cc}}^{-1}}{\partial k_i}\mathbf{K_{cr}}\frac{\partial \mathbf{F_r}}{\partial k_j}$$

$$\mathbf{S_2} = \frac{\partial \mathbf{K_{cc}}^{-1}}{\partial k_j}\frac{\partial \mathbf{K_{cr}}}{\partial k_i}\mathbf{F_r} + \mathbf{K_{cc}}^{-1}\frac{\partial^2 \mathbf{K_{cr}}}{\partial k_j \partial k_i}\mathbf{F_r} + \mathbf{K_{cc}}^{-1}\frac{\partial \mathbf{K_{cr}}}{\partial k_i}\frac{\partial \mathbf{F_r}}{\partial k_j}$$

and

$$\mathbf{S_3} = \frac{\partial \mathbf{K_{cc}}^{-1}}{\partial k_j}\mathbf{K_{cr}}\frac{\partial \mathbf{F_r}}{\partial k_i} + \mathbf{K_{cc}}^{-1}\frac{\partial \mathbf{K_{cr}}}{\partial k_j}\frac{\partial \mathbf{F_r}}{\partial k_i} + \mathbf{K_{cc}}^{-1}\mathbf{K_{cr}}\frac{\partial^2 \mathbf{F_r}}{\partial k_j \partial k_i}$$

Eqs. 2.44 and 2.45 involve terms which require the derivative of the inverse of a matrix. For example, in Eq. 2.44, $\frac{\partial \mathbf{K}_{cc}^{-1}}{\partial k_i}$ is needed. Terms like these can be expressed in an alternate form which will not involve the derivative of the inverse. This is possible because, for any square invertible matrix $\mathbf{A}$ and a scalar parameter t,

$$\frac{\partial \mathbf{A}^{-1}}{\partial t} = -\mathbf{A}^{-1}\frac{\partial A}{\partial t}\mathbf{A}^{-1}$$

which can be derived by differentiating $\mathbf{A}\mathbf{A}^{-1} = \mathbf{I}$, where $\mathbf{I}$ is the identity matrix.

Similar to the case of the flexibility matrix, the equations for each column as given by Eq. 2.43, can be stacked one on top of the other and then solved iteratively for Δk. In this procedure it is assumed that the model of the undamaged structure is known. Thus the undamaged stiffness values are used in calculating the flexibilities associated with the condensed degrees of freedom.

The idea leading to the development of the curvature flexibility matrix was to incorporate the rotational degrees of freedom into the analysis. This was motivated by the idea that considering the rotational degrees-of-freedom might help in identifying which column in a story suffers a damage. As an example, we consider a two story single bay frame. This is shown in Figure 2.16. The model consists of 4 columns and 2 beams. The stiffness of these members are denoted by k_i ($i = 1 \ldots 6$). A total of 6 DOF's were considered, 2 translational (U_1 and U_2) and 4 rotational (U_i, $i = 3, 4, 5, 6$). For defining the curvature flexibility, curvature was used at both ends of each of the stiffness elements. A total of 12 points were therefore used. These are shown in Figure 2.17. The dimensions of the various matrices are listed in Table 2.9. With the two translational DOF's being the retained DOF's the size of $\mathbf{F_r}$ is 2×2. The four rotational DOF's are condensed and thus the size of $\mathbf{F_c}$ is 4×2. This leads to $\mathbf{F_{str}}$ being 6×2. With 12 curvature points defined as in Figure 2.17 the size of $\mathbf{T}$ is 12×6. This matrix

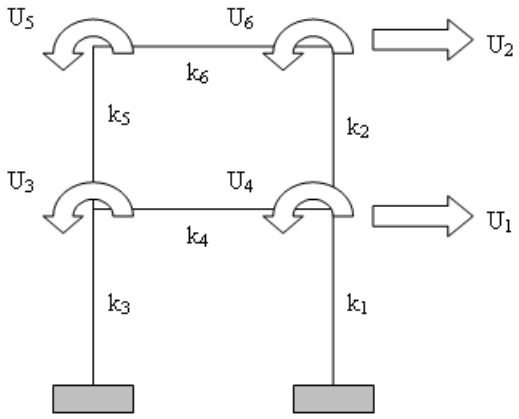

Figure 2.16: The framed structure considered in the curvature flexibility approach.

is given by,

$$\mathbf{T} = \begin{bmatrix} 6 & 0 & 2 & 0 & 0 & 0 \\ 6 & 0 & 4 & 0 & 0 & 0 \\ 6 & 0 & 0 & 2 & 0 & 0 \\ 6 & 0 & 0 & 4 & 0 & 0 \\ 0 & 0 & 4 & 2 & 0 & 0 \\ 0 & 0 & 2 & 4 & 0 & 0 \\ -6 & 6 & 4 & 0 & 2 & 0 \\ -6 & 6 & 2 & 0 & 4 & 0 \\ -6 & 6 & 0 & 4 & 0 & 2 \\ -6 & 6 & 0 & 2 & 0 & 4 \\ 0 & 0 & 0 & 0 & 4 & 2 \\ 0 & 0 & 0 & 0 & 2 & 4 \end{bmatrix}$$

The size of the curvature matrix, $\mathbf{F}_\rho$ is 12×2, and that of the stiffness vector is 6.

To obtain numerical results showing the application of the curvature flexibility approach, for each member stiffness represented by the factor EI/L was assumed to be equal to 100 units. The mass at the nodes was assumed to be 1 unit. To simulate the damage, the stiffness in the column represented by stiffness k_3 was reduced by 10%. For this damaged structure, the modal properties were calculated and used as the known modal characteristics for calculating the curvature flexibilities and associated damage

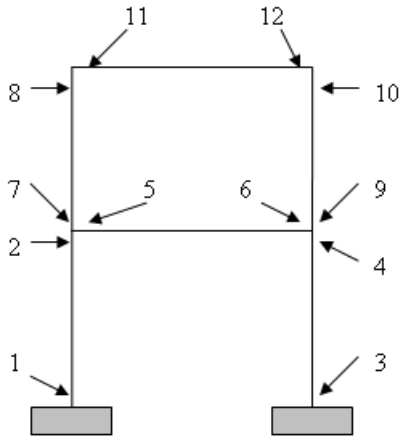

Figure 2.17: The curvature points for the framed structure considered in the curvature flexibility approach.

Table 2.9: The dimensions of various matrices and vectors for the framed structure considered in the curvature flexibility approach.

Matrix/Vector	Dimension
$\mathbf{F_r}$	2×2
$\mathbf{F_c}$	4×2
$\mathbf{F_{str}}$	6×2
$\mathbf{T}$	12×6
$\mathbf{F}_\rho$	12×2
Δk	6×1

Table 2.10: Actual and calculated percentage change in stiffness for different elements in the framed structure.

	Percentage change	
Stiffness element	Actual	Calculated
k_1	0	-5.0709
k_2	0	-0.0149
k_3	-10	-5.0709
k_4	0	0.0000
k_5	0	-0.0149
k_6	0	0.0000

index values. These damage index values were then used in the iterative scheme to calculate the change in the element stiffness values of the six elements. Table 2.10 shows the final iteration results and Figure 2.18 shows the convergence of these results to their final values for increasing number of iterations.

From Table 2.10 we note that the calculated change in the element k_3 is 5.0709% and not 10%. However, the identification approach also shows a same amount of change in the stiffness of element k_1 as in k_3, with the total change in the story stiffness of 10.1418%. This value is very near the true damage of 10% in k_3. The change in the other four elements are correctly obtained near 0. These results, thus, indicate that this approach can not differentiate between the two columns, primarily because both columns contribute symmetrically to the total story stiffness. The response acceleration measurements made corresponding to the two degree of freedom of the condensed structure do not provide enough information to distinguish between the two symmetrically placed columns. Results leading to similar observation were also obtained when a damage was introduced in one of the members of the top story. In that case also, the algorithm was not able to isolate the damaged members but it distributed the damage into all connected members of the story.

The conclusion one can draw from these results is that the condensed model will not be able to isolate the damaged member. It will distribute the damage in all con-

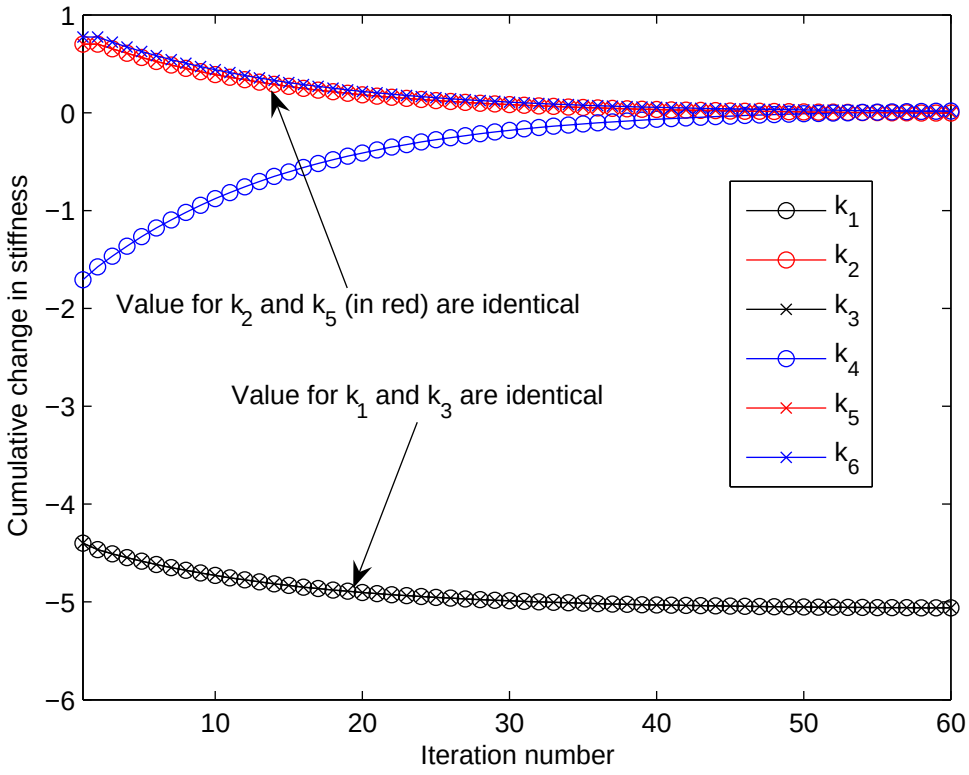

Figure 2.18: The estimated change in stiffness for the framed structure considered in the curvature flexibility approach.

nected members. To differentiate between damage in different elements, more damage specific measurements such as strains near joints on each element will be required. This situation was, however, not investigated in this study.

2.7 Conclusions

The focus of this chapter is on the use of the flexibility matrix in the identification of damage in civil engineering structures. The damage is characterized by reduction in the stiffness of structural elements. The flexibility matrix is defined in terms of the modal parameters which are assumed to have been extracted from the measured dynamic response such as accelerations. The concept of damage index matrix, defined as a difference of the damaged and undamaged flexibility matrices, is introduced. The

damage index matrix is related to the change in the stiffness of structural elements through the Taylor series expansion. For a known damage index matrix, an iterative scheme is described to solve this equation to calculate the stiffness changes. The proposed approach is then applied to the IASC-ASCE SHM problem, which was created by the joint Task force committee of the IASC and ASCE in 2004. Various cases representing modeling schemes, load application and symmetric and asymmetric structural configuration with different damage patterns are considered for damage quantification. The proposed approach is shown to work well in correct identification of all story damage patterns. The localization of the damage in braces on different faces, however, was not attempted because it was not possible to extract the torsional mode. Without this mode, it would not be possible to detect on which face of the structure the damage is confined. The impact of missing modes on the proposed damage identification scheme is also studied. It is in general observed that the missing modes can lead to errors in the estimated changes in stiffness. In some cases when the damage is small and the modes that contribute most to the flexibility of an element can not be identified, the damage detection may not be possible. The concept of displacement flexibility is also extended to define the curvature flexibility with the objective of better damage localization in the elements and joints connecting them. Then the damage can be detected and its general location can be identified, but for better localization in the elements near the joints, it is necessary to make measurement of other response quantities such as the strains that are related to damage near the joint.

Chapter 3

Detection of Sudden Changes in Stiffness Using High-Frequency Components

3.1 Introduction

In the previous chapter the problem of damage identification was addressed using flexibility approach. From the measured acceleration response the modal parameters were first extracted and then used to estimate the flexibility matrix, followed by the damage identification procedure. This was an off-line technique. For real time damage identification it is of interest to detect when certain structural parameters suffer a change in their values. The present chapter deals with the identification of the time at which a sudden change in stiffness occurs.

Several researchers have explored this issue of detection of sudden changes in stiffness. Some of the most common methods for detecting damage, and the discontinuities either in the time or spatial domains, have been the continuous and discrete wavelet transform-based methods (Carden and Fanning (2004), Kim and Melhem (2004), Taha *et al.* (2006), Wang and Deng (1999), Oxafor and Dutta (2000), Amaravadi *et al.* (2001), Hong *et al.* (2002), Sun and Chang (2002), Melhem and Kim (2003), Demetriou and Hou (2003), Chang and Chen (2003), Chang and Chen (2004), Sun and Chang

(2004), Zhong and Oyadiji (2007), Bayissa *et al.* (2008), Ren and Sun (2008), Hao *et al.* (2000), Robertson *et al.* (2003), Hera and Hou (2004), Peng *et al.* (2007), Zhu *et al.* (2008), Basu *et al.* (2008), Nagarajaiah and Basu (2009)) although there are also several researchers that have used the Hilbert-Huang Transform approach (Huang *et al.* (1998), Chen *et al.* (2007), Xu and Chen (2004), Yang *et al.* (2004)). Very good reviews of the application of the wavelet-based methods in structural health monitoring is provided by Carden and Fanning (2004), Kim and Melhem (2004), Taha *et al.* (2006), Nagarajaiah and Basu (2009). The specific applications to detect discontinuities in spatial domains such as along a beam or a plate are described in References: Wang and Deng (1999), Oxafor and Dutta (2000), Amaravadi *et al.* (2001), Hong *et al.* (2002), Sun and Chang (2002), Melhem and Kim (2003), Demetriou and Hou (2003), Chang and Chen (2003), Chang and Chen (2004), Sun and Chang (2004), Zhong and Oyadiji (2007), Bayissa *et al.* (2008), Ren and Sun (2008). The application for detecting discontinuities or track changes in time domain in References Hou *et al.* (2000), Robertson *et al.* (2003), Hera and Hou (2004), Peng *et al.* (2007), Zhu *et al.* (2008), Basu *et al.* (2008), Nagarajaiah and Basu (2009).

When making use of the discrete wavelet transform (DWT), singularities in the measured signal are indicated by the presence of significant non-zero value(s) or spikes (Zu *et al.* (2008), Kim and Melhem (2004)). The spikes in level-1 details of the discrete wavelet transform have been used to detect singularity in harmonically excited single-degree-of-freedom system by Hou and Noori (2000) and in multi-degree-of-system by Demetriou and Hou (2003). The approach was also applied to the ASCE benchmark structure (Johnson *et al.* (2004)) where the excitation was filtered white noise (Hera and Hou, (2004)). These studies have shown that the time at which the stiffness reduces suddenly is indicated by the spikes in the processed acceleration response. In addition, researchers (Hera and Hou, (2004), Hou *et al.* (2000)) have observed that the presence of noise makes it difficult to discern these spikes.

Although in many studies the spikes in the DWT details indicate the presence of discontinuities, what exactly constitutes a spike is not clearly understood. In this study, it is formally shown that a sudden change in stiffness introduces a jump discontinuity

in the response acceleration. In addition, a theoretical explanation is provided for why spikes noted in earlier studies occur and what exactly constitutes a spike. In particular, it is shown that a spike is the scaled step-response of a high-pass filter. Herein, the relationship of the spike and the high-pass filter helps in explaining the effect of measurement noise on the ability to detect sudden changes when we use a high-pass filter or the DWT.

This chapter is organized as follows. In Section 3.2 it is shown how an isolated singularity affects the high frequency components. This motivates the use of high-pass filters for singularity identification. In Section 3.3, we formally show that a sudden change in stiffness is associated with a jump singularity in the acceleration response. In Section 3.4, using the Gibb's phenomenon, an explanation is provided of what constitutes a spike. The effect of measurement noise on the identification of damage instant when using the high-pass filters is also explained. In Section 3.5, the numerical results demonstrating the application of high-pass filters in detecting damage instant are presented. First, a multi-story structure with sudden changes in story stiffness values while under base excitation is considered. This is followed by another numerical example, showing the use of a high-pass filter to detect a crack causing bilinear stiffness change in the system. Finally, the chapter summary and conclusions are presented in Section 3.6.

3.2 Isolated Singularities and High-Frequency Content

In this section, for illustration a sine wave with an isolated singularity is considered. It is shown that the isolated singularity affects the Fourier spectrum and that the high-frequency content can be used to identify the location of this singularity.

Consider a signal $x_1[t]$ given by,

$$x_1[t] = sin(2\pi t), \quad t = k\Delta t$$

This signal represents the sampled version of a sinusoidal function of frequency 1 Hz.

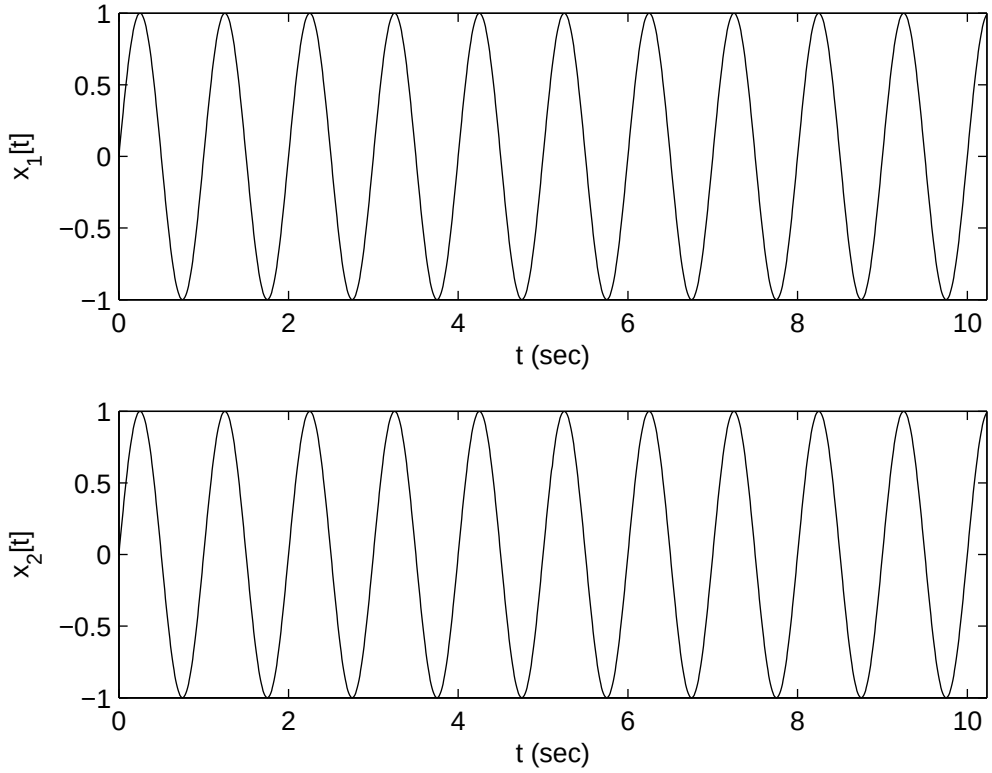

Figure 3.1: Plot of the sinusoidal function without (top, $x_1[t]$) and with (bottom), $x_2[t]$ the singularity. The identification of the singularity simply based on the comparison of the time domain plots is hard.

The sampling time step is Δt and $k = 0, 1, \ldots N-1$, where N is the length of the discrete signal. Another signal $x_2[t]$ is defined as

$$x_2[t] = x_1[t] + e[t]$$

where $e[t]$ is zero everywhere except at $t = k_0\Delta t$ where it is set equal to -0.02. Thus $x_1[t]$ represents the sampled version of a smooth signal and $x_2[t]$ the same smooth signal but with an isolated singularity at $k = k_0$. The values of the parameters used in the simulation were, $\Delta t = 0.01$, $N = 1024$, and $k_0 = 512$.

In Figure 3.1 the plots of the two signals are shown. Based on these plots it is hard to identify the location of the change in $x_2[t]$. In a practical situation, such visual

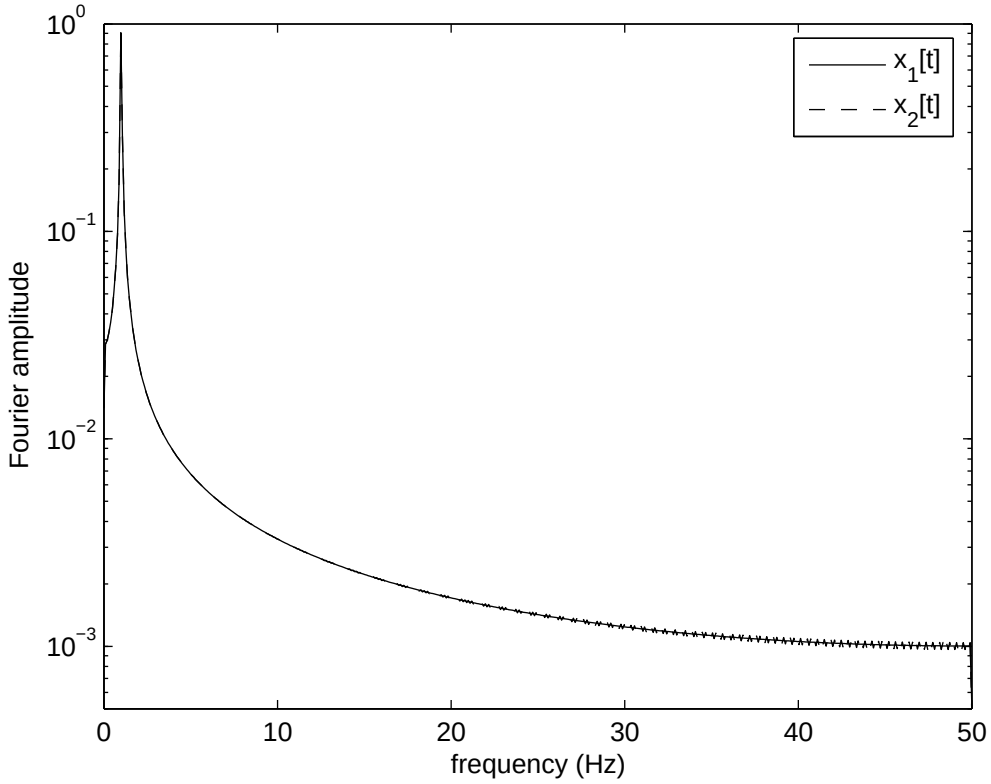

Figure 3.2: The Fourier amplitude (absolute value) spectrum of $x_1[t]$ and $x_2[t]$.

identification will be much harder when the signal being studied would be far from a single smooth sinusoidal function and most likely corrupted with noise.

Figure 3.2 shows the Fourier amplitude spectrums of the two signals. In the low-frequency range the spectrums are similar and the difference is hard to observe. However, since $x_1[t]$ has no singularity its spectrum is expected to decay smoothly at higher frequencies. In comparison a smooth decay is not expected in the spectrum of $x_2[t]$. This is based on the fact that the overall regularity of a signal affects the decay of the Fourier coefficients at higher frequencies. A zoomed-in portion of the two spectrums at higher frequencies is shown in Figure 3.3. It can be seen that the two spectra differ and, indeed, the spectrum of $x_2[t]$ does not decay smoothly. This leads to the idea that since the singularity introduces a difference which is prominent in the high-frequency range, it might be possible to identify the singularity by reconstructing $x_2[t]$ using just

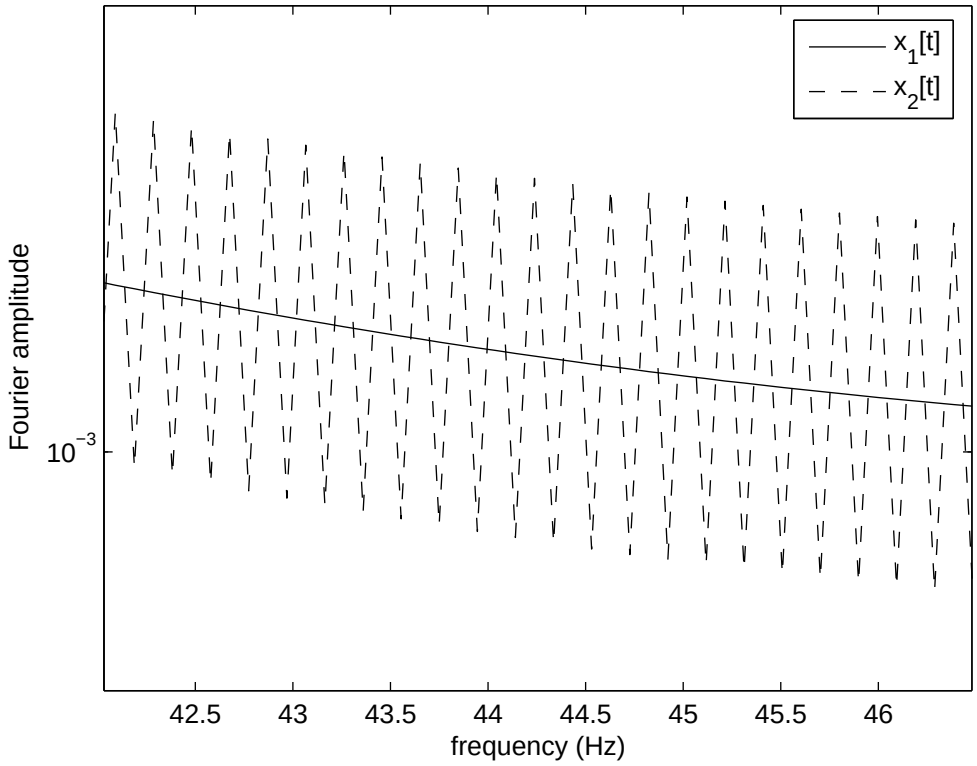

Figure 3.3: Zoomed-in view of the spectrum of $x_1[t]$ and $x_2[t]$.

the high-frequency components.

Towards this end, the signal $x_2[t]$ was passed through a high-pass filter with a cut-off frequency of 20 Hz. The output of the filter is shown in Figure 3.4. It can be seen that the location of the singularity can, indeed, be identified by the significant non-zero values in the middle of the plot. The non-zero values at the very beginning of the plot can be ignored because they are caused by the end effects. This example motives the use of high-pass filters for the identification of singularities. Note that the high-pass filter was designed and used without any reference to the multi-resolution analysis as is done in wavelet analysis. Thus for damage detection purposes it might be possible to identify the damage instance by simply analyzing the high-frequency content of the acceleration response.

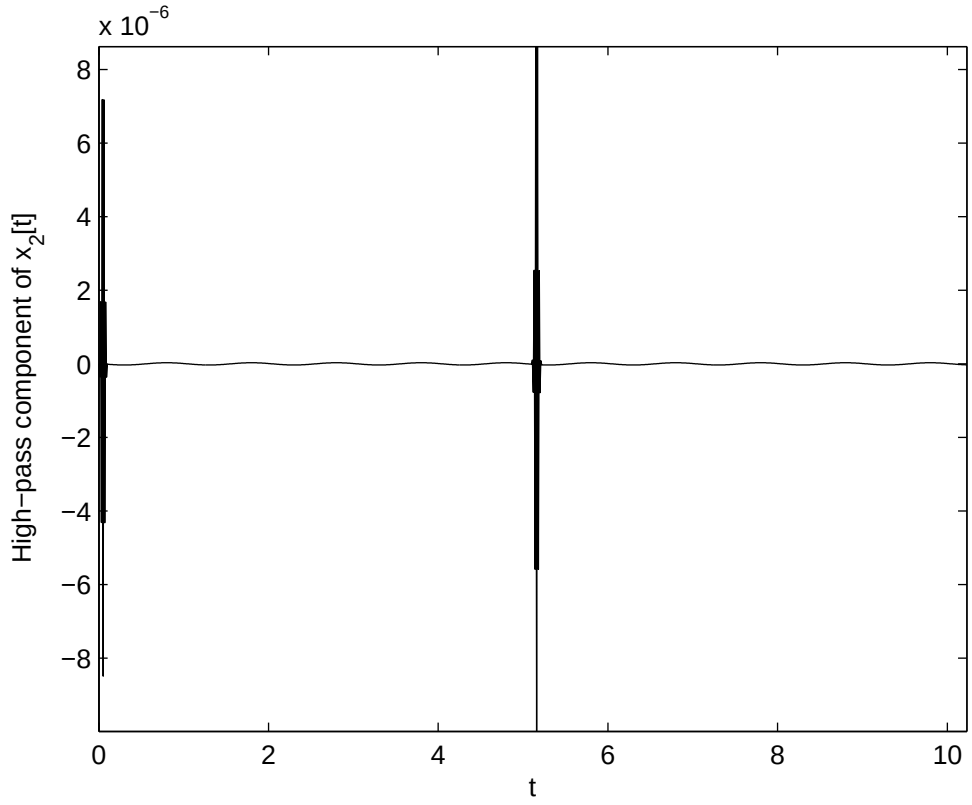

Figure 3.4: Output obtained by passing $x_2[t]$ through a high pass filter. The presence of the singularity is indicated by the spike near $t = 5$.

3.3 Sudden Change in Stiffness and Singularity

Herein we formally show that a sudden change in structural stiffness introduces a jump discontinuity in the response acceleration. The equation of motion for a N degree-of-freedom (DOF) system can be written as,

$$\mathbf{M}\ddot{x}(t) + \mathbf{E}\dot{x}(t) + \mathbf{K}x(t) = f(t) \tag{3.1}$$

where $\mathbf{M}$, $\mathbf{E}$, and $\mathbf{K}$, respectively, are the $N \times N$ mass, damping, and stiffness matrices; $\ddot{x}(t)$, $\dot{x}(t)$ and $x(t)$ are the $N \times 1$ acceleration, velocity, and displacement vectors respectively; and $f(t)$ is the $N \times 1$ input excitation vector. By defining the state vector as

$$q(t) = \left\{ \begin{array}{c} x(t) \\ \dot{x}(t) \end{array} \right\} \tag{3.2}$$

the equations of motion, Eq. 3.1, can be expressed in the standard state-space form as,

$$\dot{q}(t) = \mathbf{A}q(t) + \mathbf{B}f(t) \tag{3.3}$$

where

$$\mathbf{A} = \left[\begin{array}{cc} \mathbf{0} & \mathbf{I} \\ -\mathbf{M^{-1}K} & -\mathbf{M^{-1}E} \end{array} \right] \qquad \mathbf{B} = \left[\begin{array}{c} \mathbf{0} \\ \mathbf{M^{-1}} \end{array} \right] \tag{3.4}$$

The size of the matrices $\mathbf{A}$ and $\mathbf{B}$ are $2N \times 2N$ and $2N \times N$ respectively and $\mathbf{0}$ and $\mathbf{I}$ are the null and identity matrices of appropriate dimensions. The measurement equation associated with this state-space model can be written as,

$$y(t) = \mathbf{C}q(t) + \mathbf{D}f(t) \tag{3.5}$$

where $y(t)$ is the vector of measured quantities, and $\mathbf{C}$ and $\mathbf{D}$ are the matrices that describe the vector $y(t)$. For the case of acceleration response measurements, the matrices $\mathbf{C}$ and $\mathbf{D}$ are given by,

$$\mathbf{C} = \left[\begin{array}{cc} -\mathbf{M^{-1}K} & -\mathbf{M^{-1}E} \end{array} \right] \qquad \mathbf{D} = \mathbf{M^{-1}} \tag{3.6}$$

For earthquake induced base excitation and absolute acceleration measurements, the input vector $f(t) = -\mathbf{M}\gamma\ddot{x_g}(t)$, where $\ddot{x_g}(t)$ is the base acceleration, γ is the ground displacement influence vector of length N with all its entries equal to 1 in the direction

of ground motion and zero otherwise, and the matrix $\mathbf{D} = \mathbf{0}$. The solution for the state vector for a given initial state $q(t_0)$ $(t_0 < t)$ can be written as,

$$q(t) = e^{\mathbf{A}(t-t_0)}q(t_0) + \int_{t_0}^{t} e^{\mathbf{A}(t-\tau)}\mathbf{B}f(\tau)d\tau \tag{3.7}$$

Now consider a case where the system experiences a sudden change in stiffness matrix at time $t = t_0$. Due to this change, let the matrix $\mathbf{A}$ change to $\mathbf{A_1}$. The state vector at $t = t_0 + \epsilon$ $(\epsilon > 0)$ can then be expressed as,

$$q(t_0 + \epsilon) = e^{\mathbf{A_1}(t_0+\epsilon-t_0)}q(t_0) + \int_{t_0}^{t_0+\epsilon} e^{\mathbf{A_1}(t_0+\epsilon-\tau)}\mathbf{B}f(\tau)d\tau \tag{3.8}$$

In the limit as $\epsilon \to 0$,

$$\lim_{\epsilon \to 0} q(t_0 + \epsilon) = q(t_0) \tag{3.9}$$

Thus a sudden change in stiffness matrix does not change the state vector. However, due to a change in stiffness matrix, matrix $\mathbf{C}$ in Eq. 3.5 changes, thus leading to a change in the response acceleration. Denoting this change by Δy, we have

$$\Delta y = \Delta \mathbf{C} q(t_0) \tag{3.10}$$

where $\Delta\mathbf{C}$ is the change in the matrix $\mathbf{C}$. For the case when only the stiffness matrix changes, we have,

$$\Delta y = \begin{bmatrix} -\mathbf{M^{-1}}\Delta\mathbf{K} & \mathbf{0} \end{bmatrix} q(t_0) = -\mathbf{M^{-1}}\Delta\mathbf{K}x(t_0) \tag{3.11}$$

where $\Delta\mathbf{K}$ is the change in the stiffness matrix. Therefore, a sudden change in stiffness introduces a jump discontinuity in the acceleration response. The magnitude of this jump discontinuity is proportional to the change in stiffness. We observe that, in principle, one may not get a jump discontinuity in acceleration even if a sudden change in the stiffness occurs. This can occur if the displacement vector $x(t_0)$ happens to be zero. However, this is not likely to be a common case as in a practical situation a sudden loss in stiffness in a structural element will typically occur when displacement or deformation value is large and not zero.

3.4 Singularity Identification Using High-Pass Filters

The previous discussion shows that a sudden change in stiffness introduces a jump discontinuity in the response acceleration. From the perspective of structural health monitoring (SHM), the problem then is to identify the occurrence, location, and magnitude of this singularity in the response acceleration. Using the concept of Gibbs phenomenon, here an explanation is provided as to why one observes spikes in the high-frequency content of signals containing singularities. Based on this, the use of the high-pass filters in singularity detection is suggested.

The Gibbs phenomenon is well-known in Fourier series analysis literature where it is commonly discussed from the point of view of the convergence of a Fourier series. Although the analytical treatment of Gibbs phenomenon can be found in the texts on Fourier analysis, in the context of this study, the Gibbs phenomenon is briefly described to highlight the importance of high-frequency content in the identification of singularities. This helps in explaining what exactly the "spikes" are in the plots of the high-frequency content, how they help in singularity identification using high-pass filters, and when can they be identified. Later its application to identify anomalies in discrete data is suggested.

3.4.1 Gibbs Phenomenon and High-Pass Filters

Consider a function $f(t)$ which has an isolated jump discontinuity at $t = t_0$. This function can be expressed as

$$f(t) = f_c(t) + \alpha \mathcal{U}(t - t_0) \tag{3.12}$$

where $f_c(t)$ is an appropriately defined function which is continuous in the neighborhood of t_0. α is the size of the jump discontinuity and $\mathcal{U}(s)$ is the Heaviside or unit-step function given by

$$\mathcal{U}(s) = \begin{cases} 1 & s \geq 0 \\ 0 & \text{otherwise} \end{cases} \tag{3.13}$$

Let $h_{\omega_0}(t)$ and $l_{\omega_0}(t)$ be the impulse responses of ideal high-pass, $H(\omega)$, and low-pass, $L(\omega)$, filters with their respective frequency response functions defined as follows,

$$H(\omega) = \begin{cases} 0 & |\omega| \leq \omega_0 \\ 1 & \text{otherwise} \end{cases} \quad L(\omega) = \begin{cases} 1 & |\omega| \leq \omega_0 \\ 0 & \text{otherwise} \end{cases} \tag{3.14}$$

where ω_0 is the cut-off frequency. Consider a function $g(t)$ obtained by convolving the function $f(t)$ with $h_{\omega_0}(t)$ as follows,

$$g(t) = f(t) \star h_{\omega_0}(t) \tag{3.15}$$

where the convolution operation is denoted by $\star$. Substituting for $f(t)$ from Eq. 3.12 we obtain,

$$g(t) = [f_c(t) + \alpha \mathcal{U}(t - t_0)] \star h_{\omega_0}(t) = f_c(t) \star h_{\omega_0}(t) + \alpha \mathcal{U}(t - t_0) \star h_{\omega_0}(t) \tag{3.16}$$

Since $f_c(t)$ is a continuous function and $h_{\omega_0}(t)$ and $l_{\omega_0}(t)$ are ideal filters, we can write the first term in the above equation as,

$$f_c(t) \star h_{\omega_0}(t) = f_c(t) - f_c(t) \star l_{\omega_0}(t) = p(t) \tag{3.17}$$

Denoting the second term in Eq. 3.16 as $I(t) = \alpha \mathcal{U}(t - t_0) \star h_{\omega_0}(t)$, we can re-write this equation as,

$$g(t) = p(t) + I(t) \tag{3.18}$$

Consider the behavior of $g(t)$ as ω_0 is increased and in the limit $\omega_0 \to \infty$. As ω_0 increases, the first term $p(t)$ in Eq. 3.18 goes to zero because $f_c(t) \star l_{\omega_0}(t)$ converges to $f_c(t)$ uniformly. The second term, however, does not go to zero. Using the expression for the step response of an ideal high-pass filter (Papoulis (1962)), and for convenience assuming $t_0 = 0$, this term can be written as

$$I(t) = \alpha \mathcal{U}(t - t_0) \star h_{\omega_0}(t) = \alpha \left\{ \mathcal{U}(t) - \frac{1}{2} \left\{ 1 + \frac{2}{\pi} \int_0^{\omega_0 t} \frac{sin(x)}{x} dx \right\} \right\} \tag{3.19}$$

The sine integral in Eq. 3.19,

$$Si(\omega_0 t) = \int_0^{\omega_0 t} \frac{sin(x)}{x} dx \tag{3.20}$$

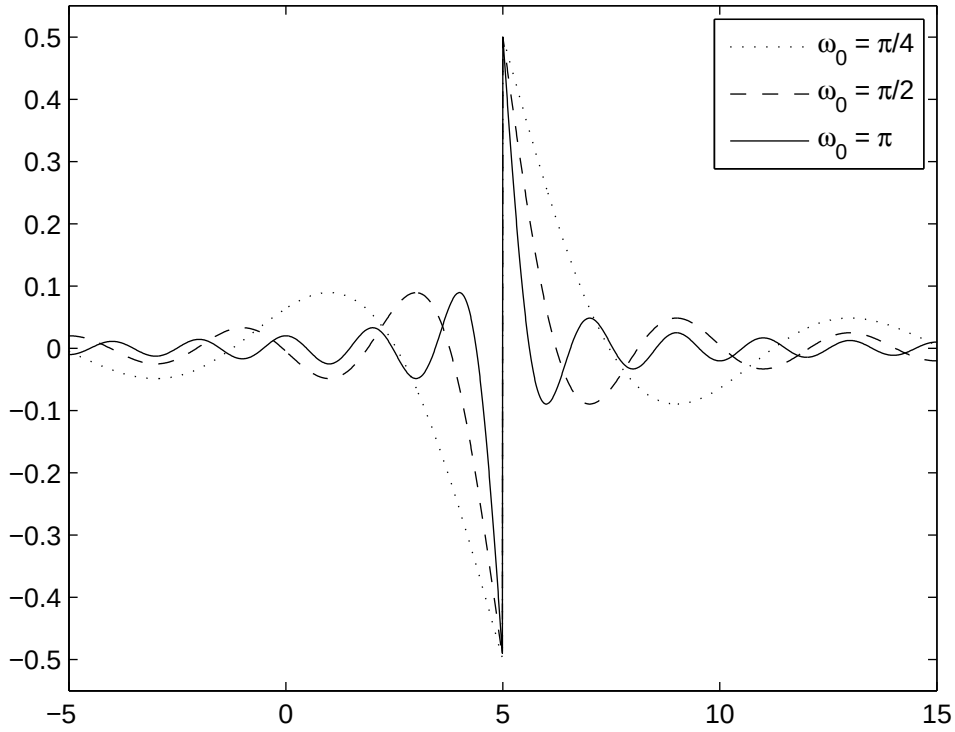

Figure 3.5: Unit-step response for an ideal high-pass filter with $\omega_0 = \pi/4, \pi/2$ and $\pi/1.1$ and $t_0 = 5$.

reaches its maximum and minimum value of ± 1.8519 at $\omega_0 t = \pm\pi$. Using these values in Eq. 3.19 the maximum and minimum values of $I(t)$, or the Gibbs oscillations, turn out to be $\pm 0.0895\alpha$. Therefore due to the presence of the singularity, as ω_0 is increased, $g(t)$ or the high-frequency content of $f(t)$ does not go to zero; it, rather, shows up as the Gibbs phenomenon in the neighborhood of t_0 with an amplitude which is independent of ω_0 and which is proportional to the size of the jump discontinuity. This function $I(t)$ for $\alpha = 1$ and for three different values of ω_0, ($\pi/4, \pi/2$ and π) is plotted in Figure 3.5 for $t_0 = 5$. We note that unit-step response exhibits oscillatory behavior near $t_0 = 5$. With an increase in the value of ω_0 the oscillations die off faster; however, their peak value always remains the same at ± 0.0895.

The spikes described above only occur when there are discontinuities. Also, the size

of these spikes is directly proportional to the size of the jump discontinuities. Therefore, one can identify the presence of singularities by analyzing the high-frequency content of a signal.

Based on Eq. 3.18, in general, three situations can occur depending on the relative magnitude of $p(t)$ with respect to $I(t)$. In the first situation, $p(t) \approx 0$. In this case, the low frequency components of the signal can be filtered out by high-pass filtering and what remains is then the contribution of the singularity. In the second situation, $p(t) << I(t)$. This would correspond to a situation where the function $f(t)$, besides the singularity, may also consist of high frequency components. However these high-frequency components are not strong enough to completely mask the step response of the high-pass filter due to the singularity. Thus, the singularity can still be identified. In the third case, $p(t) \approx I(t)$ or $p(t) > I(t)$. This will correspond to a situation where the signal itself has strong enough high frequency components. In such a situation, one can not identify the singularity.

3.4.2 Discrete-Time Case

The Gibb's phenomenon is not observed in the discrete-time case simply because a discrete-time signal $f[n]$, $n = k\Delta t$, $k = 0, 1 \ldots N-1$ (Δt is the sampling time-step) of size N can be perfectly reconstructed as long as all N Fourier coefficients are utilized. This is in contrast to the continuous-time case where N is infinite. However, based on the conclusions outlined in the last paragraph of the previous subsection a method for identification of singularities in the response acceleration using its sampled version can still be developed.

Let $f[n]$ denote the sampled version of the response acceleration. Assume that the energy of $f[n]$ lies mainly in the frequency range $0 - f_{signal}$. Now let a sudden reduction in stiffness occur at $t = t_0$, which induces a jump discontinuity of magnitude α in the acceleration response. This α is defined by Eq. 3.11. In the sampled version this might correspond to say $k = k_0$ or lie between $k = k_0 - 1$ and $k = k_0$. To detect this singularity, the sampling needs to be fast enough. Let f_N and f_s denote the Nyquist and sampling frequencies ($f_N = f_s/2 = 1/(2\Delta t)$). If the Nyquist frequency is significantly

larger than the signal frequency and if we pass the sampled function $f[n]$ through a high-pass filter with the cut-off frequency higher than f_{signal}, then the output $f_h[n]$ would essentially be the scaled unit-step response of the high-pass filter shifted by k_0.

It is mentioned here that in a digitally designed high-pass filter there will be a small shift in the spike location from the time instant at which the discontinuity occurs. This is shown by an example of a high-pass digital filter of length 11 in Figure 3.6. This filter has been used in calculations later. The first part of the figure shows the magnitude of the frequency response of the filter where the frequencies below 150 Hz are suppressed. The next sub-figure shows the unit-step response function for this filter. We note that the maximum absolute value of the step-response first occurs at the 5^{th} sampled point. Thus, if this filter is used the spike location will be shifted by 5 sampled points; that is, a sudden change in the stiffness occurring at time step $k = k_0$ will appear as a spike on the $k = k_0 + 5$ time step in the filtered function.

The observations made earlier about the conditions for the detectability of the spike for the continuous function also hold in the present discrete-time case. Depending upon the frequency content of the signal and the characteristics of the noise in the acceleration measurement, the following three singularity detection scenarios can arise.

1. If $f_{signal} << f_N$ and the signal is noise free then the singularity can be identified using an appropriate cut-off frequency f_0 for the high-pass filter. As f_{signal} approaches f_N the identification will become difficult because the underlying signal (besides the singularity) will also start to contribute to the filtered output.

2. If the signal consists of measurement noise with frequency spectrum spreading over the frequency range of $0 - f_{noise}$ and if $f_{noise} << f_N$ then the singularity can be identified even for large noise levels by an appropriate selection of f_0.

3. If the signal consists of measurement noise such that its frequency spectrum spreads over the entire frequency range that is between $0 - f_N$, and if the noise level is low enough not to mask the step-response of the high-pass filter, the singularity can be identified. In this case, the term $p(t)$ in Eq. 3.18 is much smaller than the term $I(t)$. As is shown later by the numerical example, the

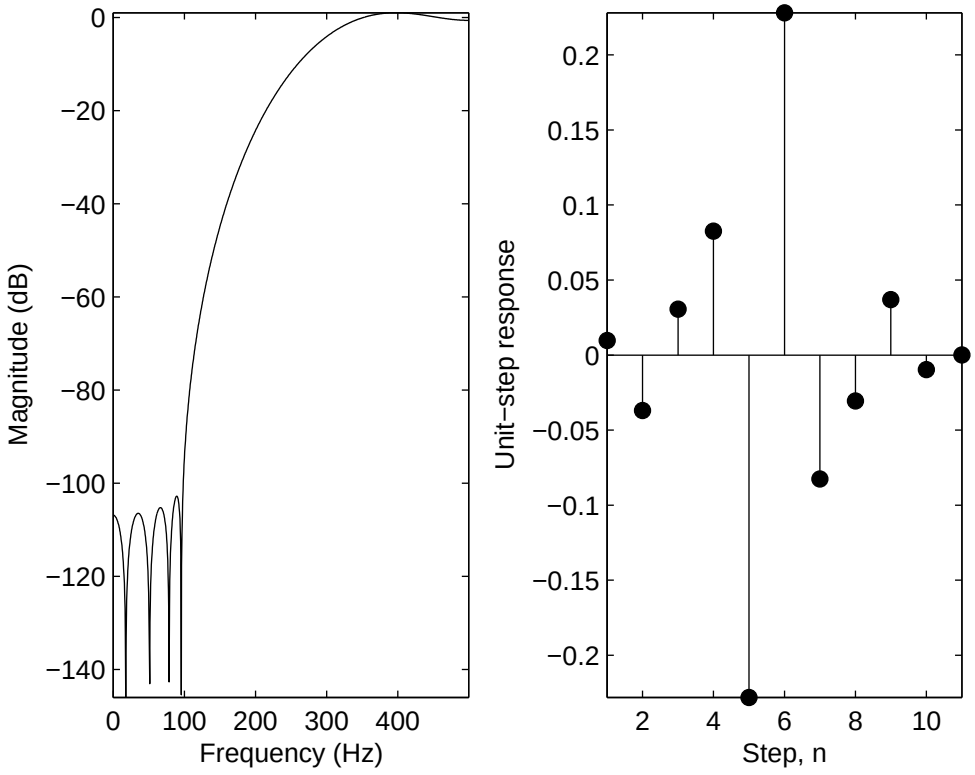

Figure 3.6: The high-pass filter characteristics - magnitude of the frequency response and unit-step response

Table 3.1: Mass and stiffness properties for the 6-DOF shear beam model

DOF	Mass (kg $\times 10^4$)	Stiffness (N/m $\times 10^7$)
1	4.8	8.34
2	4.8	8.34
3	4.32	5.34
4	4.32	5.34
5	3.84	3.34
6	3.84	3.34

noise level for which singularity identification is possible can be rather low.

3.5 Numerical Results

Numerical studies have been carried out to illustrate the use of high-pass filters for damage identification and to study the effect of measurement noise. Two systems were considered. First, a multi-degree-of-freedom (MDOF) system which suffers a sudden reduction in stiffness when under base excitation. The second example considers a single-degree-of-freedom (SDOF) system with bilinear stiffness excited by a sinusoidal input.

3.5.1 6-Degrees-of-Freedom System

A 6-degrees-of-freedom (DOF) shear beam model is considered. The mass and stiffness properties for this model are given in Table 3.1. The undamped natural frequencies of the structure are 1.5119 Hz, 3.8036 Hz, 6.0855 Hz, 7.6825 Hz, 9.6063 Hz and 11.487 Hz. To construct the damping matrix, a 2% damping is assumed for all the modes. First the results for two cases of damage at multiple locations are shown. Later, using a single damage scenario the effect of measurement noise on the damage identification procedure is illustrated.

The base excitation used in the simulations is shown in Figure 3.7. A sampling frequency of 1000 Hz is used. The absolute acceleration response calculated at different

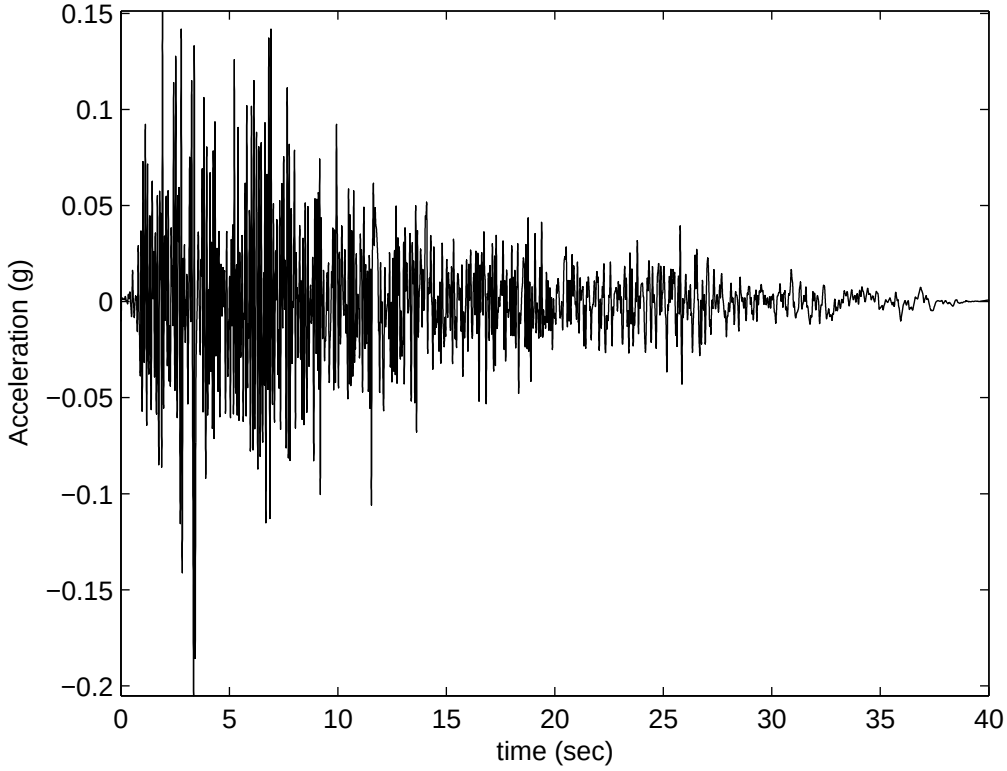

Figure 3.7: Base excitation used in the 6-DOF example.

DOF's are treated as the measured data for damage identification. To extract the high-frequency content of these responses, they are passed through a high-pass filter. Figure 3.6 shows the magnitude of the frequency response, and the unit-step response of the filter used in this study.

Figure 3.8 shows the displacement and acceleration responses at the first and second floors for the case when the stiffness in stories 1 and 2 are reduced by 2% and 1%, respectively, at 5 seconds. In Figure 3.9 the filtered accelerations at different floors are plotted for this case. The clear spikes in the filtered accelerations of the first and second floors which are affected by these changes in the stiffness value, indicate the damage instant. There are also indiscernibly small spikes in the filtered accelerations at other floors (especially floor 3) as the accelerations calculated by time-stepping procedures at adjacent degrees of freedom are also affected by the changes in stiffness in story 1

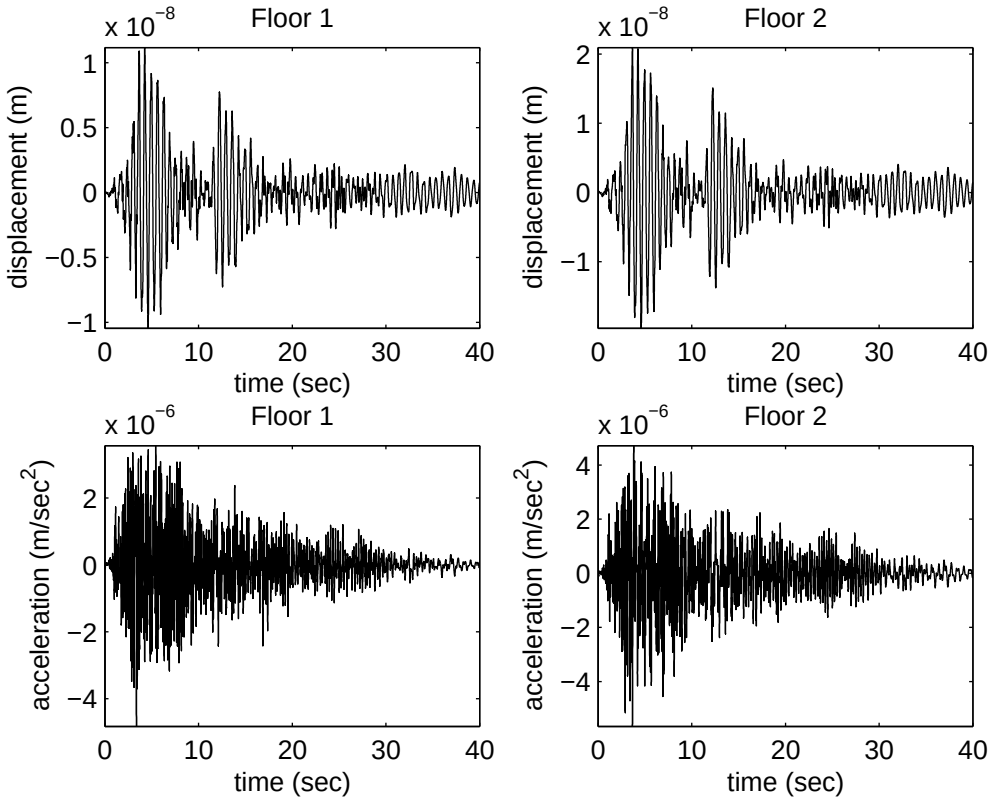

Figure 3.8: Displacement and acceleration response at floor 1 and 2 for the case when stories 1 and 2, respectively, suffer a 2% and 1% reduction in stiffness at 5 seconds.

and 2. However, the accelerations at the degrees of freedom further removed from the damaged structural element are affected much less. This helps in locating the damaged structural element in a shear building model easily.

The ability of the proposed method being able to detect damage occurrences at multiple time instants is shown by the next set of results. In Figure 3.10 are plotted the filtered outputs for the case when the stiffness in story 1 and story 6 are reduced by 2% at 5 seconds and 10 seconds, respectively. The spikes in the plots of the filtered acceleration responses of floors 1 and 6 clearly identify the damage instants. A spike is also seen in the plot for floor 5 as the acceleration at this floor is also affected by the change in the stiffness of the 6^{th} story. The absence of a spike in the filtered acceleration of floor 4 clearly eliminates the possibility of damage in story 5.

To study the affect of measurement noise, four different cases are considered. Case 1 involves no additive noise, thus the simulated accelerations represent the available data. In Case 2, some band-limited white noise with energy distributed within the frequency range of 0-50 Hz is added to the simulated responses as the measurement error. Case 3 and Case 4 involve the addition of noise with its energy spreading over the complete spectrum, i.e., 0-500 Hz. The difference in these two last cases is that the noise level in Case 3 is much smaller than the noise level in Case 4. Figure 3.11 shows the spectrum of the added noise for the last three cases. The level of noise in these cases is listed in Table 3.2 where % σ is defined as the ratio of the standard deviation of the added noise to the standard deviation of the acceleration response. These cases are created to demonstrate the three detection scenarios enumerated in the last part of Section 4.

The noise-free (Case 1) and noise contaminated (Cases 2, 3, and 4) acceleration responses are treated as the measured acceleration data. For damage identification they are passed through a high-pass filter. Damage in all these 4 cases is introduced at 4.252 seconds by reducing stiffness of the first story by 2%. At this particular time the acceleration response of the undamaged structure was high, thus detecting such a small change in acceleration could be challenging, at least to the naked eye.

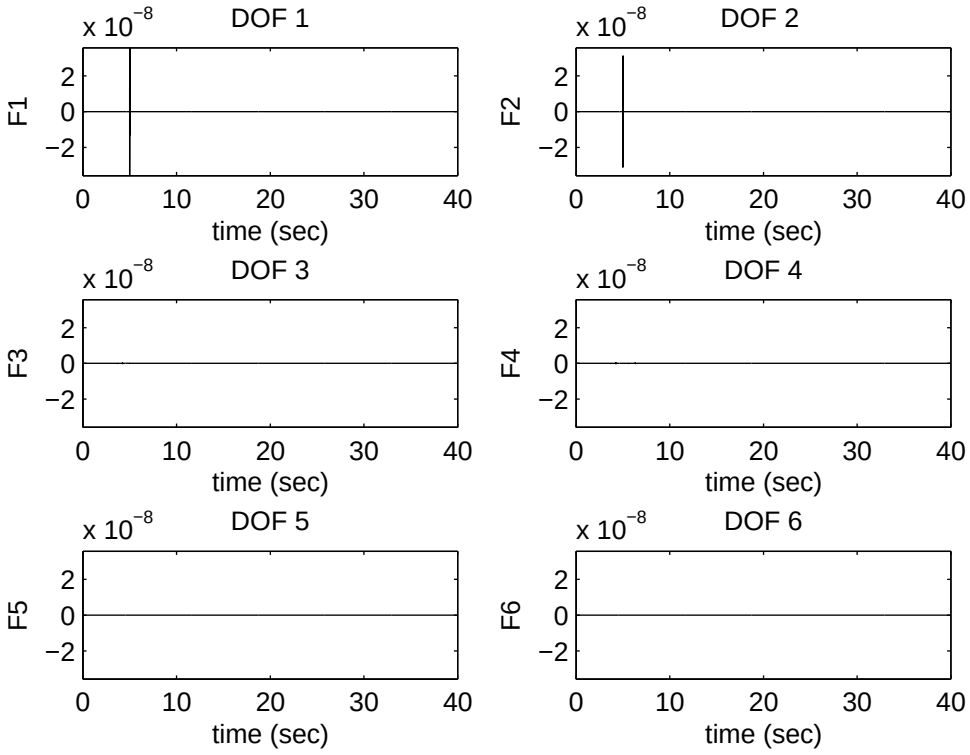

Figure 3.9: Filter outputs F1 to F6 at various degrees of freedom for the case when stories 1 and 2, respectively, suffer a 2% and 1% reduction in stiffness at 5 seconds. Fi (i= $1 \ldots 6$) is used to denote the filter output for the i^{th} DOF.

Table 3.2: Cases studied for the 6-DOF example. Noise type is "F" for filtered noise and "UF" for unfiltered noise.

Case	Noise added	Noise type	% σ
1	None	-	-
2	Yes	F	20.07
3	Yes	UF	1.25
4	Yes	UF	4.96

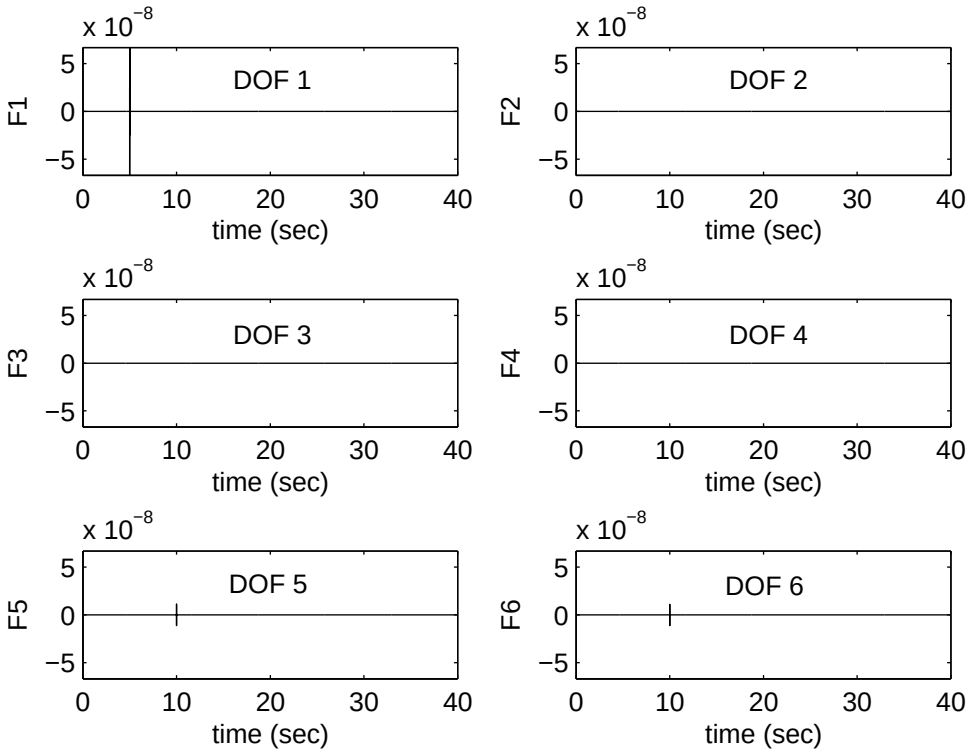

Figure 3.10: Filter outputs F1 to F6 at various degrees of freedom when the stiffness in story 1 is reduced by 2% at 5 seconds and the stiffness in story 6 is reduced by 2% at 10 seconds. Fi (i= $1 \ldots 6$) is used to denote the filter output for the i^{th} DOF.

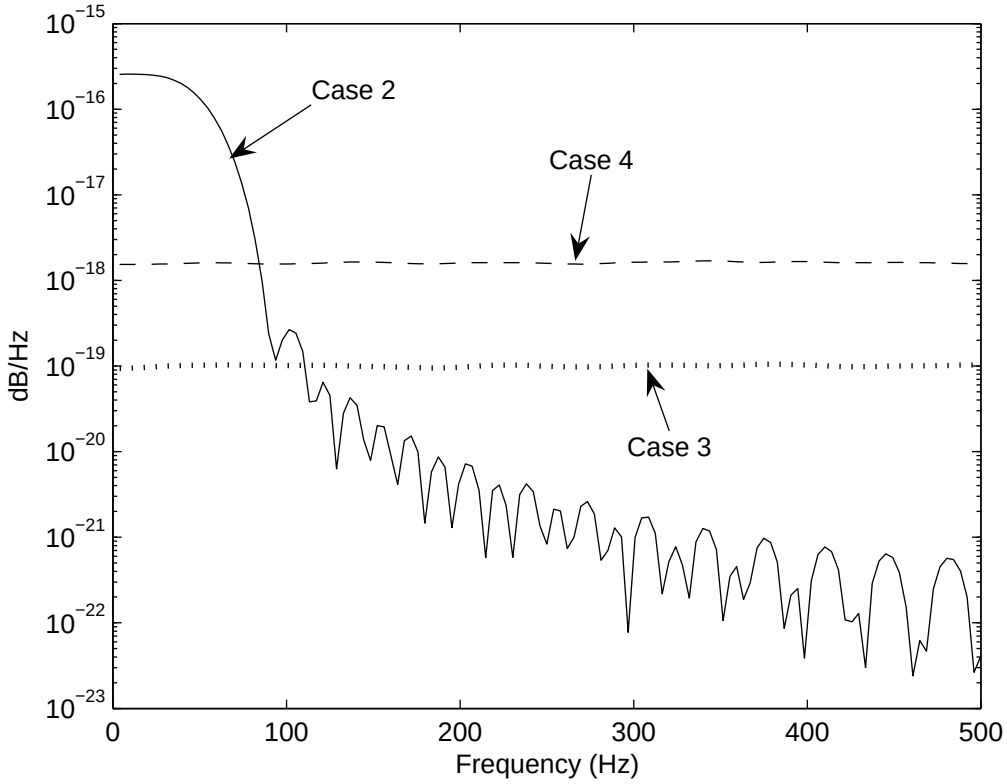

Figure 3.11: Noise spectrum for Cases 2, 3 and 4.

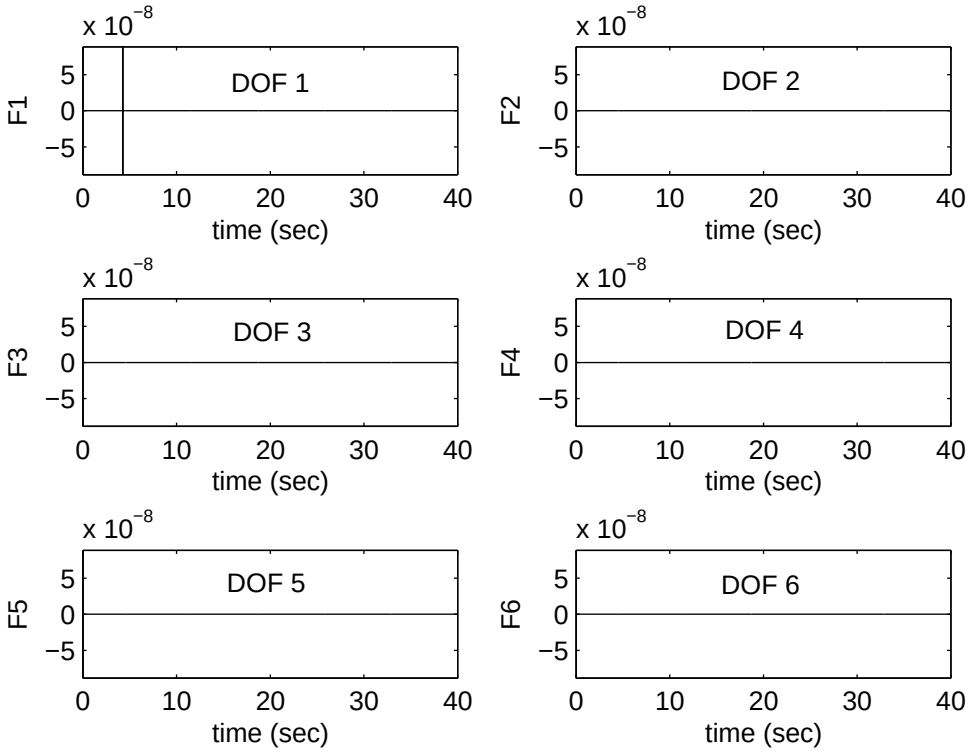

Figure 3.12: Filter outputs F1 to F6 for Case 1 - noise free data: Story 1 stiffness reduced by 2%. Fi (i= 1 . . . 6) is used to denote the filter output for the i^{th} DOF.

For Case 1, where the acceleration data at different floors is noise free, Figure 3.12 shows the filtered outputs for the six absolute acceleration responses. The spike appearing in the output corresponding to the degree of freedom 1 clearly identifies the damage instant.

Next we show the results for the noise contaminated acceleration responses. The filtered outputs are shown for the three cases in Figure 3.13. The results are only shown for DOF 1 as this degree of freedom is affected by the stiffness change in story 1. A clear identification of the spike is possible in Case 2 even though the level of measurement noise is unusually high (20.07%). It is primarily because this noise as well as the signal can be easily filtered out by the high-pass filter used, and the remain-

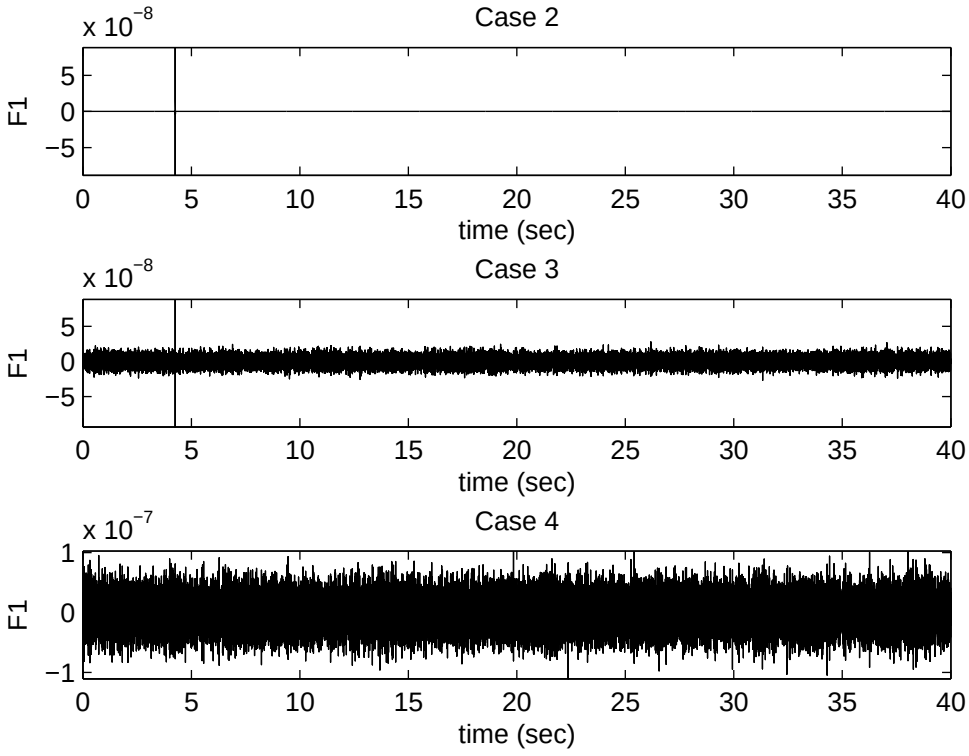

Figure 3.13: Filter outputs for response at DOF 1 Cases 2, 3 and 4 - Noise contaminated acceleration: Story 1 stiffness reduced by 2%. F1 is used to represent the filter output for the 1^{st} DOF.

ing output just shows spike reflecting the high frequency content introduced by the sudden stiffness/acceleration change. This case corresponds to situation 2 mentioned in the previous section. We can also identify the presence of spike in Case 3, as seen from Figure 3.13. In this case, although the added noise spectrum spreads over the entire frequency range and, thus, the filter output will contain contribution from the measurement noise, the noise level being relatively small (1.25%) does not mask the step-response caused by the sudden change. This case corresponds to the situation 3 mentioned in the previous section. Finally in Case 4, in addition to the noise spectrum spreading over the entire range the level of noise is also high (4.96%). In this case the noise contribution to the filter output is large enough to mask the step-response of the filter caused due to the jump discontinuity.

Thus a contaminated data with high-level noise containing high frequencies comparable to the Nyquist frequency can cause problem in the identification of the instant of damage of very small level. Equation 3.11 relates the magnitude of sudden change in the acceleration caused by a change ΔK in the stiffness matrix. It is the magnitude of this change in the acceleration that can be easily masked by the measurement error if this error is distributed over high frequencies as well.

Although the quantification of the damage level is not addressed in this paper, Eq. 3.11 can help in this regard. Knowing the size of the spike, one can estimate the level of change in acceleration with the help of Eq. 3.11 which states that the magnitude of spike is directly proportional to the magnitude of the jump in the acceleration. This defines the left hand side of Eq. 3.11 which, in principle, can be solved to calculate ΔK. There are, however, serious difficulties in doing this as calculating the displacement vector needed in Eq. 3.11 from measured acceleration responses is not error free because of serious drift caused by numerical integration.

3.5.2 SDOF with Bilinear Stiffness

An example of a nonlinear system simulating the opening and closing of a gap in a cracked beam or shaft is considered next. To simulate this in a simple manner, a single degree of freedom system with bi-linear stiffness values for opened and closed crack

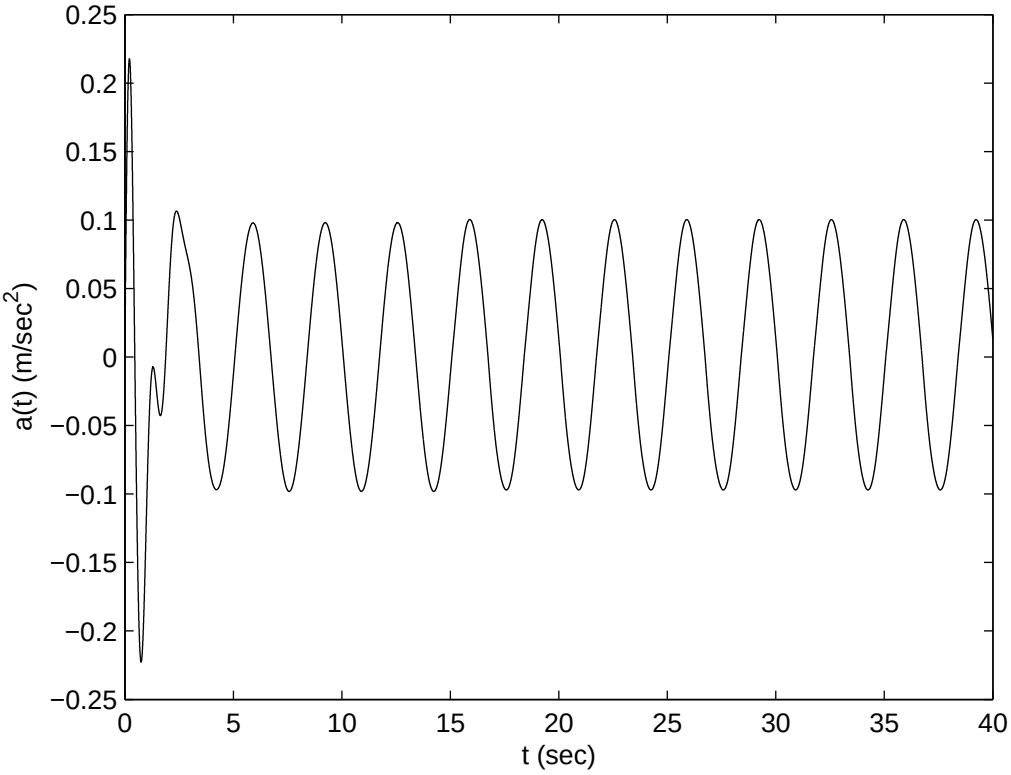

Figure 3.14: Time history of the simulated acceleration for the SDOF bilinear system.

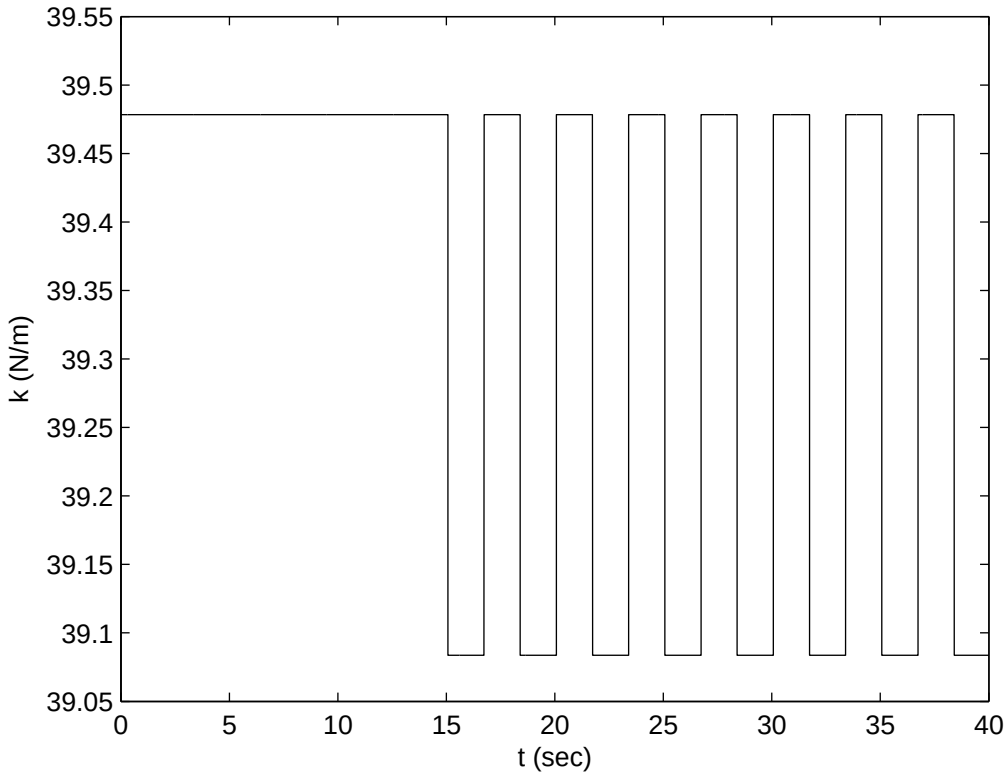

Figure 3.15: Value of stiffness parameter for the SDOF bilinear system. For clarity the plot is shown only for the duration 14 to 24 seconds.

conditions is considered. The system is represented by the following equation:

$$ma(t) + cv(t) + kd(t) = u(t) \tag{3.21}$$

where $a(t)$, $v(t)$, and $d(t)$ are the acceleration velocity and displacement of the mass, respectively. m, c, and k are the mass, damping coefficient and stiffness, respectively. $u(t)$ is the input force. The stiffness coefficient representing the open and closed crack conditions is defined as:

$$k = k(t, d(t)) = \begin{cases} 4\pi^2 & t < 15 \\ 0.99 \times 4\pi^2 & t > 15 \text{ and } d(t) \leq 0 \\ 4\pi^2 & t > 15 \text{ and } d(t) > 0 \end{cases} \tag{3.22}$$

For numerical simulation, using a time step of 0.001, the acceleration response of the mass for $m = 1$, and $c = 2(0.2)(2\pi)$ was calculated for a sinusoidal input $u(t) = sin(0.6\pi t)$ of frequency 0.3 Hz. The MATLAB[1] function *ode45* which implements the Runge-Kutta based numerical integration scheme was used. The frequency of the SDOF system for $t < 15$ is 1 Hz. The time history of the simulated acceleration is shown in Figure 3.14. The value of the stiffness parameter k is shown in Figure 3.15. The simulated acceleration response was passed through a high-pass filter to detect the time of change in the stiffness. In Figure 3.16, the high-pass filtered acceleration, is shown. The filter output is negligible for $t < 15$. Beyond $t = 15$, spikes are obtained at regular intervals, determined by the excitation frequency, when the displacement has a zero-crossing. To compare the time history of the filter output and the displacement, both are shown in Figure 3.17. The high-pass filter used in this simulation had 31 filter coefficients with the 16^{th} value being the maximum one. Thus the filter output was also shifted by 16 samples for this figure. It can be seen that the spikes in the filter output correspond to the time at which the displacement has a zero crossing.

Therefore, the high frequency content of the response acceleration can be used to identify the occurrences of change in stiffness in the bilinear model. This may have relevance in devising a procedure to detect a crack in a shaft or a beam. The approach would require exciting the beam with a low frequency sinusoidal load, and the

[1]MATLAB is a registered trademark of The MathWorks, Inc.

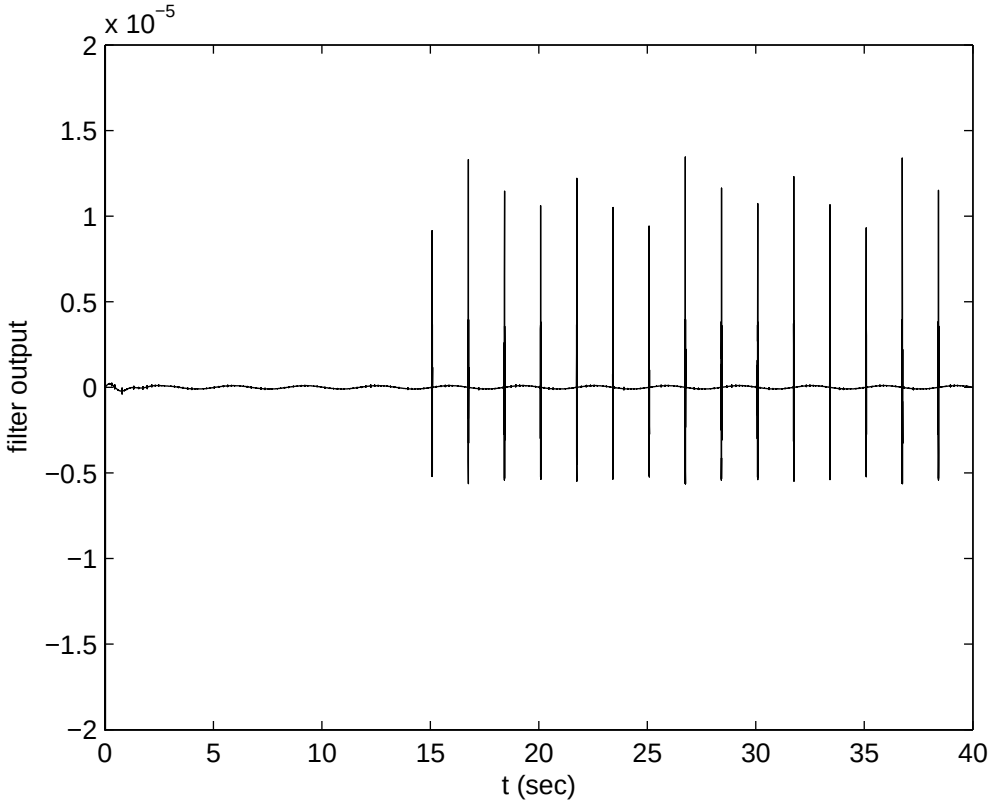

Figure 3.16: Filter output for the SDOF bilinear system.

measurement of acceleration response of the beam at an appropriate location. High-pass filtering of the measured acceleration with a spike appearing at regular interval determined by the frequency of excitation will indicate a crack.

3.6 Conclusions

In several studies researchers have shown that the discrete-wavelet transform can be used to identify the damage instant corresponding to a sudden change in stiffness. In such studies the damage instant has been shown to be indicated by the presence of spikes in the plot of the details. In this chapter it is shown that a sudden change in the system stiffness introduces discontinuities in the acceleration response. These discontinuities are the high frequency events, and the Fourier series representation of a function with such discontinuities shows the overshooting Gibb's oscillations. With

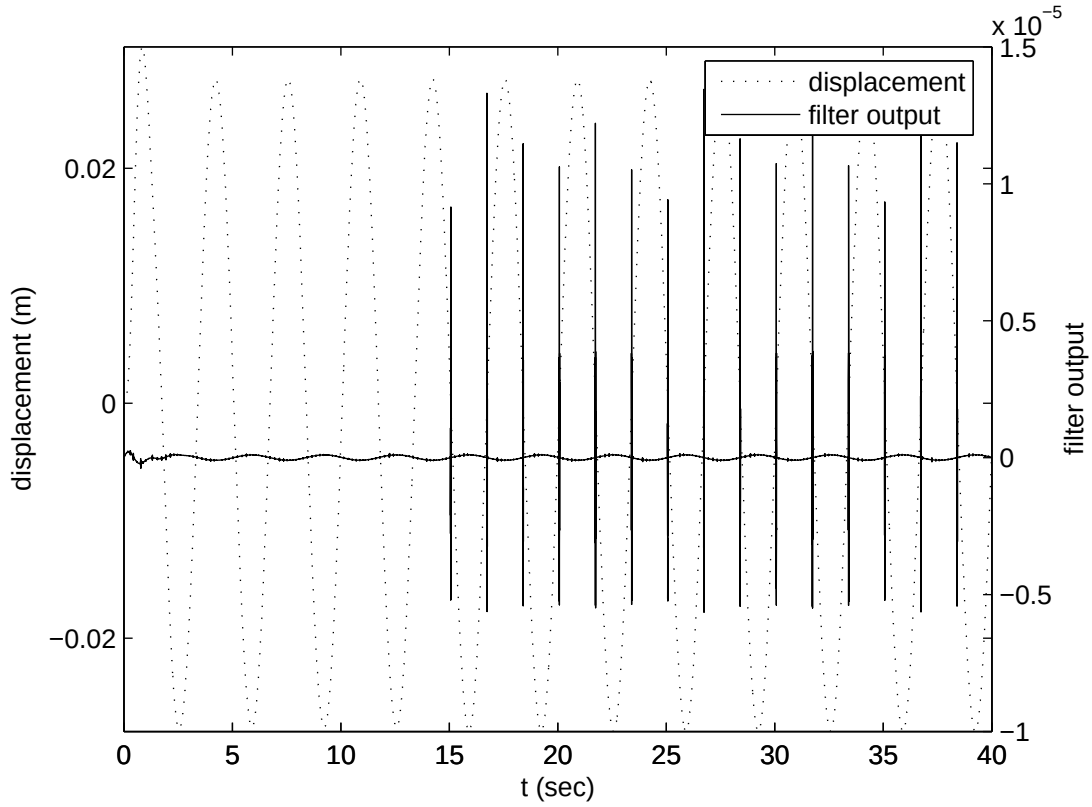

Figure 3.17: Scaled filter output and displacement for the SDOF bilinear system.

increasing terms in the Fourier series, these oscillations coalesce into up and down spikes close to the discontinuity. The heights of these spikes are directly proportional to the size of the discontinuity. Thus, by a high-frequency analysis of the discontinuous function with proper filtering of the smooth original function without the discontinuity, one can identify the time instant as well as the size of the sudden change. For this, the use of simple high-pass filters that extract the high frequency components and filter out the smooth low frequency content of the signal is proposed. The paper provides the basic analytical underpinning of the rationale behind the approach which explains the relationship of the spikes to the discontinuity being detected. This analysis also allows one to show the impact of the noise and the characteristics of the noise under which it would be possible to detect the sudden change. Numerical results for a MDOF system under base excitation and a SDOF bilinear system are presented to illustrate the methods and impact of noise in damage instant identification. Even though the instant at which the stiffness changes can be identified, calculating the change in stiffness requires the knowledge of displacement values, which are typically not available. In the next chapter a different approach is presented using which stiffness values can be tracked without having to explicitly know the displacement values.

Chapter 4

An Adaptive Unscented Kalman Filter for Tracking Sudden Stiffness Changes

4.1 Introduction

In Chapter 3, the problem of identifying the instant of damage causing a sudden change in the stiffness was addressed using the high frequency filtering of the measured response. It was noted that to obtain the magnitude of the sudden change it was necessary to know the displacement response just prior to the change. In principle, it seemed possible to obtain the displacement response by double integration of the measured acceleration response. However, it is well-known that such integration is usually associated with large drift errors (Yang and Lin (2005); Yang *et al.* (2006a, 2006b), Smyth and Wu (2007)), thus making it difficult to calculate the magnitude of the sudden change even if we know the instant of the change.

In this chapter, thus, we develop a scheme to address the issue of calculating the changes in stiffness as well as damping values without explicitly calculating the displacement response. In particular, we develop a recursive approach to track the structural parameter values such as damping and stiffness for a multi-degree of freedom structure subjected to earthquake excitation. The recursive feature of the approach also enables

us to implement this in real-time. Simply stated the problem is as follows: given the response acceleration and earthquake excitation data, calculate the values of damping and stiffness parameters in a recursive fashion.

Problem of tracking changes in the parameters of mechanical and chemical systems has been of continued interest, particularly for controlling these systems. One common approach for tracking changes in system parameters has been to use the recursive least squares (RLS) method with a forgetting factor. The forgetting factor is used to weigh the most recent measurements more than the past measurements. By properly choosing the values of the forgetting factor one can track both sudden and gradual time variations (Ljung (1999), Ljung and Soderstrom (1983)). In an early work Fortescue *et al.* (1981) showed the use of the RLS algorithm with a (variable) forgetting factor to track changes in a large-scale chemical plant. In their work the authors developed a method to track both slow and sudden changes in the plant dynamics (a step change in set point, change in pressure in the adsorption column etc.). They achieved this by calculating the forgetting factor at each time step such that the information content of the estimator was kept constant. This leads to a decrease in the value of the forgetting factor each time there is a sudden change in the parameter value allowing the tracking of time variations. Similarly, Hagglud (1984) suggested a two step procedure, first to identify when a change occurs and then to change the algorithm once the change is detected.

For civil engineering applications, Wang and Haldar (1994) used the least squares technique to estimate the parameters of shear beam models of structures for the case of unknown excitations. In a later work, they extended their approach to the cases where measurements at only a limited degrees-of-freedom were available (Wang and Haldar, (1997)). In their study, however, the velocities and displacements were assumed to be known. Smyth *et al.* (1999) have used a modified least squares adaptive method with a forgetting factor (Ioannou and Sun (1996)) for the identification of the parameters of a nonlinear single-degree-of-freedom system with the Bouc-Wen hysteretic element and also with polynomial-type nonlinear terms. They also consider non-linear multi-degree-of-freedom systems under white noise excitation, again to identify the parameters of

their nonlinear model. The validity of their proposed method is also experimentally demonstrated through the online identification of hysteretic parameters for a reinforced concrete joint system. Lin *et al.* (2001) developed a scheme for upgrading the diagonal elements of the gain matrix to track time variations of the parameters of the linear and nonlinear models of the restoring force in their system. They assumed the knowledge of input ground acceleration and the structural accelerations. The velocities and displacements were calculated by numerical integration. The identification of time invariant and time varying systems was demonstrated through simulation studies considering the Duffing, the van der Pole oscillators and the Bouc-Wen type hysteretic models. They also consider the case of damage identification when damping is reduced linearly over time. More recently, Yang and Lin (2004) have developed a least-squares based adaptive tracking technique for the identification of systems with gradual and sudden time variations. They use different forgetting factors for different parameters, obtained through an optimization approach. The application of their approach has been illustrated on single and multi-degree-of-freedom linear and non-linear systems experiencing a sudden change in structural parameter value (Yang and Lin (2005), Yang *et al.* (2006)). They have further extended this method for cases when displacement and velocities are also estimated through recursive scheme and to account for the cases when input is not measured (Yang *et al.* (2007)). The use of the optimization to estimate the forgetting factor, however, may make it difficult for its on-line application.

The problem of tracking structural parameter values can also be cast as a state-estimation problem. One of the most popular methods for state-estimation is the Kalman filter. This algorithm achieves the minimum error covariance for systems described by linear state and measurement equations. However, if the displacement and velocities, along with stiffness and damping coefficients are assumed to be unknown, and are a part of the state vector, then the state and measurement equations become non-linear. To solve such a nonlinear problem, the researchers have used the extended Kalman filter (EKF) approach in which the nonlinear equations are linearized so that the standard Kalman filter approach can be applied.

Lately to avoid linearization and associated inaccuracies caused by linearization,

a new approach called the Unscented Kalman Filteri (UKF) approach has emerged. This approach utilizes the well-known features of the Kalman filter approach but uses the method of unscented transform (UT) to obtain better estimates for the mean and variances of the nonlinear terms by employing the sigma point representation. This approach was first suggested by Julier *et al.* in 1995. Over the years this algorithm has been further studied and refined and better implementations have been developed (Julier (2002,2003), Julier *et al.* (2000), Julier and Uhlmann (2002, 2004), Tenne and Singh (2003), van der Merwe and Wan (2001)). The application of the UT and the UKF has been shown in numerous studies related to target tracking and navigation problems (Duan *et al.* (2005a), Khairnar *et al.* (2007), Leven and Lanterman (2009), Meuter *et al.* (2008), Rao and Basu (2008), Sadeghi and Moshiri (2007), Zhan and Wan (2007), Zhang and Hu (2006), Zhang *et al.* (2006)). Recently, Wu and Smyth (2007), Chatzi and Smyth (2009) have also used UKF in the area of structural health monitoring and identification of nonlinear systems.

In this chapter we propose to use the UKF approach to track sudden stiffness changes caused by damage in multi-degree of freedom structures subjected to earthquake induced ground excitations. It is assumed that we will have the measurements on ground motion as well as accelerations at different degrees of freedom of the structure. Our study indicates that the traditional UKF can not track sudden changes in the parameters and thus requires special improvements. We call this improved approach as the adaptive unscented Kalman filter (AUKF) approach. In this adaptive approach, we first detect the time of sudden changes and then propose to modify the error covariance appropriately just prior to occurrence time to appropriately track the change in the magnitude of the parameters. The time of sudden changes can also be detected by the method proposed in the previous chapter. But herein, we propose another approach that utilizes the existing KF algorithm.

This chapter is organized as follows. In Section 4.2 the Kalman filter algorithm is briefly introduced and the basic equations involved are presented as they will be used later. Next, using a simple example of estimating the mean and covariance of a random variable undergoing a non-linear transformation the idea behind the UT

is briefly described in Section 4.3. Following which the steps involved in the UKF algorithm are outlined in Section 4.4. The need for an adaptive unscented Kalman filter (AUKF) is illustrated in Section 4.5 where a scheme is suggested which can be used for tracking sudden changes in stiffness. Finally the capability of the AUKF in tracking sudden changes is illustrated through numerical examples in Section 4.6. A two degree-of-freedom and a six degree of-freedom-system each under base excitation and suffering reduction in stiffness are studied. Results are presented for the case when noise is added to both the measurement and the base excitation data. It is shown, as it is true for all estimation techniques, that the AUKF is able to track the sudden changes accurately for low noise levels. The conclusions are presented in Section 4.7.

4.2 Kalman Filter

As our proposed damage detection approach will use the concept of Kalman filtering extensively, in this section a brief overview of the Kalman filter algorithm is presented followed by a very short description of the equations that are used. The Kalman filter is a recursive algorithm for estimating the value of an unknown quantity from the available measurements which are related to that unknown quantity. The details in the presentation here are kept to minimum. For a rigorous theoretical treatment of the topic one can refer to Maybeck (1979).

Here we first introduce the Kalman filter through a simple example. Suppose we are interested in knowing the voltage across a resistor. The true value of the voltage is a constant 10 V, i.e.

$$x(t) = 10V$$

where $x(t)$ is the voltage at time t. We have at our disposal an instrument with which we can measure the voltage across the resistor. However, the instrument is not perfect and from past experience we know that the measurements would be corrupted by white noise which can be characterized by a mean value of zero and a covariance of 1 V^2. As it is numerically expedient to work with discrete time representation of the systems, the equations describing this problem in the discrete-time representation can be written as

follows:,

$$x[k+1] = x[k] \tag{4.1}$$

$$y[k] = x[k] + v[k] \tag{4.2}$$

where $x[k]$ is the true voltage at time step k, $y[k]$ is the actual measured value and $v[k]$ is a zero mean white sequence with a covariance of 1 V^2. The time index $k = 1, 2, \ldots$. These two equations define the state-space model for this simple problem.

Before taking any measurements, suppose we have no knowledge of the value of the voltage and are asked to make an initial guess. With no knowledge we might as well guess the value to be 0. Next we take a measurement and obtain $y[1] = 9.8V$. Following this, we take another measurement and obtain $y[2] = 10.02V$. We know that both of these measurements are corrupted by noise. The question then is how to combine our initial guess and the information $y[1]$ and $y[2] \ldots y[k]$ to obtain an estimate of the voltage. Also, once we have an estimate, how would that change if a new measurement $y[k+1]$ is made available. Another consideration is that, for real time application, we would like to update our estimate each time a new measurement comes in (instead of storing all the previous measurements) and calculate the estimate each time. In order words, we would like to calculate the estimate recursively. One way of doing this is as follows.

An initial guess for the value of the voltage is made, say $\hat{x}[0|0] = 0V$. This is the estimate of the voltage at time step 0, based on the knowledge that we have at that time step, and thus the notation "[0|0]". The confidence that we have in this estimate is reflected in the covariance of this estimate denoted by $P[0|0]$. Since we have no prior knowledge, our confidence is not much and, thus we can set $P[0|0]$ to be a large value as a large value means a large uncertainty. In the discussion which follows, a hat ($\hat{}$) is used to denote the estimate of a quantity. The notation $[i|j]$ for an estimate is the value of the estimate at time step i based on the measurements up to time step j. Similar notation is used to define the covariance of the estimate.

Once we have the value for $\hat{x}[0|0]$ and $P[0|0]$ the objective is to obtain values for $\hat{x}[1|1]$ and $P[1|1]$ which are the estimate of the voltage at step 1 based on the knowl-

edge that we have at step 1, i.e., based on the measurement $y[1]$ and the associated covariance. This is achieved in two steps. In the first step we estimate the voltage based on the knowledge at step 0. In the second step, we update this estimate based on the available measurement at step 1. The first step is known as the "time-update" step and the second one as the "measurement-update" step.

Time-update: $\hat{x}[0|0] \rightarrow \hat{x}[1|0]$
Before the measurement at step 1 becomes available, an estimate of the voltage at time step 1 is obtained. Let this estimate be denoted by $\hat{x}[1|0]$. The value of this estimate can be obtained using Eq. 4.1, i.e.,

$$\hat{x}[1|0] = \hat{x}[0|0]$$

Measurement-update: $\hat{x}[1|0] \overset{y[1]}{\rightarrow} \hat{x}[1|1]$
Based on the estimate $\hat{x}[1|0]$ one can obtain an estimate of the measurement at time step 1, i.e., $\hat{y}[1|0]$ using Eq. 4.2. Since the additive noise term has a mean value of 0 we have,

$$\hat{y}[1|0] = \hat{x}[1|0]$$

This is the estimate of the measurement at step 1, based on the knowledge of the state at step 0. When the actual measurement at step 1 becomes available, i.e., $y[1] = 9.8$, the error in the estimated measurement can be calculated,

$$e[1|0] = 9.8 - \hat{y}[1|0]$$

The final estimate of voltage at step 1 next is calculated as:

$$\hat{x}[1|1] = \hat{x}[1|0] + \mathbf{K}e[1|0]$$

where $\mathbf{K}$ is the Kalman gain which needs to be calculated. Associated with this estimate is a covariance $P[1|1]$. One way of interpreting the covariance is as follows. If the covariance is large, then it indicates that the estimate is far from the true value. If the value is small, then it shows that the estimate is close to the true value. We choose the Kalman gain value such that it minimizes the value of $P[1|1]$, since we want our estimate to be as close to the true value as possible. Once $\hat{x}[1|1]$ and $P[1|1]$ are calculated the same steps can be followed again. This in essence is the Kalman filter algorithm.

We will come back to the above problem again a little later after we have introduced the basic equations that are used in the implementation of the Kalman filter algorithm.

State Estimation: Kalman Filter Algorithm

Consider a linear time invariant system which is described by the discrete state and measurement equations as:

$$x[k+1] = \mathbf{A}x[k] + \mathbf{B}u[k] + w[k] \tag{4.3}$$

$$y[k] = \mathbf{C}x[k] + \mathbf{D}u[k] + v[k] \tag{4.4}$$

where $x[.]$ is the n dimensional state vector, $y[.]$ is the m dimensional measurement vector and $u[.]$ is the r dimensional input vector. $w[.]$ and $v[.]$ are zero mean white process and measurement noise sequences with covariance matrices $\mathbf{Q}$ and $\mathbf{R}$, respectively. $\mathbf{A}$, $\mathbf{B}$, $\mathbf{C}$, and $\mathbf{D}$ are matrices of appropriate dimensions. The problem of state-estimation is to estimate the state at step k, i.e., $x[k]$ recursively, based on the measurements $\mathbf{Y_k} = [y[1], y[2], \ \ldots \ y[k]]$. In the following we define these system matrices for our problem of a multi-degree of freedom structure excited by earthquake induced ground motion. The equations of motion for such a system can be writen in classical form as follows:

$$\mathbf{M}\ddot{q}(t) + \mathbf{E}\dot{q}(t) + \mathbf{K}q(t) = -\mathbf{M}\gamma\ddot{u}(t) \tag{4.5}$$

where $\mathbf{M}$, $\mathbf{E}$, and $\mathbf{K}$, are respectively the mass, damping and stiffness matrices of size $n \times n$. The vector $q(t)$ is the displacement vector of length n, γ is a vector of length n with all its entries equal to 1, and $u(t)$ is the earthquake induced ground motion. If the measurements are made to record absolute acceleration of the structure, then the measurement equation can be written as:

$$y(t) = \mathbf{M}^{-1}(-\mathbf{K}q(t) - \mathbf{E}\dot{q}(t)) \tag{4.6}$$

Using the state vector defined as,

$$x(t) = \left\{ \begin{array}{c} q(t) \\ \dot{q}(t) \end{array} \right\}$$

we can re-write the equation of motion in the continuous-time state form as,

$$\dot{x}(t) = \mathbf{A_c}x(t) + \mathbf{B_c}\ddot{u}(t)$$

where

$$\mathbf{A_c} = \begin{bmatrix} \mathbf{0}_{n\times n} & \mathbf{I}_{n\times n} \\ -\mathbf{M}^{-1}\mathbf{K} & -\mathbf{M}^{-1}\mathbf{E} \end{bmatrix} \quad \mathbf{B_c} = \begin{Bmatrix} 0_{n\times 1} \\ -\gamma \end{Bmatrix}$$

The discrete-time state equation can then be written in the form of Eq. 4.3 with the corresponding discrete-time state matrices defined as follows,

$$\mathbf{A} = e^{\mathbf{A_c}\Delta t} = \sum_{i=1}^{\infty} \frac{1}{i!}(\mathbf{A_c}\Delta t)^i \qquad \mathbf{B} = \int_0^{\Delta t} e^{\mathbf{A_c}\tau} d\tau \mathbf{B_c} = \left[\sum_{i=1}^{\infty} \frac{1}{i!}(\mathbf{A_c}\Delta t)^i \Delta t\right] \mathbf{B_c}$$

where Δt is the time-step. Using Eq. 4.6, the measurement equation can be written in the discrete form as given in Eq.4.4 with the matrices defined as,

$$\mathbf{C} = \begin{bmatrix} -\mathbf{M}^{-1}\mathbf{K} & -\mathbf{M}^{-1}\mathbf{E} \end{bmatrix} \qquad \mathbf{D} = \mathbf{0}$$

We now continue with the description of the basic steps of Kalman filter algorithm. In the discussion that follows a hat ($\hat{}$) is used to denote the estimate of a quantity. The notation $[i|j]$ for an estimate (and its covariance) is the value of the estimate (or its covariance) at time step i based on the measurements upto time step j. The basic steps are:

Initialization

At time step k let $\hat{x}[k|k]$ be the estimate of the true state $x[k]$ based on the measurements $\mathbf{Y_k}$. Let $\mathbf{P}[k|k]$ be the associated error covariance matrix which is defined as,

$$\mathbf{P}[k|k] = E[(x[k] - \hat{x}[k|k])(x[k] - \hat{x}[k|k])^T] \tag{4.7}$$

Time-update: $\hat{x}[k|k] \rightarrow \hat{x}[k+1|k]$

Using the state equation and the fact that $w[.]$ is a zero-mean white sequence, the best estimate of the state at the next step can be expressed as,

$$\hat{x}[k+1|k] = \mathbf{A}x[k|k] + \mathbf{B}u[k] \tag{4.8}$$

The error covariance associated with this estimate can then be written as:

$$\mathbf{P}[k+1|k] = E[(x[k+1] - \hat{x}[k+1|k])(x[k+1] - \hat{x}[k+1|k])^T] = \mathbf{A}\mathbf{P}[k|k]\mathbf{A}^T + \mathbf{Q} \tag{4.9}$$

Measurement-update $\hat{x}[k+1|k] \overset{y[k+1]}{\rightarrow} \hat{x}[k+1|k+1]$

Since $v[.]$ is zero-mean and white, the estimated measurement at time step $k+1$ can be expressed as,

$$\hat{y}[k+1] = \mathbf{C}\hat{x}[k+1|k] + \mathbf{D}u[k+1] \tag{4.10}$$

When the actual measurement at step $k+1$ is available, the state estimate is updated as per the following equation:

$$\hat{x}[k+1|k+1] = \hat{x}[k+1|k] + \mathbf{K}_{k+1}(y[k+1] - \hat{y}[k+1]) \tag{4.11}$$

The matrix $\mathbf{K}_{k+1}$ is known as the Kalman gain which needs to be defined. In essence, Eq. 4.11 states that the updated estimate = estimate before measurement is available + (some gain)(error committed in estimated measurement). We choose the Kalman gains such that it minimizes the covariance of the error between the true value and the estimate. The covariance of this error can be defined in the following form:

$$\mathbf{P}[k+1|k+1] = E[(x[k+1] - \hat{x}[k+1|k+1])(x[k+1] - \hat{x}[k+1|k+1])^T]$$

which after simplification can be written as

$$\mathbf{P}[k+1|k+1] = [\mathbf{I} - \mathbf{K_{k+1}C}]\mathbf{P}[k+1|k][\mathbf{I} - \mathbf{K_{k+1}C}]^T + \mathbf{K_{k+1}R}{\mathbf{K_{k+1}}}^T \tag{4.12}$$

The Kalman gain $\mathbf{K}_{k+1}$ is then selected such that the error covariance $\mathbf{P}[k+1|k+1]$ is minimized. This optimal gain is given by:

$$\mathbf{K_{k+1}} = \mathbf{P}[k+1|k]\mathbf{C}^T[\mathbf{CP}[k+1|k]\mathbf{C}^T + \mathbf{R}]^{-1} \tag{4.13}$$

Corresponding to this optimal gain value, the error covariance expression can be obtained by substituting Eq. 4.13 in Eq. 4.12 to provide the following:

$$\mathbf{P}[k+1|k+1] = (\mathbf{I} - \mathbf{K_{k+1}C})\mathbf{P}[k+1|k] \tag{4.14}$$

The recursive Kalman filter algorithm can now be summarized as follows:

1. ***Initialization***

   Time step k: $\hat{x}[k|k]$ and $\mathbf{P}[k|k]$ are known.

2. ***Time-update***

   Predicted state and error covariance are calculated as:

$$\hat{x}[k+1|k] = \mathbf{A}\hat{x}[k|k] + \mathbf{B}u[k] \tag{4.15}$$

$$\mathbf{P}[k+1|k] = \mathbf{A}\mathbf{P}[k|k]\mathbf{A}^T + \mathbf{Q} \tag{4.16}$$

3. ***Measurement-update***

   At time step $k+1$, we next define the error in estimated measurement, or also called as the innovation as:

$$e[k+1|k] = y[k+1] - \hat{y}[k+1] = y[k+1] - \mathbf{C}\hat{x}[k+1|k] - \mathbf{D}u[k+1] \tag{4.17}$$

   and use the Kalman gain:

$$\mathbf{K_{k+1}} = \mathbf{P}[k+1|k]\mathbf{C}^T[\mathbf{C}\mathbf{P}[k+1|k]\mathbf{C}^T + \mathbf{R}]^{-1} \tag{4.18}$$

   to calculate the updated state and the update error covariance as follows:

$$\hat{x}[k+1|k+1] = \hat{x}[k+1|k] + \mathbf{K}_{k+1}e[k+1] \tag{4.19}$$

$$\mathbf{P}[k+1|k+1] = (\mathbf{I} - \mathbf{K_{k+1}}\mathbf{C})\mathbf{P}[k+1|k] \tag{4.20}$$

The Kalman filter algorithm equations can be written in another standard form involving the covariance matrix of the innovation or the error in the estimated measurement $\mathbf{P}^{ee}$ and the cross-covariance of $\hat{x}[k+1|k]$ and $\hat{y}[k+1|k]$, i.e., $\mathbf{P}^{xy}$. When expressed in this form, it can be seen that the recursive algorithm needs the estimates of the mean and covariance at each time step. This then emphasizes the importance of the method of unscented transform which estimates these quantities for non-linear transformations. These equations can be obtained as follows.

Using $y[k+1] = \mathbf{C}x[k+1] + \mathbf{D}u[k+1] + v[k+1]$ in Eq. 4.17 the error or innovation can be expressed as,

$$\begin{aligned} e[k+1|k] &= \mathbf{C}x[k+1] + \mathbf{D}u[k+1] + v[k+1] - \mathbf{C}\hat{x}[k+1|k] - \mathbf{D}u[k+1] \\ &= \mathbf{C}\left(x[k+1] - \hat{x}[k+1|k]\right) + v[k+1] \end{aligned}$$

In terms of this, the covariance of the innovation can be written as,

$$\mathbf{P}^{ee} = E[e[k+1|k]e[k+1|k]^T]$$

$$= \mathbf{C}E[(x[k+1] - \hat{x}[k+1|k])(x[k+1] - \hat{x}[k+1|k])^T]\mathbf{C}^T + E[v[k+1]v[k+1]^T]$$

or,

$$\mathbf{P}^{ee} = \mathbf{C}\mathbf{P}[k+1|k]\mathbf{C}^T + \mathbf{R} \tag{4.21}$$

It is noted the inverse of this appears in the expression for the Kalman gain in Eq. 4.18. Next we define the cross-covariance between $\hat{x}[k+1|k]$ and $\hat{y}[k+1|k]$,

$$\mathbf{P}^{xy} = E[(x[k+1] - \hat{x}[k+1|k])(y[k+1] - \hat{y}[k+1|k])^T]$$

$$= E[x[k+1]y[k+1]^T - \hat{x}[k+1|k]y[k+1]^T - x[k+1]\hat{y}[k+1|k]^T + \hat{x}[k+1|k]\hat{y}[k+1|k]^T]$$

Substituting $y[k+1] = \mathbf{C}x[k+1] + \mathbf{D}u[k+1] + v[k+1]$, and $\hat{y}[k+1|k] = \mathbf{C}\hat{x}[k+1|k] + \mathbf{D}u[k+1]$ in the above expression, and after some simplification, we obtain for this covariance as follows:

$$\mathbf{P}^{xy} = E[x[k+1](\mathbf{C}x[k+1] + \mathbf{D}u[k+1] + v[k+1])^T$$

$$-\hat{x}[k+1|k](\mathbf{C}x[k+1] + \mathbf{D}u[k+1] + v[k+1])^T$$

$$-x[k+1](\mathbf{C}\hat{x}[k+1|k] + \mathbf{D}u[k+1])^T$$

$$\hat{x}[k+1|k](\mathbf{C}\hat{x}[k+1|k] + \mathbf{D}u[k+1])^T]$$

$$= E[(x[k+1] - \hat{x}[k+1|k])(x[k+1] - \hat{x}[k+1|k])^T]\mathbf{C}^T$$

This in terms of the error covariance can be written as:

$$\mathbf{P}^{xy} = \mathbf{P}[k+1|k]\mathbf{C}^T \tag{4.22}$$

We note that this term also appears in the expression for the Kalman gain in Eq. 4.18. Using the expressions as given by Eq. 4.21 and Eq. 4.22 in the expression for the Kalman gain (Eq. 4.18), the Kalman filter can be written in a different form as:

$$\mathbf{K}_{k+1} = \mathbf{P}^{xy}(\mathbf{P}^{ee})^{-1} \tag{4.23}$$

The basic set of equations describing the algorithm is as follows:

$$\hat{x}[k+1|k+1] = \hat{x}[k+1|k] + \mathbf{K}_{k+1} e[k+1|k] \tag{4.24a}$$

$$\mathbf{P}[k+1|k+1] = \mathbf{P}[k+1|k] - \mathbf{K}_{k+1}(\mathbf{P}^{ee})^{-1}\mathbf{K}_{k+1}^{T} \tag{4.24b}$$

This form is more useful in understanding the use of the unscented transform. In deriving the Kalman filter equations along these lines one key step is that the Kalman gain $\mathbf{K_{k+1}}$ is selected such that the error covariance is minimized. In this sense the filter is optimal i.e. it achieves the minimum possible error covariance. The filter equation (Eq.4.11) is of the linear form. Therefore, the Kalman filter estimator is also the linear minimum variance estimator (LMVE). That is, among all the linear filters the Kalman filter achieves the minimum variance for the error.

Example revisited

Here, the example mentioned at the beginning of this section is revisited. We will apply the algorithm defined by Eqs. 4.15 - 4.20 to this simple problem. A set of 20 random numbers were generated around the value of 10 to represent the measurement $y[k]$. The random noise in these measurements had a variance of 1. Based on these, we will estimate $x[k]$ using the algorithm. Using these noisy measurements with an initial guess of 0 and a covariance value of 100 i.e. $x[0|0] = 0$ and $P[0|0] = 100$ the estimated voltage i.e. $\hat{x}[k|k]$ was calculated.

As mentioned before, the state and the measurement equations for this problem are given by,

$$x[k+1] = x[k] \qquad y[k] = x[k] + v[k]$$

With A=1, B=0, C= 1, R= 1 and Q =0 for this discrete-time representation, the recursive Kalman filter equations (Eqs. 4.15 - 4.20) can be written specialized as follows:

$$\hat{x}[k+1|k] = x[k|k]$$

$$\mathbf{P}[k+1|k] = \mathbf{P}[k|k]$$

$$e[k+1|k] = y[k+1] - \hat{y}[k+1] = y[k+1] - \hat{x}[k+1|k]$$

$$\mathbf{K_{k+1}} = \mathbf{P}[k|k][\mathbf{P}[k|k] + \mathbf{R}]^{-1}$$

$$\hat{x}[k+1|k+1] = \hat{x}[k+1|k] + \mathbf{K_{k+1}} e[k+1|k]$$

$$\mathbf{P}[k+1|k] = (1 - \mathbf{K_{k+1}})\mathbf{P}[k|k]$$

With the first of the 20 observed values being equal to 10.623, $y[1] = 10.623$. We start the estimation process with the initial values for the state $x[0|0] = 0$, and error covariance of $P[0|0] = 100$. The covariance of the measurement is $\mathbf{R} = 1$. Applying sequentially the steps defined by the above set of equations with these intial values, we calculate the estimate of the voltage at step 1 i.e. $\hat{x}[1|1]$ and the error covariance $\mathbf{P}[1|1]$ that will be used for the following steps as follows:

$$\hat{x}[1|0] = 0$$

$$\mathbf{P}[1|0] = \mathbf{P}[0|0] = 100$$

$$e[1|0] = y[1] - \hat{y}[1|0] = y[1] - 0 = y[1] = 10.623$$

$$\mathbf{K_1} = 100[100 + 1]^{-1} = \frac{100}{101}$$

$$\hat{x}[1|1] = 0 + \frac{100}{101} 10.623 = 10.5178$$

$$\mathbf{P}[1|1] = (1 - \frac{100}{101})100 = \frac{100}{101}$$

The steps are successively applied to obtain new estimate of the voltage and the error covariance. In Figure 4.1 we plot the observed and estimated voltage values versus the true values. It is seen that the estimate converges quickly to the true value. Figure 4.2 shows the innovation sequence ($e[k+1|k] = y[k+1] - \hat{y}[k+1|k]$) the covariance ($P[k|k]$) and the Kalman gain values. The (absolute) value of the innovation decreases over time as the estimate converges to the true value. Similarly the covariance value decreases with time. The large value of the initial covariance matrix leads to a large gain value which later slowly decreases as the covariance decreases (and the estimate converges).

Finally, in Figure 4.3, we show the effect of initial covariance choice on the convergence of the estimated values to the true values. The figure shows the estimated values as well as Kalman gains obtained for the same initial value of $x[0|0] = 0$ but for two

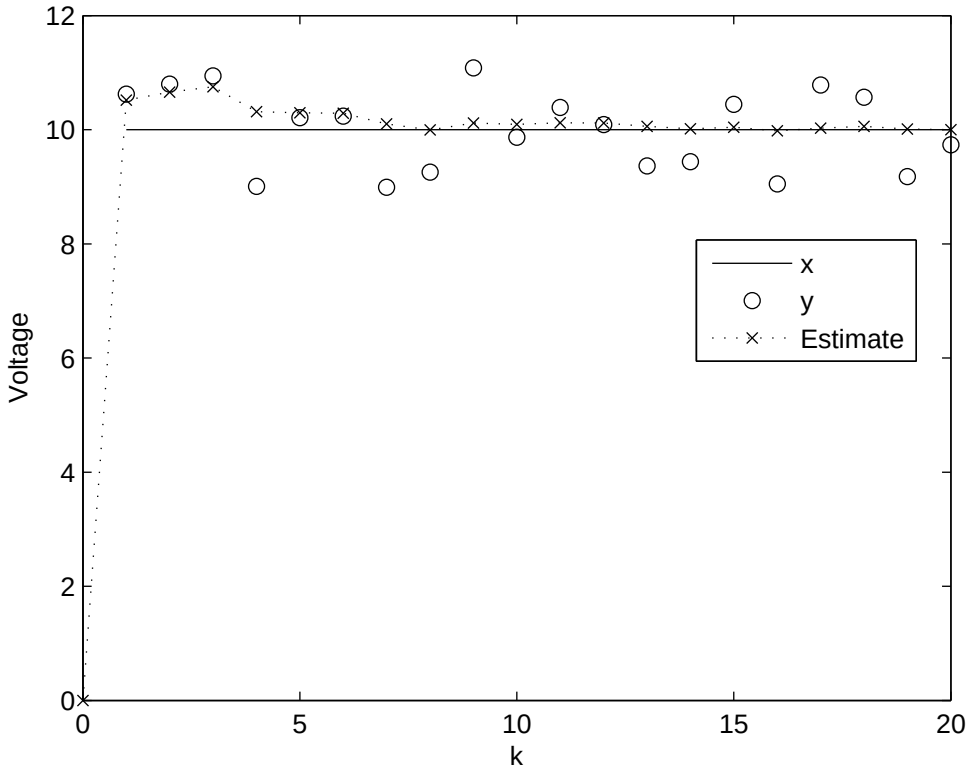

Figure 4.1: The voltage estimates for the Kalman filter example. Starting from an initial value of 0, the estimate of the voltage (identified by "Estimate") converges to the true value (x). The noisy measurements from which the estimates are calculated are also shown (y).

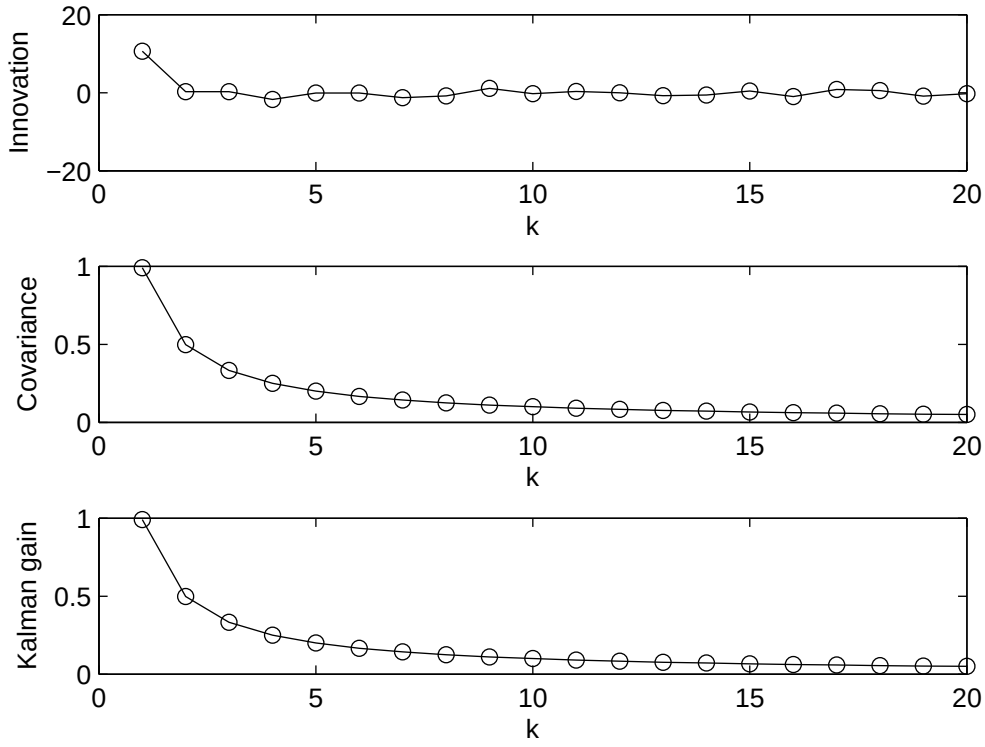

Figure 4.2: The innovation, covariance, and the Kalman gain for the estimation of the constant voltage. The error in the estimate is initially large which leads to a large value of these quantities in the initial phase. With an improvement in the estimate, the value of these quantities decreases.

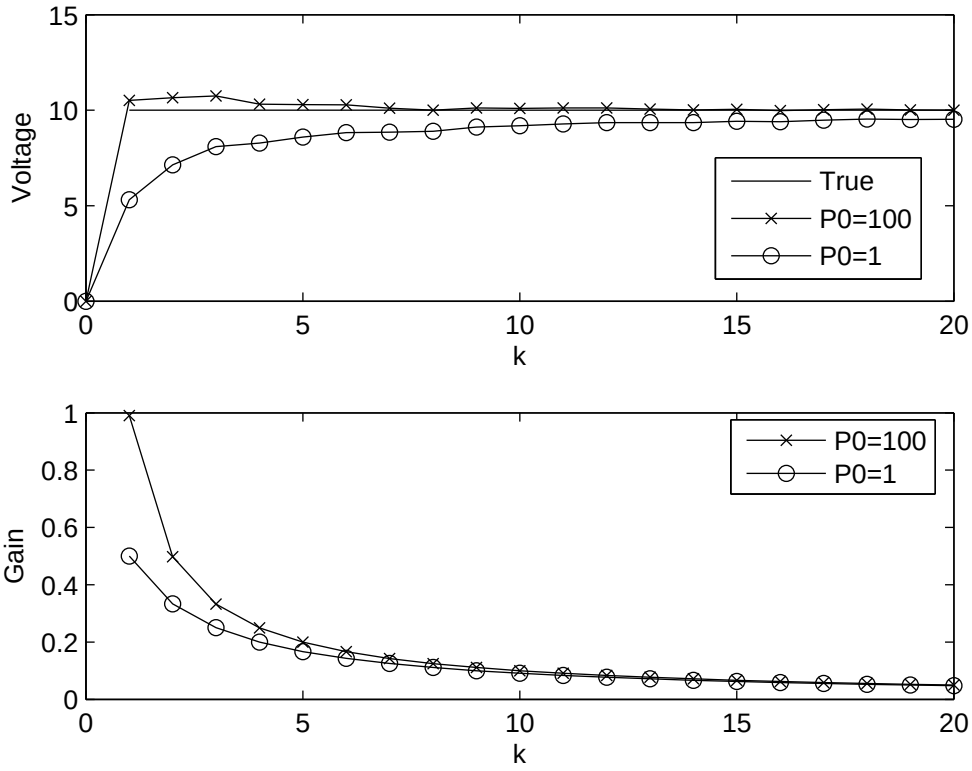

Figure 4.3: The estimated voltage and the Kalman gain for two different values of the initial covariance. A large initial covariance leads to a higher gain value. In the long run the estimates converge for either of the covariance values.

different value of the initial covariance, $P[0|0] = 1$ and $P[0|0] = 100$. In the long run, the estimates in both cases converge to the true value for both the cases. The difference in the estimates is mainly in the initial phase. For the larger initial covariance value the initial gain is also larger, this helps the estimate to converge faster. This is most evident in the first estimated value after the initial guess of 0. For the case with the larger covariance the first estimate is closer to the true value as compared to the estimate calculated using the lower covariance value. This observation about the impact of the choice of initial covariance was of relevance in the formulation of the proposed new adaptive Kalman filter approach with unscented transform to be presented later.

4.3 Unscented Transform

The equations derived in the previous section are applicable only to the linear time invariant systems. That is, the Kalman filter is not directly applicable to systems which are described by non-linear state and measurement equations. As we discuss later, we obtain nonlinear states and measurement equations when the system parameters are a part of the state vector. A popular approach for state estimation for nonlinear systems has been the extended Kalman filter (EKF). The basic idea behind the EKF is to linearize the non-linear equations and then apply the Kalman filter. This, however, can introduce error in the estimation. An approach which has become popular now with non-linear state estimation is the unscented Kalman filter (UKF) proposed by Julier *et al.* (1995). The UKF was developed primarily to avoid the linearization process and to obtain better state estimates. The UKF makes use of the unscented transform (UT) to calculate mean and covariances of random quantities undergoing non-linear transformations.

The general problem addressed by the UT is as follows: Given a vector of random variables $\mathbf{x}$ with mean $\mu_{\mathbf{x}}$ and covariance matrix $\mathbf{P}^{\mathbf{xx}}$ estimate the mean and covariance of the random variable $\mathbf{y}$ which is obtained by some non-linear transformation $f(\mathbf{x})$ of $\mathbf{x}$. The UT method can be divided into two steps. First, a set of discrete points referred to as the sigma points, are generated which capture (atleast) the mean and variance of $\mathbf{x}$. Next, these points are transformed using the non-linear function $f(\mathbf{x})$ to obtain

a new set of sigma points. The mean and covariance of the new set is the estimate of the mean and covariance of $\mathbf{y}$. In Julier and Uhlmann (1996), the authors have studied the properties of the UT and have shown that the error in the estimated mean and covariance is lower than if these quantities were estimated by using linearization of the non-linear function $f(\mathbf{x})$. In this section the basic idea behind the sigma points and the working of the UT are briefly presented.

Sigma points

In practical situations, it is fair to assume that for a random quantity at least the first two moments would be available. The sigma points with their weights are defined such that they can provide accurate estimates of the first two moments of random variables in both the linear and non-linear transformations. To explain this by example, consider a random vector $\mathbf{x}$ with a mean value $\mu_{\mathbf{x}}$ and covariance matrix $\mathbf{P^{xx}}$. This random vector $\mathbf{x}$ can also be written as,

$$\mathbf{x} = \mu_{\mathbf{x}} + \sqrt{\mathbf{P^{xx}}}\,\mathbf{z} \tag{4.25}$$

where $\mathbf{z}$ is a standard Gaussian random variable with zero mean and unit covariance and $\sqrt{\mathbf{P^{xx}}}$ is the matrix square root of $\mathbf{P^{xx}}$ i.e. $\sqrt{\mathbf{P^{xx}}}\sqrt{\mathbf{P^{xx}}}^T = \mathbf{P^{xx}}$. It can be seen that,

$$E[\mathbf{x}] = \mu_{\mathbf{x}}$$

and

$$E[(\mathbf{x} - \mu_{\mathbf{x}})(\mathbf{x} - \mu_{\mathbf{x}}{}^T)] = \sqrt{\mathbf{P^{xx}}}\; E[\mathbf{z}\mathbf{z}^T]\; \sqrt{\mathbf{P^{xx}}}^T = \mathbf{P^{xx}}$$

For the ease of illustration, consider $\mathbf{x}$ to be 2 dimensional. Therefore $\mathbf{z}$ is a 2 dimensional standard Gaussian random variable with mean $\mu_{\mathbf{z}} = \mathbf{0}$ and unit covariance i.e. $\mathbf{P^{zz}} = I$. This continuous Gaussian vector is represented by five sigma points, which are discrete points with assigned probability of occurrences or the weight. Since the Gaussian distribution is symmetric these five sigma points are selected as follows:

$$\mathbf{Z}_0 = \begin{Bmatrix} 0 \\ 0 \end{Bmatrix}, \quad \mathbf{Z}_1 = \begin{Bmatrix} -s_1 \\ 0 \end{Bmatrix} \quad \mathbf{Z}_2 = \begin{Bmatrix} s_1 \\ 0 \end{Bmatrix} \quad \mathbf{Z}_3 = \begin{Bmatrix} 0 \\ -s_2 \end{Bmatrix} \quad \mathbf{Z}_4 = \begin{Bmatrix} 0 \\ s_2 \end{Bmatrix}$$

Associated with each point $\mathbf{Z}_i$ is a weight W_i. The weights for symmetric points (with respect to the mean) must be equal, i.e. $W_1 = W_2$ and $W_3 = W_4$. Also, note that due to

the symmetry of the distribution of $\mathbf{z}$ we can also set $s_1 = s_2$ and $W_1 = W_2 = W_3 = W_4$. The weights should be such that their sum adds up to 1:

$$\sum_{i=0}^{4} W_i = W_0 + 2W_1 + 2W_3 = W_0 + 4W_1 = 1 \tag{4.26}$$

One interpretation of the sigma point is that a continuous probability distribution (of $\mathbf{z}$) is being approximated by a finite number of discrete points $\mathbf{Z}_i$ with associated probabilities W_i. The sigma points and weights are selected such that this approximation is accurate for the mean and covariance of $\mathbf{z}$. With these point and their weights, the mean of $\mathbf{z}$ is calculated as:

$$\mu = \sum_{i=0}^{4} \mathbf{Z}_i W_i = \begin{Bmatrix} 0 \\ 0 \end{Bmatrix} W_0 + \begin{Bmatrix} -s_1 \\ 0 \end{Bmatrix} W_1 + \begin{Bmatrix} s_1 \\ 0 \end{Bmatrix} W_2 + \begin{Bmatrix} 0 \\ -s_2 \end{Bmatrix} W_3 + \begin{Bmatrix} 0 \\ s_2 \end{Bmatrix} W_4$$

$$= \begin{Bmatrix} 0 \\ 0 \end{Bmatrix} = \mu_{\mathbf{z}}$$

Therefore, the requirement that the mean of the sigma points match that of $\mathbf{z}$ is satisfied simply due to the symmetry of the sigma points and the way the weights are assigned. The covariance of the sigma points is calculated as,

$$\mathbf{P} = \sum_{i=0}^{4} \mathbf{Z}_i \mathbf{Z}_i^T W_i$$

$$= \begin{Bmatrix} 0 \\ 0 \end{Bmatrix} \begin{Bmatrix} 0 & 0 \end{Bmatrix} W_0 + \begin{Bmatrix} -s_1 \\ 0 \end{Bmatrix} \begin{Bmatrix} -s_1 & 0 \end{Bmatrix} W_1 + \begin{Bmatrix} s_1 \\ 0 \end{Bmatrix} \begin{Bmatrix} s_1 & 0 \end{Bmatrix} W_2$$

$$+ \begin{Bmatrix} 0 \\ -s_2 \end{Bmatrix} \begin{Bmatrix} -s_1 & 0 \end{Bmatrix} W_3 + \begin{Bmatrix} 0 \\ s_2 \end{Bmatrix} \begin{Bmatrix} s_1 & 0 \end{Bmatrix} W_4$$

$$= \begin{bmatrix} 2W_1 s_1^2 & 0 \\ 0 & 2W_3 s_2^2 \end{bmatrix}$$

For $\mathbf{P}$ to be equal to $\mathbf{P}^{\mathbf{zz}}$ we have,

$$2W_1 s_1^2 = 1 \tag{4.27}$$

Eqs. 4.26 and 4.27 need to be solved to define the sigma points for $\mathbf{z}$. Since $W_1 = W_2 = W_3 = W_4$ and $s_1 = s_2$, there are three unknowns: s_1, W_1 and W_0 but only two

equations Eq. 4.26 and 4.27. We introduce a free parameter κ to obtain the solution. Defining $s_1 = s_2 = \sqrt{2+\kappa}$, the solution to these equations can be obtained as,

$$W_0 = \frac{\kappa}{2+\kappa} \quad W_1 = W_2 = \frac{1}{2(2+\kappa)} \quad W_3 = W_4 = \frac{1}{2(2+\kappa)}$$

with

$$s_1 = \sqrt{2+\kappa} \quad s_2 = \sqrt{2+\kappa}$$

Therefore the sigma point set for $\mathbf{z}$ becomes,

$$\mathbf{Z}_0 = \begin{Bmatrix} 0 \\ 0 \end{Bmatrix}, \quad \mathbf{Z}_1 = \begin{Bmatrix} -\sqrt{2+\kappa} \\ 0 \end{Bmatrix} \quad \mathbf{Z}_2 = \begin{Bmatrix} \sqrt{2+\kappa} \\ 0 \end{Bmatrix}$$

$$\mathbf{Z}_3 = \begin{Bmatrix} 0 \\ -\sqrt{2+\kappa} \end{Bmatrix} \quad \mathbf{Z}_4 = \begin{Bmatrix} 0 \\ \sqrt{2+\kappa} \end{Bmatrix}$$

The sigma point set for $\mathbf{x}$ can now be calculated using Eq. 4.25 as,

$$\mathbf{X}_0 = \begin{Bmatrix} \mu_{x1} \\ \mu_{x2} \end{Bmatrix} + \sqrt{\mathbf{P^{xx}}}\, \mathbf{Z}_0 = \begin{Bmatrix} \mu_{x1} \\ \mu_{x2} \end{Bmatrix}$$

$$\mathbf{X}_1 = \begin{Bmatrix} \mu_{x1} \\ \mu_{x2} \end{Bmatrix} + \sqrt{\mathbf{P^{xx}}}\, \mathbf{Z}_1 = \begin{Bmatrix} \mu_{x1} \\ \mu_{x2} \end{Bmatrix} - \sqrt{2+\kappa}(\sqrt{\mathbf{P^{xx}}})_1$$

$$\mathbf{X}_2 = \begin{Bmatrix} \mu_{x1} \\ \mu_{x2} \end{Bmatrix} + \sqrt{\mathbf{P^{xx}}}\, \mathbf{Z}_2 = \begin{Bmatrix} \mu_{x1} \\ \mu_{x2} \end{Bmatrix} + \sqrt{2+\kappa}(\sqrt{\mathbf{P^{xx}}})_1$$

$$\mathbf{X}_3 = \begin{Bmatrix} \mu_{x1} \\ \mu_{x2} \end{Bmatrix} + \sqrt{\mathbf{P^{xx}}}\, \mathbf{Z}_3 = \begin{Bmatrix} \mu_{x1} \\ \mu_{x2} \end{Bmatrix} - \sqrt{2+\kappa}(\sqrt{\mathbf{P^{xx}}})_2$$

$$\mathbf{X}_4 = \begin{Bmatrix} \mu_{x1} \\ \mu_{x2} \end{Bmatrix} + \sqrt{\mathbf{P^{xx}}}\, \mathbf{Z}_4 = \begin{Bmatrix} \mu_{x1} \\ \mu_{x2} \end{Bmatrix} + \sqrt{2+\kappa}(\sqrt{\mathbf{P^{xx}}})_2$$

where $(\sqrt{\mathbf{P^{xx}}})_i$ is used to denote the i^{th} column of the matrix square root.

The above result can be generalized to the case of a n dimensional vector. The sigma point set for a n-dimensional random vector will consists of $2n+1$ sigma points. These points and their weights are given by,

$$\mathbf{X}_0 = \mu_{\mathbf{x}} \quad W_0 = \frac{\kappa}{n+\kappa}$$

$$\mathbf{X}_i = \mu_{\mathbf{x}} + \sqrt{n+\kappa}(\sqrt{P^{xx}})_i \quad W_i = \frac{1}{2(n+\kappa)} \quad i = 1 \dots n$$

$$\mathbf{X}_i = \mu_{\mathbf{x}} - \sqrt{n+\kappa}(\sqrt{P^{xx}})_i \quad W_i = \frac{1}{2(n+\kappa)} \quad i = n+1 \dots 2n$$

In the following, two examples are presented to illustrate the application of the sigma points in nonlinear transformations. The first example is a quadratic function for which the sigma points provide accurate moment estimations. In the second example where the transformation is cubic, the sigma point being accurate only up to the second order, do introduce some error. This error is then compared with the error that would be obtained if the linearlization is used. For a theoretical treatment of the performance of the UT in comparison to the linearization process one can refer to Julier and Uhlmann (1996).

In the first example, a random variable y is obtained by a nonlinear transformation of x as,

$$y = x^2 \tag{4.28}$$

Let x be Gaussian distributed with mean μ_x and variance σ_x^2. The objective is to obtain the mean and variance of y. The true mean and variance of y may be obtained as follows.

$$\mu_y = E[y] = E[x^2] = \mu_x^2 + \sigma_x^2 \tag{4.29}$$

$$\sigma_y^2 = E[(y-\mu_y)^2] = E[y^2] - \mu_y^2 = E[x^4] - \mu_y^2$$

$$\sigma_y^2 = \mu_x^4 + 6\mu_x^2\sigma_x^2 + 3\sigma_x^4 - (\mu_x^2 + \sigma_x^2)^2$$

For a Gaussian random variable, expressing the fourth order moment in terms of the mean and variance values of x, we obtain:

$$\sigma_y^2 = 2\sigma_x^2 + 4\mu_x^2\sigma_x^2 \tag{4.30}$$

Now consider the linearized approximation of the nonlinear transformation. By expanding about the mean value of x and only retaining the linear terms, we obtain:

$$y_{lin} = f(x)_{lin} = 2\mu_x\tilde{x} + \mu_x^2$$

where $\tilde{x}$ is a mean zero Gaussian random variable with covariance σ_x^2. With this the mean and variance of y are

$$\mu_{y,lin} = E[y]_{lin} = \mu_x^2 \tag{4.31}$$

$$\sigma_{y,lin}^2 = E[(y_{lin} - \mu_{y,lin})^2] = E[y_{lin}^2] - \mu_{y,lin}^2 = 4\mu_x^2\sigma_x^2 \tag{4.32}$$

The effect of linearization is easy to see. Comparing Eq. 4.29 with Eq. 4.31 it can be seen that the mean has a bias. Also comparing Eq. 4.30 with Eq. 4.32 it can be seen that the variance is underestimated.

Next consider using sigma points to estimate the mean and variance for this non-linear transformation. To begin with, a set of sigma points $\{X_i\}$ and their associated weights $\{W_i\}$ are selected such that they capture the mean and variance of x and the symmetry of its distribution. For this consider,

$$x = \mu_x + z$$

where z has the Gaussian distribution with mean zero and variance σ_x^2. If a set of points is selected which appropriately captures the mean and covariance of z then adding μ_x to this set would give the corresponding points for x. Since x is one-dimensional ($n = 1$), the minimum number of points needed to capture this information is $2n + 1 = 3$. This set of points is given by:

$$\{X_1 \;\; X_2 \;\; X_3\} = \{\mu_x \;\; \mu_x - \sigma \;\; \mu_x + \sigma\}$$

where $\sigma = \sqrt{(n+\kappa)\sigma_x^2}$ and κ is a free parameter. The corresponding weights are given by,

$$\{W_1 \;\; W_2 \;\; W_3\} = \{\frac{\kappa}{n+\kappa} \;\; \frac{1}{2(n+\kappa)} \;\; \frac{1}{2(n+\kappa)}\}$$

For the current example, as noted earlier $n = 1$. The mean is obtained as the weighted average as,

$$X_1W_1 + X_2W_2 + X_3W_3 = \mu_x$$

and

$$(X_1 - \mu_x)^2W_1 + (X_2 - \mu_x)^2W_2 + (X_3 - \mu_x)^2W_3 = \sigma_x^2$$

Thus the set of selected points along with their associated weights provide an accurate measure of the mean and variance of x. κ does not appear in either of these expressions.

The value of κ can be fixed by match a higher order moment. For example, chose the fourth order moment the correct values of which is z is $3\sigma_x^4$. Using the sigma point, this value can be calculated as:

$$0W_1 + (1+\kappa)^2\sigma_x^4 W_2 + (1+\kappa)^2\sigma_x^4 W_3 = (1+\kappa)\sigma_x^4$$

Setting this equal to the correct fourth order moment, one obtains κ equal to 2. To obtain the mean and variance of Y, the set of sigma points is passed though the nonlinear function $f(.)$ to obtain the transformed set of points as:

$$\{Y_1 \;\; Y_2 \;\; Y_3\} = \{\mu_x^2 \quad \mu_x^2 + \sigma^2 - 2\mu_x\sigma \quad \mu_x^2 + \sigma^2 + 2\mu_x\sigma\}$$

The weights associated with these transformed points are the same as before i.e. $\{W_1 \;\; W_2 \;\; W_3\}$. The mean and variance of y can now be calculated:

$$\mu_{y,UT} = Y_1W_1 + Y_2W_2 + Y_3W_3 = \mu_x^2 + \sigma_x^2 \tag{4.33}$$

and

$$\begin{aligned}\sigma_{y,UT}^2 &= (Y_1 - \mu_{y,UT})^2W_1 + (Y_2 - \mu_{y,UT})^2W_2 + (Y_3 - \mu_{y,UT})^2W_3 \\ &= \kappa\sigma_x^4 + 4\mu_x^2\sigma_x^2\end{aligned}$$

with $\kappa = 2$,

$$\sigma_{y,UT}^2 = 2\sigma_x^4 + 4\mu_x^2\sigma_x^2 \tag{4.34}$$

Comparing Eqs. 4.29 and 4.30 with Eqs. 4.33 and 4.34 it can be seen that the mean and variance of y are correctly estimated.

In the previous example the estimated mean and covariance of y using the UT were equal to the true values. This will not be the case in general. However, as shown by Julier and Uhlmann (1996) the estimates will have lower error than that obtained using the linearization process.

Next, consider a cubic transformation as:

$$y = x^3 \tag{4.35}$$

The true mean of y can be obtained as,

$$\mu_y = E[y] = E[x^3] = \mu_x^3 + 3\sigma_x^2\mu_x \tag{4.36}$$

Similarly, the true variance of y can be calculated as,

$$\sigma_y^2 = E[(y-\mu_y)^2] = E[y^2] - \mu_y^2 = E[x^6] - (\mu_x^3 + 3\sigma_x^3\mu_x)^2$$

$$\sigma_y^2 = \mu_x^6 + 15\sigma_x^2\mu_x^4 + 45\sigma_x^4\mu_x^2 + 15\sigma_x^6 \tag{4.37}$$

The linear approximation of y can be written as:

$$y_{lin} = f(x)_{lin} = 3\mu_x^2\tilde{x} + \mu_x^3$$

where $\tilde{x}$ is a zero mean Gaussian random variable with variance σ_x^2. The mean of y using linearization is

$$\mu_{y,lin} = E[y]_{lin} = 3\mu_x^2 E[\tilde{x}] + \mu_x^3$$

or

$$\mu_{y,lin} = \mu_x^3 \tag{4.38}$$

Using linearization the estimated variance is,

$$\sigma_{y,lin}^2 = E[(y_{lin} - \mu_{y,lin})^2] = E[y_{lin}^2] - \mu_{y,lin}^2 = E[(3\mu_x^2\tilde{x} + \mu_x^3)^2] - \mu_x^6$$

$$\sigma_{y,lin}^2 = 9\sigma_x^2\mu_x^4 \tag{4.39}$$

Using the expressions for the sigma points and weights from the previous example ($\kappa = 2$) the transformed sigma point set is:

$$\{Y_1 \quad Y_2 \quad Y_3\} = \{\mu_x^3 \quad (\mu_x - \sigma)^3 \quad (\mu_x + \sigma)^3\}$$

where $\sigma = \sqrt{3}\sigma_x$ and the associated weights are given by

$$\{W_1 \quad W_2 \quad W_3\} = \{\frac{2}{3} \quad \frac{1}{6} \quad \frac{1}{6}\}$$

The mean of y using these points is given by,

$$\mu_{y,UT} = Y_1W_1 + Y_2W_2 + Y_3W_3 = \mu_x^3 + \sigma^2\mu_x = \mu_x^3 + 3\sigma_x^2\mu_x \tag{4.40}$$

Comparing Eqs. 4.36, 4.38 and 4.40 it can be seen that the mean estimated using the UT is accurate but that obtained using linearization is in error.

Finally, the variance using the UT is calculated as (using $\kappa = 2$ as in the previous example),

$$\sigma_{y,UT}^2 = \frac{2}{3}(Y_1 - \mu_x^3 - 3\sigma_x^2\mu_x)^2 + \frac{1}{6}(Y_2 - \mu_x^3 - 3\sigma_x^2\mu_x)^2 + \frac{1}{6}(Y_3 - \mu_x^3 - 3\sigma_x^2\mu_x)^2$$

$$= \frac{2}{3}(\mu_x^3 - \mu_x^3 - 3\sigma_x^2\mu_x)^2 + \frac{1}{6}((\mu_x - \sigma)^3 - \mu_x^3 - 3\sigma_x^2\mu_x)^2 + \frac{1}{6}((\mu_x + \sigma)^3 - \mu_x^3 - 3\sigma_x^2\mu_x)^2$$

This after some simplification provides:

$$\sigma_{y,UT}^2 = 9\sigma_x^2\mu_x^4 + 36\sigma_x^4\mu_x^2 + 9\sigma_x^6 \tag{4.41}$$

Using Eqs. 4.37 4.39 and 4.41 Comparing the difference in the estimated variance values,

$$\sigma_y^2 - \sigma_{y,lin}^2 = \mu_x^6 + 6\sigma_x^2\mu_x^4 + 45\sigma_x^4\mu_x^2 + 15\sigma_x^6$$

and

$$\sigma_y^2 - \sigma_{y,ut}^2 = \mu_x^6 + 6\sigma_x^2\mu_x^4 + 9\sigma_x^4\mu_x^2 + 6\sigma_x^6$$

It can be seen that the error in the estimated variance is less when using the UT.

Implementation Steps for Unscented Transform

The steps involved in the UT are now summarized. The mean μ_x and covariance P_{xx} of n dimensional random variables x are known. The objective is to calculate the mean and covariance of $y = f(x)$. This is done as follows:

1. Generate the set of $2n + 1$ sigma points, X_i and their associated weights W_i $(i = 1 \dots 2n + 1)$.
   $X_1 = \mu_x$,
   $X_j = \mu_x + \sqrt{(n+\kappa)P_{xx}}|_j$ and $X_{j+n} = \mu_x - \sqrt{(n+\kappa)P_{xx}}|j$ for $j = 2 \dots n + 1$.
   Where $\sqrt{(n+\kappa)P_{xx}}|_j$ is the j^{th} column of the matrix square-root of $(n+\kappa)P_{xx}$.
   The weights are given by,
   $W_1 = \kappa/(\kappa + n)$, $W_j = 1/2(\kappa + n)$ for $j = 2 \dots 2n + 1$.

2. Apply the function $f(.)$ to the sigma points to obtain the $2n + 1$ transformed sigma points $Y_j = f(X_j)$ $j = 1 \dots 2n + 1$.

3. The mean of y is given by $\mu_y = \sum Y_i W_i$.

4. The covariance of y is given by $\sum(Y_i - \mu_y)(Y_i - \mu_y)^T W_i$.

The UT can be used to calculate the mean and covariance matrices the estimates of which are better than those obtained by linearization. In the following section, we describe the unscented Kalman filter approach in which the sigma point are used to transform the nonlinear state equations to linear ones so that standard Kalman filter algorithm can be used.

4.4 Unscented Kalman Filter

The unscented Kalman filter (UKF) retains the basic structure of the Kalman filter but utilizes the unscented transform to calculate mean and covariance values. Consider a system described using the state and measurement equations as,

$$x[k+1] = F[x[k], u[k]] + w[k] \tag{4.42}$$

and

$$y[k] = H[x[k], u[k]] + v[k] \tag{4.43}$$

where $F[.]$ and $H[.]$ can be non-linear functions and $w[k]$ and $v[k]$ are additive process and measurement noise sequences which are zero mean white and with covariance matrices $\mathbf{Q}$ and $\mathbf{R}$ respectively. The four basic steps involved in the UKF are as follows:

1. *Initialization*
   Time step k: $\hat{x}[k|k]$ and $\mathbf{P}[k|k]$ are known.

2. *Generate sigma points*
   Calculate the sigma point set $\{X_i\}$ $i = 1 \ldots 2n+1$

3. *Time-update*

   - Propagate the sigma points $\{X_i\}$ through the state equation $F[.]$ and calculate the transformed sigma points $\{X_i^t\}$.
   - Predicted state: $\hat{x}[k+1|k]$ is given by the (weighted) mean of $\{X_i^t\}$.
   - Error covariance: $\mathbf{P}[k+1|k]$ is the covariance of the transformed sigma points $\{X_i^t\} + \mathbf{Q}$.

4. *Measurement-update*

   - Propagate the transformed sigma points $\{X_i^t\}$ through the measurement equation $H[.]$ to obtain sigma point set $\{Y_i\}$.
   - Calculate the predicted measurement $\hat{y}[k+1|k]$ as the weighted mean of $\{Y_i\}$.
   - Obtain $\mathbf{P}^{yy}$ be the covariance of the sigma points $\{Y_i\} + \mathbf{R}$.
   - Obtain $\mathbf{P}^{xy}$ be the cross covariance between the sigma points $\{X_i^t\}$ and $\{Y_i\}$.
   - Obtain the Kalman gain: $\mathbf{K_{k+1}} = \mathbf{P}^{xy}(\mathbf{P}^{yy})^{-1}$.
   - Calculate the Error in estimated measurement: $e[k+1|k] = y[k+1] - \hat{y}[k+1]$
   - Calculate the updated state: $\hat{x}[k+1|k+1] = \hat{x}[k+1|k] + \mathbf{K}_{k+1}e[k+1]$
   - Error covariance: $\mathbf{P}[k+1|k+1] = \mathbf{P}[k+1|k] - \mathbf{K}_{k+1}(\mathbf{P}^{yy})^{-1}\mathbf{K}_{k+1}^T$.

It can be seen that the state and measurement equations being linear is not a requirement. Thus the UKF is applicable in the general case. Next we apply this algorithm to estimate the parameters of a simple two degree of freedom system, and observe its limitations,

Consider the equation of motion for a 2 degree-of-freedom shear beam model system under base excitation.

$$\begin{bmatrix} m_1 & 0 \\ 0 & m_2 \end{bmatrix} \begin{Bmatrix} \ddot{q_1} \\ \ddot{q_2} \end{Bmatrix} + \begin{bmatrix} c_1 + c_2 & -c_2 \\ -c_2 & c_2 \end{bmatrix} \begin{Bmatrix} \dot{q_1} \\ \dot{q_2} \end{Bmatrix} + \begin{bmatrix} k_1 + k_2 & -k_2 \\ -k_2 & k_2 \end{bmatrix} \begin{Bmatrix} q_1 \\ q_2 \end{Bmatrix}$$
$$= - \begin{bmatrix} m_1 & 0 \\ 0 & m_2 \end{bmatrix} \begin{Bmatrix} 1 \\ 1 \end{Bmatrix} u \tag{4.44}$$

where m_i c_i and k_i are the mass damping and stiffness values associated with the i^{th} floor $(i = 1, 2)$, q_i is the i^{th} relative displacement and u is the base excitation. Considering that displacement and velocity values are not directly available as measurements

a state vector is defined as,

$$x = \left\{ \begin{array}{c} x_1 \\ x_2 \\ x_3 \\ x_4 \\ x_5 \\ x_6 \\ x_7 \\ x_8 \end{array} \right\} = \left\{ \begin{array}{c} q_1 \\ q_2 \\ \dot{q}_1 \\ \dot{q}_2 \\ c_1 \\ c_2 \\ k_1 \\ k_2 \end{array} \right\}$$

Using this state vector and the equation of motion for the 2-DOF system, the state equation can be written as

$$\dot{x} = \left\{ \begin{array}{c} \dot{x}_1 \\ \dot{x}_2 \\ \dot{x}_3 \\ \dot{x}_4 \\ \dot{x}_5 \\ \dot{x}_6 \\ \dot{x}_7 \\ \dot{x}_8 \end{array} \right\} = \left\{ \begin{array}{c} x_3 \\ x_4 \\ \frac{1}{m_1}\left[-(x_5+x_6)x_3 + x_6x_4 - (x_7+x_8)x_1 + x_8x_2 - m_1u\right] \\ \frac{1}{m_2}\left[x_6x_3 - x_6x_4 + x_8x_1 - x_8x_1 - m_2u\right] \\ 0 \\ 0 \\ 0 \\ 0 \end{array} \right\} \tag{4.45}$$

If the measurements available from this 2-DOF system are the absolute accelerations then the measurement equation is given by:

$$y = \left\{ \begin{array}{c} y_1 \\ y_2 \end{array} \right\} = \left\{ \begin{array}{c} \ddot{q}_1 + u \\ \ddot{q}_2 + u \end{array} \right\} = \left\{ \begin{array}{c} \dot{x}_3 + u \\ \dot{x}_4 + u \end{array} \right\}$$

$$y = \left\{ \begin{array}{c} \frac{1}{m_1}\left[-(x_5+x_6)x_3 + x_6x_4 - (x_7+x_8)x_1 + x_8x_2\right] \\ \frac{1}{m_2}\left[x_6x_3 - x_6x_4 + x_8x_1 - x_8x_1\right] \end{array} \right\} \tag{4.46}$$

Both the state (Eq. 4.45) and measurement (Eq. 4.46) equations are non-linear. If the available information consists of the measurement and the base excitation then the unscented Kalman filter can be used to estimate the state or in other words the displacements velocities damping and stiffness coefficients.

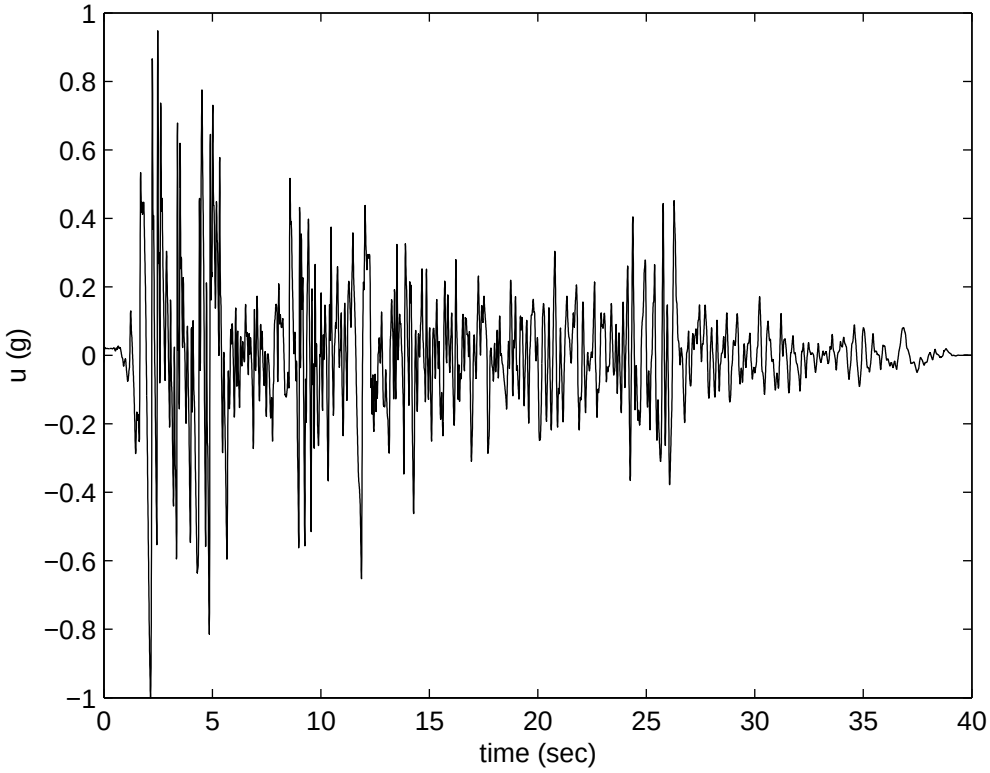

Figure 4.4: Base excitation used.

For implementation the state equation needs to be transformed to its discrete counterpart. For this consider the state equation in a general form given by

$$\dot{x} = f(x, u, t)$$

This can be transformed to the discrete domain using,

$$x[k+1] = x[k] + \int_{k\Delta t}^{(k+1)\Delta t} f(x, u, t)dt \tag{4.47}$$

where $x[k]$ is the state at time step k and Δt is the discretization step size. The integration can be evaluated using the 4^{th} order Runge-Kutta method.

The response of the 2-DOF system was simulated and the UFK was used to estimate the state vector. The base excitation data used was for the 1940 May 19^{th} Imperial Valley earthquake. Data from "USGS station 117 El Centro Array #9" was

used[1]. This available data was scaled to 1g peak acceleration value. This is shown in Figure 4.4. The structural parameter values used were $m_1 = m_2 = 1$, $c_1 = 0.6$, $c_2 = 0.5$, $k_1 = 12$ and $k_2 = 10$. The duration of the base excitation used was 40 seconds. The value of the stiffness parameter k_1 was reduced suddenly by 10% at 9 seconds. Also, in order to simulate realistic scenarios 2% RMS noise was added to the simulated response and the base excitation data. A η% RMS noise implies that the ratio of the standard deviation of the noise to the standard deviation of the signal is $\eta/100$. Since at the very beginning the value of both the base excitation and the response are small no noise is added to the first 1 second of the data.

The true and the estimated damping and stiffness values are shown in Figure 4.5. For clarity only the first 15 seconds are shown. It can be seen that in the initial phase (before the value of k_1 is changed) the estimated values converge to the true ones. However after the value of k_1 is suddenly reduced, the estimated value of k_1 does go down but at a very slow rate. The slow convergence happens because the covariances decrease as the estimate converges to the true value. The covariance in turn affects the Kalman gain value, thus affecting the ability of the filter to track the true value.

4.5 Tracking Sudden Changes: Adaptive Unscented Kalman Filter

We observe that although the unscented Kalman filter (UKF) is capable of tracking the states of a system described by non-linear state and measurement equation it is unable to track sudden changes in the parameter values. To track such changes, we propose to adopt a modified algorithm consisting of two basic steps. In the first step we identify when the instant when the sudden change occurs in the system. Knowing this instant, we then modify the covariance estimate to track the change in the parameter values. The methods to implement these steps are described in the following.

Detecting sudden changes

[1]http://peer.berkeley.edu/svbin/Detail?id=P0006

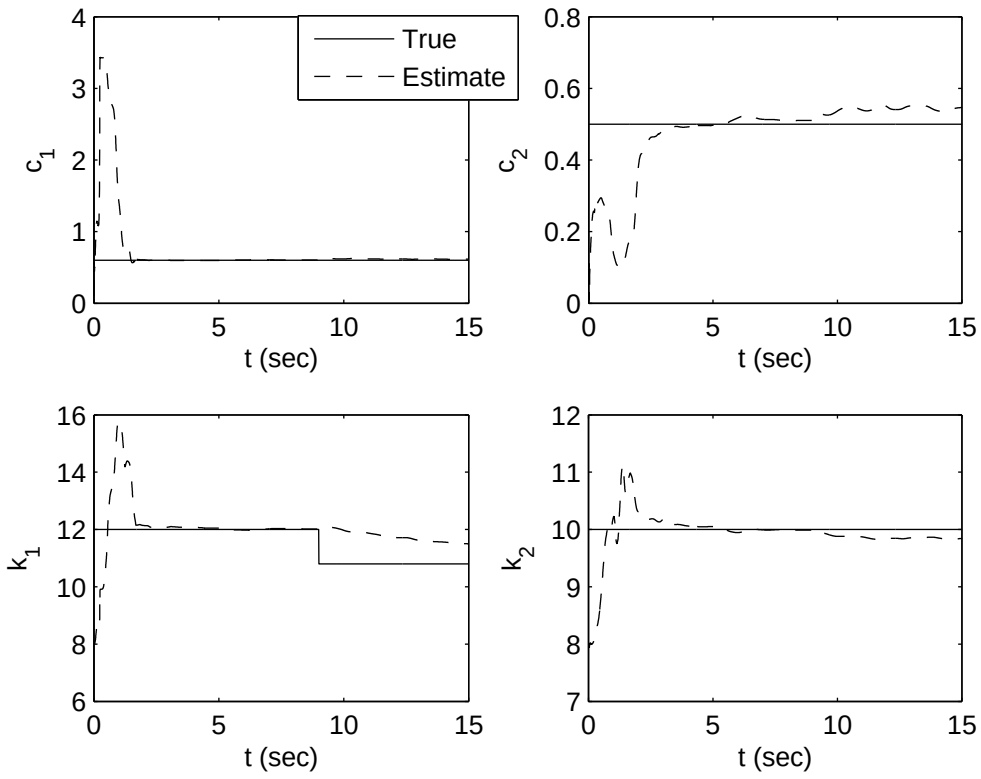

Figure 4.5: Estimated damping and stiffness values for the 2-DOF system under base excitation when the 1^{st} floor stiffness i.e. k_1 reduces by 10% at t=9sec.

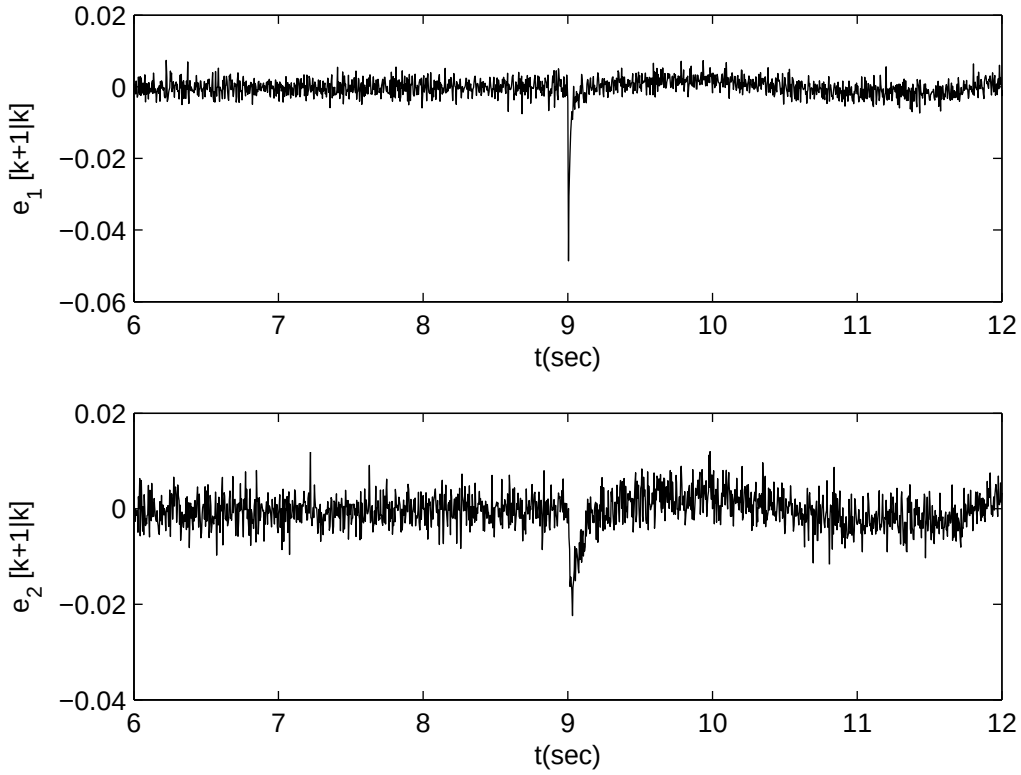

Figure 4.6: Plot of the innovation sequence for the 2-DOF system under base excitation when the state is estimated using the UKF and the 1^{st} floor stiffness i.e. k_1 reduces by 10% at t=9sec. 2% noise case.

In the UKF the error in the estimated measurement at each time step is calculated as follows:

$$e[k+1|k] = y[k+1] - \hat{y}[k+1|k]$$

where $y[k+1]$ is the available measurements at time step $k+1$, $\hat{y}[k+1|k]$ is the estimate of the measurement at time step $k+1$ based on the state estimate at time step k. As mentioned earlier, $e[k+1|k]$ is commonly referred to as the innovation. The covariance of this innovation is denoted by $\mathbf{P}^{yy}$ and is also calculated at each time step. Once the filter has converged the innovation values are small. If any of the parameters change suddenly then the value of the innovation increases. The plot of the innovation sequence for the 2-DOF system under base excitation which suffers a 10% reduction in

stiffness at t=9 sec is shown in Figure 4.6. It can be seen that the innovation values increase after 9 seconds.

A zoomed-in plot of the same sequences along with their $\pm 3\sigma$ values (indicated by the solid lines) are shown in Figure 4.7. If the innovations are assumed to follow a zero-mean Gaussian distribution then the probability of their value being greater than $\pm 3\sigma$ is about 0.003. So on an average, there is small chance (three times in 1000) that the value of innovation might be greater than $\pm 3\sigma$. However if this happens frequently then it would indicate that some error (damage in the structure causing a significant mismatch in the estimated and true values) has occurred. For example, in Figure 4.7 the innovation values do exceed the 3σ range once in a while, but it happens more frequently around 9 seconds when the change in the stiffness was introduced.

First a simple attempt was made to detect the occurrence of a sudden change using a simple counting scheme. At every time step, the number of times the innovation values exceeded their $\pm 3\sigma$ limit was counted for the previous W time steps. If this number was more than 50% of W it was assumed that a damage had occurred. However, using this approach one has to wait for several time steps after the actual damage occurs for it to be identified.

An alternative scheme was then implemented in which a norm of the innovation value, defined below, was calculated and compared to a pre-decided value.

$$\beta = e[k+1|k]^T (\mathbf{P}^{yy})^{-1} e[k+1|k]^T \tag{4.48}$$

If the innovation can be assumed to be zero-mean Gaussian random variable then β is Chi-square distributed. We note that at each time step both $e[k+1|k]$ and $\mathbf{P}^{yy}$ are calculated in the algorithm, and thus available to calculate this norm. In Figure 4.8 the value of β are plotted for the two degree-of-freedom example problem. The left plot shows the value for time 0 to 20 seconds and the right plot is a close-up showing the β values around 9 seconds. In the right plot it can be seen that the value of β is significantly more at $t = 9$ sec. That is, this parameter is highly sensitive to sudden changes. Thus, based on this observation the value of β is used indicate a sudden change in the stiffness. A threshold value β_0 can be selected such that if $\beta > \beta_0$ a

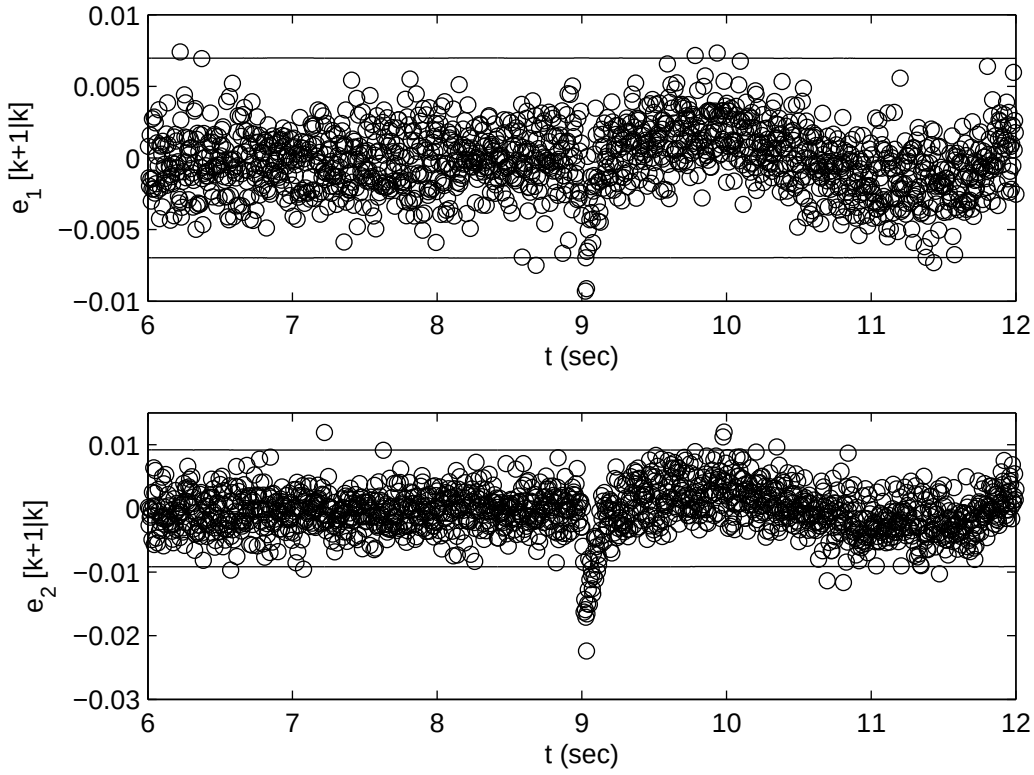

Figure 4.7: Plot of the innovation sequence along with their 3σ values (solid lines) for the 2-DOF system under base excitation when the state is estimated using the UKF and the 1^{st} floor stiffness i.e. k_1 reduces by 10% at t=9sec. 2% noise case.

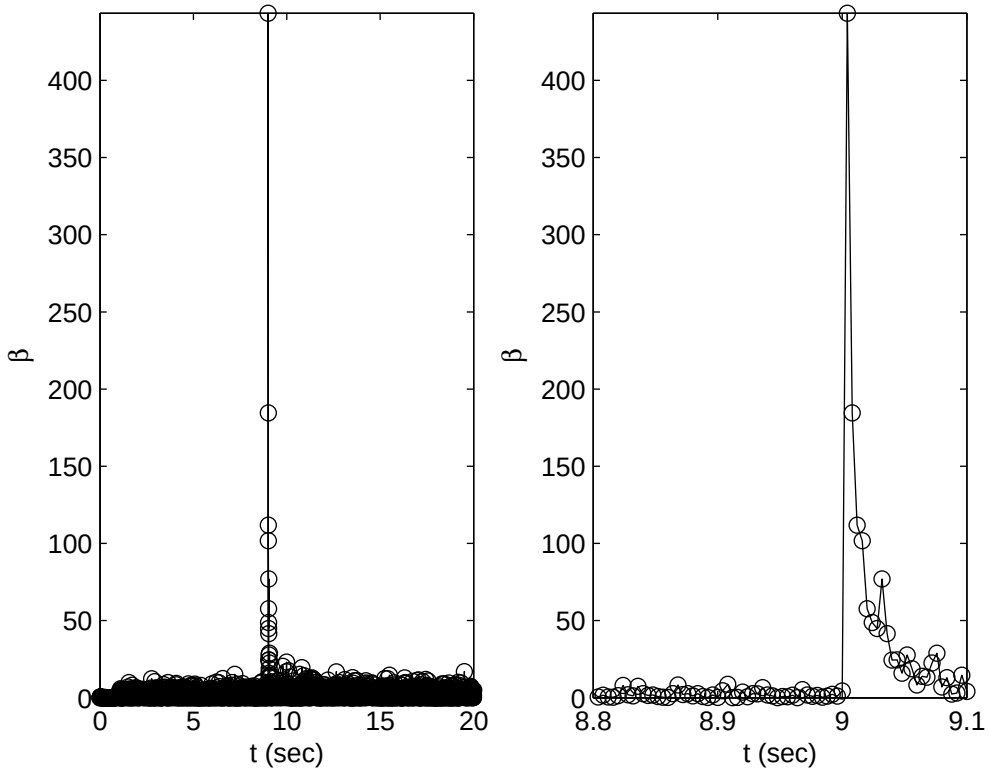

Figure 4.8: β values for the first 20 seconds along with a close-up showing the values around 9 seconds. The value of β shows a substantial increase at $t = 9$ sec.

sudden change is indicated.

The selection of an appropriate threshold value for β_0 is addressed next. For this, we examine the values of this parameter prior to the change. We assume that the algorithm has converged to the true values in a time period prior to the occurrence of the sudden change. During this initial phase of convergence the values for β are calculated at each time step and stored. The maximum of the stored values (or a slightly higher value) is chosen as a benchmark value β_0 .

For the 2-DOF system under base excitation the plot of β for the first 8 seconds is shown in Figure 4.9. Based on these previous values in the first 8 seconds, the value for β_0 was set equal to 20 or slightly higher. This value was used to detect the sudden

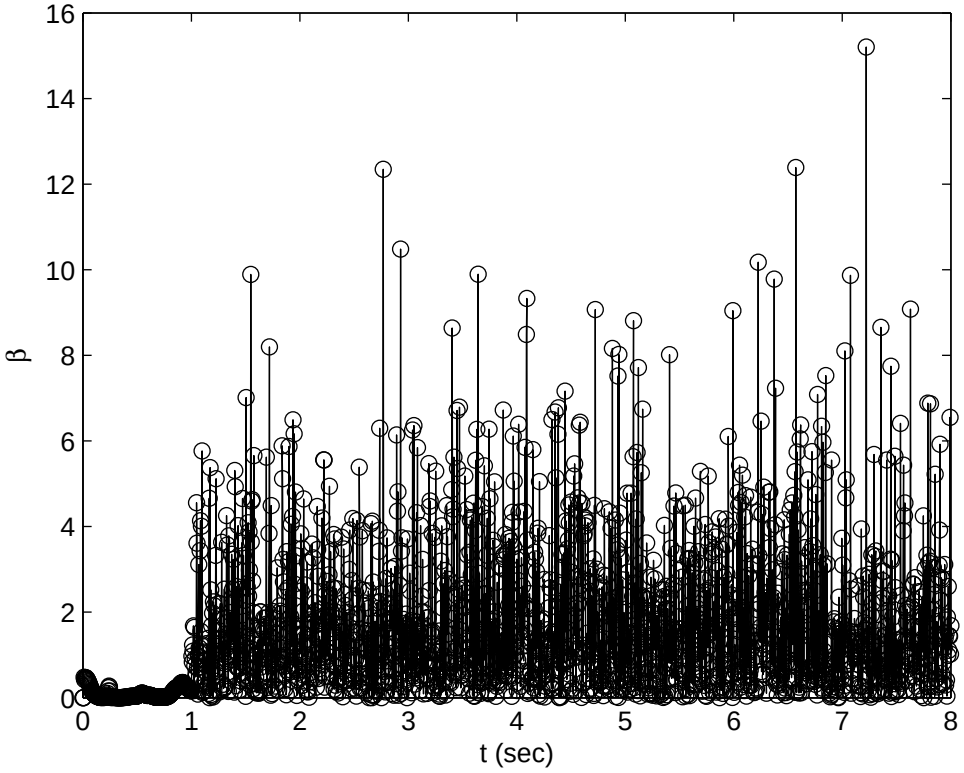

Figure 4.9: β values for the 2-DOF system under base excitation for the first 8 seconds. 2% noise case.

changes. Figure 4.8 clearly shows that at 9 seconds or after, the calculates β values are significantly higher than this limiting value, clearly indicating the occurrence of a sudden change.

Modifying the covariance matrix

Once a sudden change has been identified the next step consists of modifying the covariance matrix to allow the algorithm to track the change. For this, the diagonal value corresponding to the structural parameter which has changed was significantly increased indicating little confidence in the estimated value. For example, for the 2-DOF system considered above the covariance matrix is of size 8×8. The first two diagonal elements correspond to displacement, the next two to velocities, followed by

damping and stiffness. Therefore if it is decided that k_1 has changed then then 7^{th} diagonal element must be increased.

Two questions now arise. First, how to decide which diagonal element to modify, or in other words which structural parameter has changed. And second, by how much we increase the covariance value.

For the second question, it was first noted that when working in the recursive least squares framework, it is common to set limits on the gain or a bound on the covariance matrix, in order to be able to track changes in systems (Landau *et al.* (1998)). Following this idea, a first attempt was made by selecting a value of 0.1. That is, each time a change is detected the covariance value corresponding to the structural element would be set equal to 0.1. This value is suggested as the lower limit on the gain in the constant trace method (Landau *et al.* (1998)) and has been used in the variable trace approach in the study by Lin *et al.* (2001). However, it was noted that this value might or might not work, depending on the covariance value. That is, if the covariance value when a sudden change is detected, is already larger than 0.1, then setting it equal to 0.1, will cause a decrease in its value instead of an increase. It was then decided that a ten times increase in the covariance value will be used.

Next, to identify the diagonal element that need to be increased the following is used. The diagonal elements corresponding to the structural parameters are increased one at a time and the UKF is run for a single time step. In the UKF (and also in the Kalman filter) the innovation is calculated at each time step as it is needed in the measurement update step. Once the state estimate $\hat{x}[k+1|k+1]$ has been calculated, the residual $r[k+1|k+1] = y[k+1] - \hat{y}[k+1|k+1]$ can also be available. The value of this residual residual and its associated covariance matrix $\mathbf{P}^{rr}$ are used to identify structural parameter that has changed as follows:

1. While going from step k to $k+1$ if $\beta > \beta_0$ then a sudden change is suspected and the following steps are implemented. Otherwise the UKF is implemented as usual.

2. Let n be the dimension of the state vector. Thus there are n diagonal elements

in the covariance matrix $\mathbf{P}[k|k]$. Let n_s be the number of structural parameters.

3. For $j = n - n_s + 1$ to n
   - Increase the j^{th} element of $\mathbf{P}[k|k]$ by setting it equal to $10 \times \mathbf{P}[k|k]$
   - Calculate $r[k+1|k+1]$ and $\mathbf{P}^{rr}$ using the UKF.
   - Calculate $\gamma_j = r[k+1|k+1]^T(\mathbf{P}^{rr})^{-1}r[k+1|k+1]$
4. The state having the minimum value of γ_j is selected as the one which has changed.

The proposed adaptive unscented Kalman filter (AUKF) scheme is summarized in Table 4.1, and is illustrated in Figure 4.10. Note that, the adaptive feature (i.e. detecting the change based on the value of β and increasing the covariance matrix by 10 times) is used after the estimates have initially converged. Therefore, it is possible that when the covariance corresponding to a structural parameter, which has not suffered a change in its value, is increased by 10 times, then the estimates at the next time step may be unrealistic. If this happen, then the value of γ corresponding to this structural parameter is not considered in selecting the parameter which has changed. As example, consider the 2-DOF system described above. At $t = 9$ a damage is detected. Following which, first the 5^{th} diagonal element of the covariance matrix will be set equal to 10 times its present value. This element corresponds to c_1. Using this covariance matrix, the estimated state vector at the next time step will be calculated. Since c_1 has not changed, and there is no constraint on the values of the structural parameters, it is possible that, for example a negative value of k_1 is obtained. If any such unrealistic value is obtained for any structural parameter, then, γ_j ($j = 5$) is not considered when selecting the minimum γ value.

4.6 Numerical Results

Numerical studies are carried out to test the applicability of the proposed adaptive UKF scheme. Cases of single and multiple damages are tested in the presence of noise in the measurement data. We present the results for two and six degrees of freedom

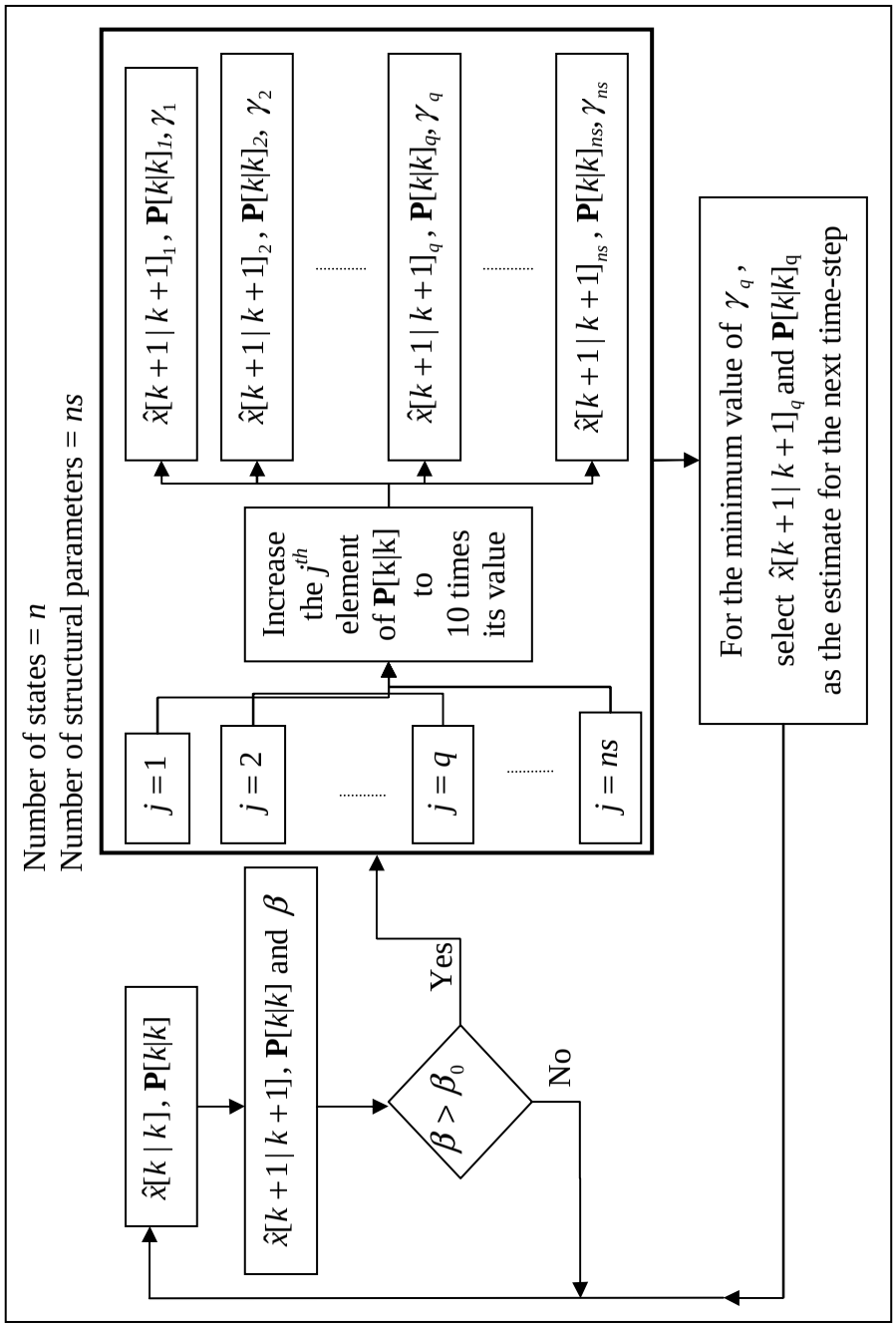

Figure 4.10: The adaptive unscented Kalman filter (AUKF) scheme.

Table 4.1: AUKF algorithm

1: $\hat{x}[k\|k]$ and $\mathbf{P}[k\|k]$ are known
2: Estimate the state and covariance at step $k+1$ using the UKF
3: Calculate β. If $\beta > \beta_0$ goto 4 else goto 1.
4: For $j = n - n_s + 1$ to n
4a: Increase j^{th} element of $\mathbf{P}[k\|k]$
4b: Run the UKF for one time step
4b: Calculate $r[k+1\|k+1]$ and $\mathbf{P}^{rr}$
4c: Calculate $\gamma_j = r[k+1\|k+1]^T(\mathbf{P}^{rr})^{-1}r[k+1\|k+1]$
5: Let j_{min} be the value of j for which the minimum value of γ_j is obtained.
6: Set $\hat{x}[k+1\|k+1]$ and $\mathbf{P}[k+1\|k+1]$ equal to the values returned by the UKF when the j^{th}_{min} diagonal value was changed.
7: Goto 1

examples.

Two Degree-of-freedom Example

The two-degree-of-freedom system described earlier was subjected to the ground acceleration record. The total duration of the excitation was 40 seconds. Three damage cases were studied. The plot of the stiffness values (k_1 and k_2) for these three cases are shown in Figure 4.11. In Case 1 the stiffness of the first floor k_1 was reduced by 10% at 9 seconds. In Case 2 the stiffness of the second floor was reduced by 10% at 9 seconds and that of the first floor was reduced by 10% at 12 seconds. Finally in Case 3, the stiffness of the first floor is reduced by 10% at 12 seconds, and the stiffness of the second floor is reduced by 10% and then by 5% at 9 and 15 seconds.

The estimated damping and stiffness are shown in Figure 4.12 for Case 1 when 2% noise was added to the measurement and to the base excitation record. The total duration of the simulation was 40 seconds, however for clarity the plot is shown for the first 15 seconds only. The AUKF is able to track the sudden change in k_1 accurately.

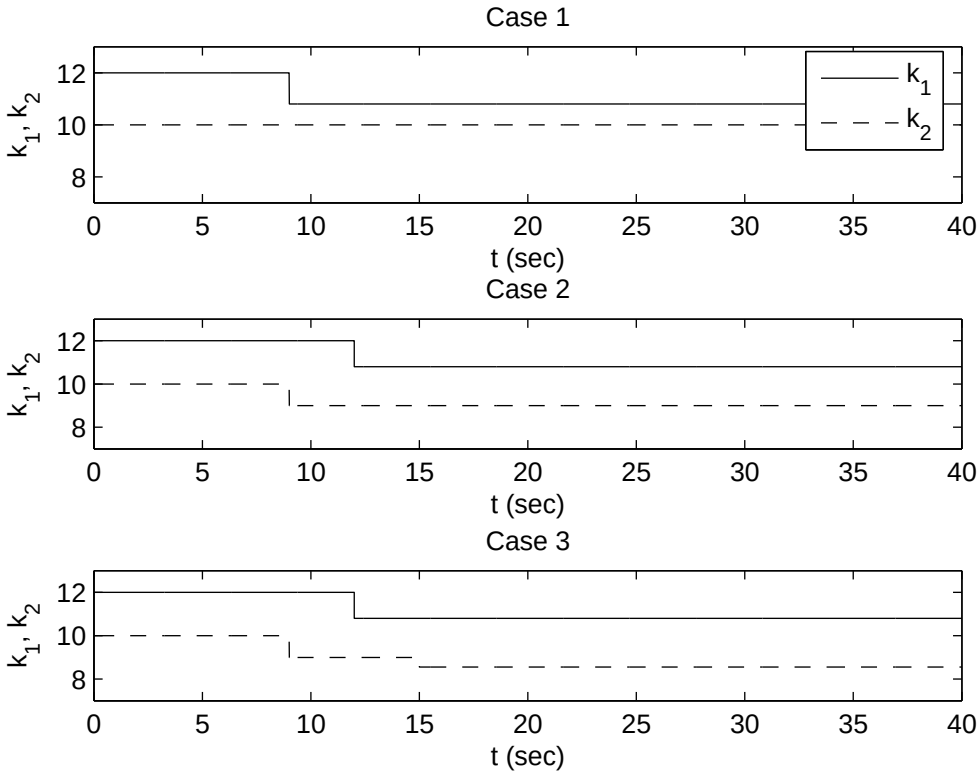

Figure 4.11: Stiffness variations for the three damage cases considered for the 2-DOF system. The value of k_1 is shown by the solid lines and that of k_2 by the dashed lines.

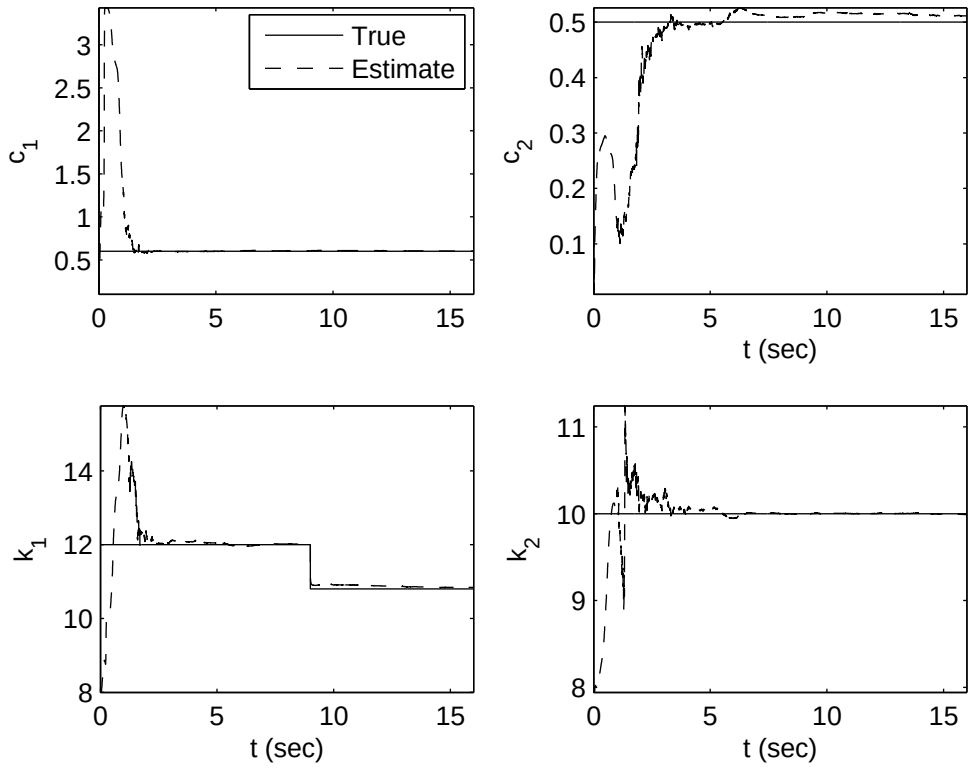

Figure 4.12: Estimated damping and stiffness values for the 2-DOF system under base excitation when k_1 reduces by 10% at 9 sec. 2% noise case.

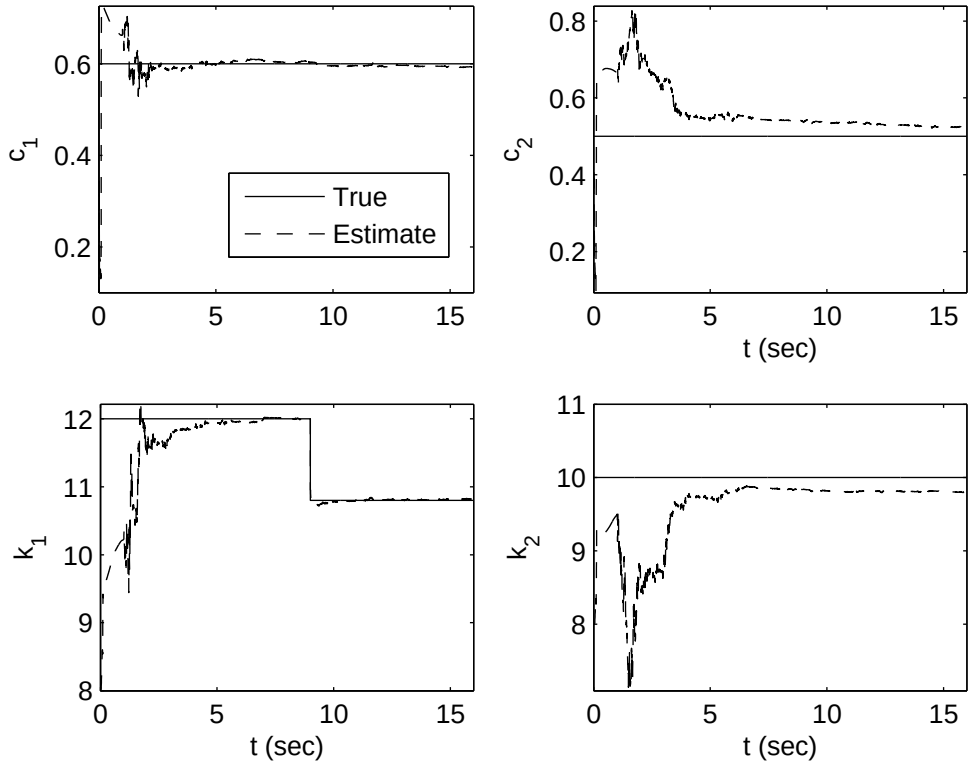

Figure 4.13: Estimated damping and stiffness values for the 2-DOF system under base excitation when k_1 reduces by 10% at 9 sec. 5% noise case.

In order to study the affect of measurement noise level on the performance of the AUKF, simulations were carried out for different noise levels. In Figure 4.13 the results for the same damage case (10% reduction in k_1) but with 5% noise are shown. The sudden change in k_1 is captured accurately though due to increase in the noise level the error in the estimates (for e.g. k_2) seems to have increased.

The results obtained with 10% and 20% noise are shown respectively in Figures 4.14 and 4.15. In both these cases the AUKF is able to track the sudden change in stiffness in k_1.

In all these cases i.e. with 2%, 5%, 10% and 20% noise, the AUKF was able to track the sudden change in k_1. The affect of measurement noise level on the AUKF can is

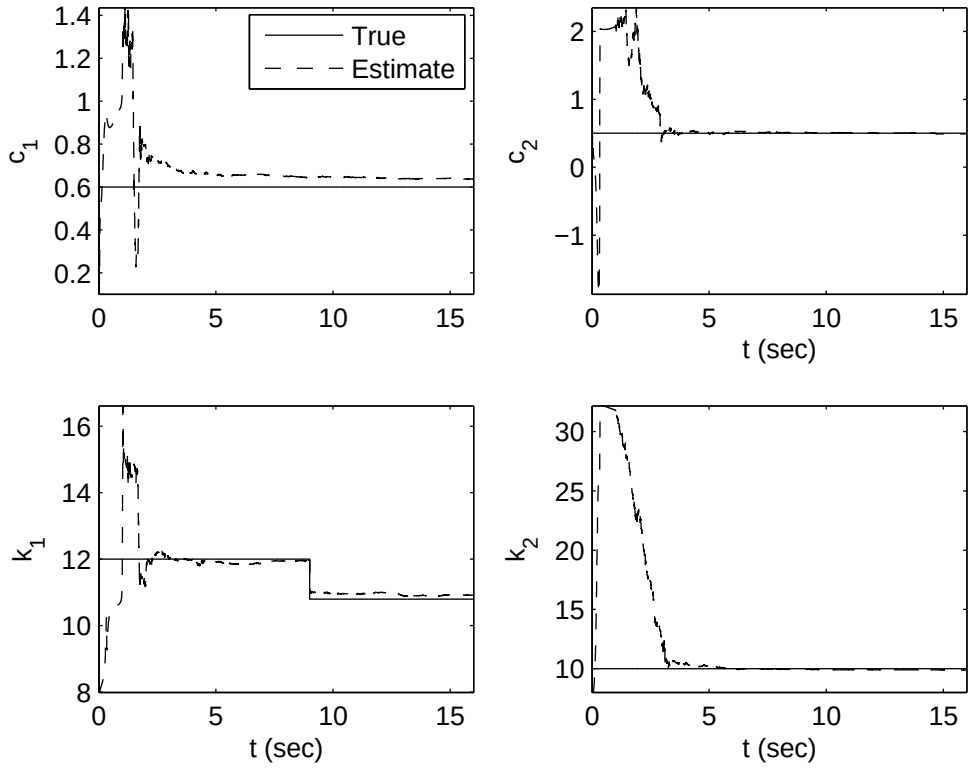

Figure 4.14: Estimated damping and stiffness values for the 2-DOF system under base excitation when k_1 reduces by 10% at 9 sec. 10% noise case.

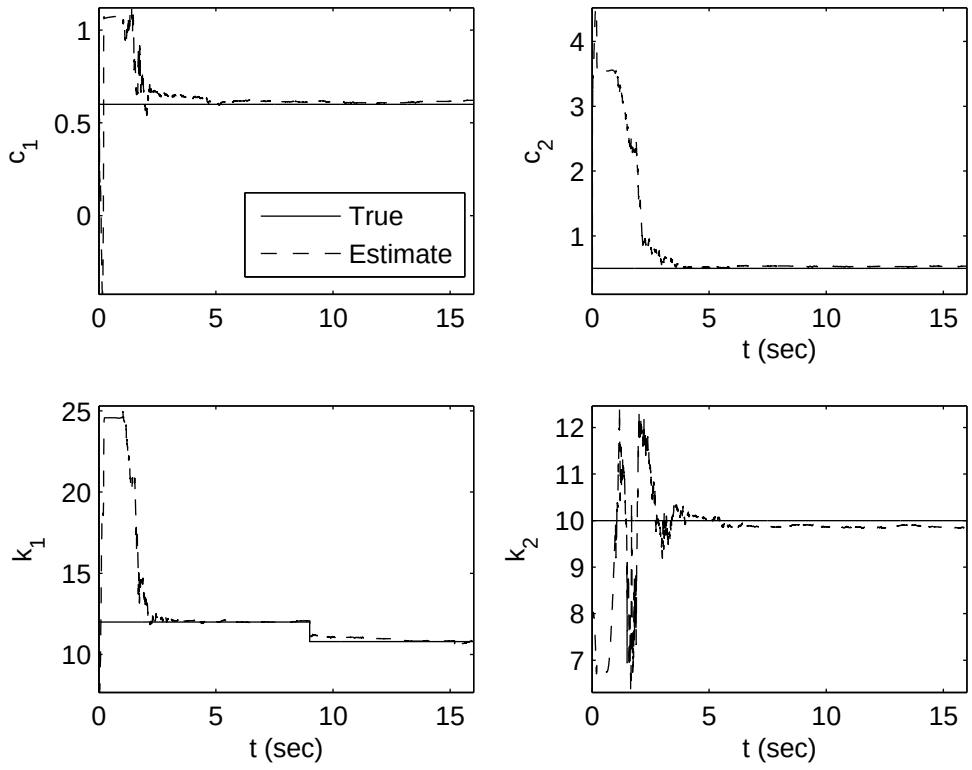

Figure 4.15: Estimated damping and stiffness values for the 2-DOF system under base excitation when k_1 reduces by 10% at 9 sec. 20% noise case.

better understood by looking at the values of β which are used for detecting a change. These are shown in Figure 4.16, where the values of β are shown for the 2%, 5%, 10% and 20% noise levels. Note that damage in this case was a 10% reduction in the value of k_1 at $t = 9$ sec. For the 2% and 5% noise cases, the value of β at $t = 9$ is significantly larger and clearly indicates the occurrence of damage. In contrast, the values of β at $t = 9$, though still the maximum, are not as significantly larger for the 10% and 20% noise cases. However, in these cases, their value was still greater than the threshold β_0 (which is based on the maximum value of β in the initial phase). Thus the change in k_1 could be tracked. This plot shows the affect of increase in the noise level on the performance of the AUKF. As the noise level increases, the value of β obtained at the damage instant will not be distinguishable from the previously obtained values. This observation is similar to the one noted in the previous chapter where, measurement noise was shown to mask the spike, which indicates the damage instant when using the high-pass filter.

The estimation results for Case 2 and Case 3 are shown respectively in Figure 4.17 and 4.18. In both these cases 2% noise was added to the measurement and base excitation data. In both these cases the AUKF was able to correctly track the structural parameters in the multiple damage scenarios.

Six degree-of-freedom

As another example illustrating the application of the AUKF with a larger state vector a six-degree of freedom system was selected. The equation of motion for this system can be written as,

$$\mathbf{M}\ddot{\mathbf{q}} + \mathbf{C}\dot{\mathbf{q}} + \mathbf{K}\mathbf{q} = -\mathbf{M}\gamma u \tag{4.49}$$

where $\mathbf{M}$, $\mathbf{C}$, and $\mathbf{K}$ are the mass damping and stiffness matrices, $\mathbf{q}$ is the displacement vector, γ is the influence vector and u is the input excitation. These matrices and

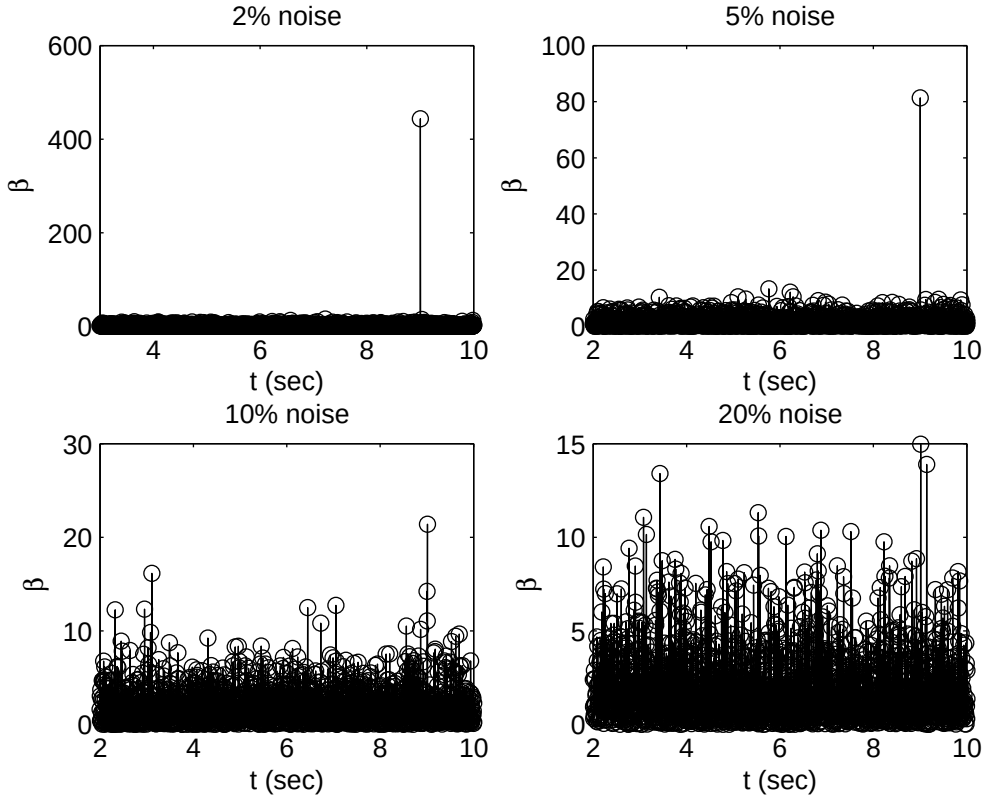

Figure 4.16: Value of β plotted for $t = 2$ to $t = 10$, for Case 1, for different noise level case. Change in stiffness in k_1 occurs at $t = 9$ sec.

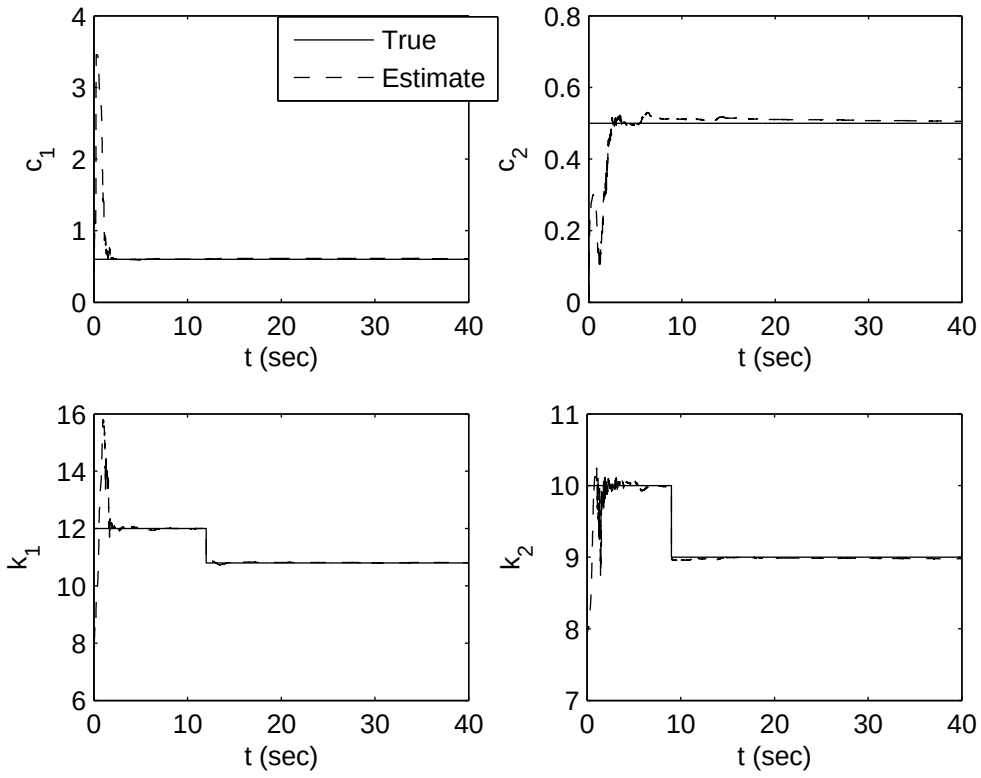

Figure 4.17: Estimated damping and stiffness values for the 2-DOF system under base excitation when k_2 and k_1 reduce by 10% at 9 sec. and 12 sec. respectively. 2% noise case.

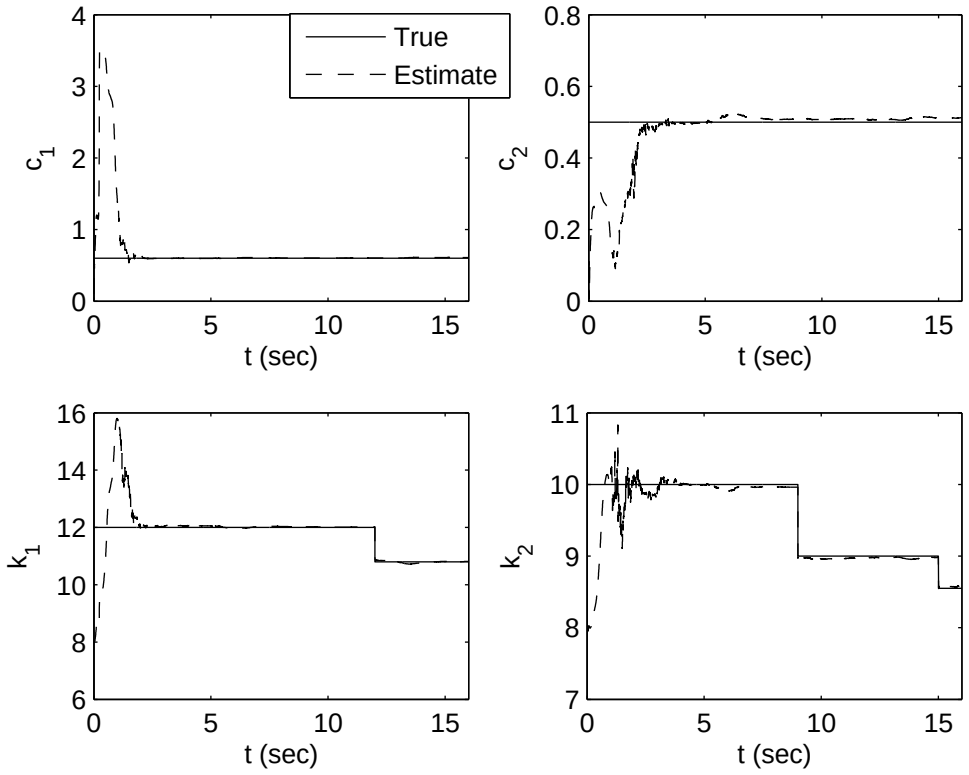

Figure 4.18: Estimated damping and stiffness values for the 2-DOF system under base excitation when k_1 reduces by 10% at 12 sec. and k_2 reduces by 10% and 5% at 9 and 15 seconds respectively. 2% noise case.

vectors are given by:

$$\mathbf{M} = \begin{bmatrix} m_1 & 0 & 0 & 0 & 0 & 0 \\ 0 & m_2 & 0 & 0 & 0 & 0 \\ 0 & 0 & m_3 & 0 & 0 & 0 \\ 0 & 0 & 0 & m_4 & 0 & 0 \\ 0 & 0 & 0 & 0 & m_5 & 0 \\ 0 & 0 & 0 & 0 & 0 & m_6 \end{bmatrix}$$

$$\mathbf{C} = \sum_{i=1}^{6} c_i \mathbf{D_i}$$

$$\mathbf{K} = \sum_{i=1}^{6} k_i \mathbf{S_i}$$

$$\mathbf{q} = \begin{Bmatrix} q_1 \\ q_2 \\ q_3 \\ q_4 \\ q_5 \\ q_6 \end{Bmatrix} \quad \gamma = \begin{Bmatrix} 1 \\ 1 \\ 1 \\ 1 \\ 1 \\ 1 \end{Bmatrix}$$

where m_i, c_i and k_i (for $i = 1 \ldots 6$) are the i^{th} story mass damping and stiffness coefficients. $\mathbf{D_i}$ (for $i = 1 \ldots 6$) is a 6×6 matrix of constant elements with values equal to 1, -1, or 0, at entries where c_i occurs with a positive sign, negative sign, or does not occur, in the complete damping matrix. The matrix $\mathbf{S_i}$ is defined similarly but using k_i.

Considering the displacements velocities damping and stiffnesses as unknowns to be estimated, the state vector of length 24 is defined as,

$$x = \begin{Bmatrix} q \\ \dot{q} \\ \mathcal{C} \\ \mathcal{K} \end{Bmatrix} = \begin{Bmatrix} x_1 \\ x_2 \\ x_3 \\ x_4 \end{Bmatrix}$$

where vectors $x_3 = \mathcal{C}$ and $x_4 = \mathcal{K}$ contain the element damping and stiffness coefficients

as follows:

$$x_3 = \mathcal{C} = \begin{Bmatrix} c_1 \\ c_2 \\ c_3 \\ c_4 \\ c_5 \\ c_6 \end{Bmatrix} \qquad x_4 = \mathcal{K} = \begin{Bmatrix} k_1 \\ k_2 \\ k_3 \\ k_4 \\ k_5 \\ k_6 \end{Bmatrix}$$

In terms of these vectors the state equation can be written as follows:

$$\dot{x} = \begin{Bmatrix} \dot{x}_1 \\ \dot{x}_2 \\ \dot{x}_3 \\ \dot{x}_4 \end{Bmatrix} = \begin{Bmatrix} \dot{q} \\ \ddot{q} \\ \dot{\mathcal{C}} \\ \dot{\mathcal{K}} \end{Bmatrix} = \begin{Bmatrix} \dot{q} \\ -\mathbf{M}^{-1} \sum_{i=1}^{6} (c_i \mathbf{D_i} \dot{q} + k_i \mathbf{S_i} q) - \gamma u \\ 0_{6\times 1} \\ 0_{6\times 1} \end{Bmatrix}$$

or

$$\dot{x} = \begin{Bmatrix} \dot{x}_1 \\ \dot{x}_2 \\ \dot{x}_3 \\ \dot{x}_4 \end{Bmatrix} = \begin{Bmatrix} x_2 \\ -\mathbf{M}^{-1} \sum_{i=1}^{6} (c_i \mathbf{D_i} x_2 + k_i \mathbf{S_i} x_1) - \gamma u \\ 0_{6\times 1} \\ 0_{6\times 1} \end{Bmatrix}$$

where $0_{6\times 1}$ is a vector of length 6 with all its entries equal to 0. This is a non-linear state equation as the right hand side contains the product of the state variables. The detailed state equation in an expanded form is given in Appendix C.

With the absolute acceleration as the available measurements, the measurement equation is given by,

$$y = \begin{Bmatrix} y_1 \\ y_2 \\ y_3 \\ y_4 \\ y_5 \\ y_6 \end{Bmatrix} = \begin{Bmatrix} \ddot{q_1} + u \\ \ddot{q_2} + u \\ \ddot{q_3} + u \\ \ddot{q_4} + u \\ \ddot{q_5} + u \\ \ddot{q_6} + u \end{Bmatrix} = -\mathbf{M}^{-1} \sum_{i=1}^{6} (c_i \mathbf{D_i} x_2 + k_i \mathbf{S_i} x_1)$$

The measurement equation in explicitly defined in the Appendix C. As in the previous example, both the state and measurement equations are non-linear. For the simulation the values of mass, stiffness, and damping were $m_1 = m_2 = 4.8$, $m_3 = m_4 = 4.32$,

$m_5 = m_6 = 3.84$, $k_1 = k_2 = 8340$, $k_3 = k_4 = 5340$, $k_5 = k_6 = 3340$, and $c_i = k_i \times 10^{-3}$ $(i = 1 \ldots 6)$. A sampling frequency of 250 Hz was used. The structure was excited by the same base excitation as before. Damage consisted of a 10% reduction in stiffness in k_1 k_6 and k_3 at 9 10 and 15 seconds respectively. 2% noise was added to the measurement and the base excitation data.

The estimated damping values are shown in Figures 4.19. The AUKF is able to estimate the damping values correctly. However at 15 seconds the estimate of c_3 seems to change. This was because at 15 seconds after a change in structural parameter is detected the AUKF indicated that c_3 had changed even though the actual change occurred in k_3. This becomes clear from Figure 4.20 where the diagonal elements of the covariance matrix corresponding to the damping coefficients are plotted for the time range 8-16 seconds. Because c_3 was indicated to have changed its covariance value at that time step has been increased. This then leads to a (visible) change in the value of c_3 as seen in Figure 4.19.

In Figure 4.21 the estimated stiffness values are plotted. The diagonal elements of the covariance matrix corresponding to the stiffness coefficients are shown for the time 8-16 seconds in Figure 4.22. The AUKF was able to track all the changes correctly. However as mentioned above, at 15 seconds the AUKF indicated a change in c_3. But after two time steps it again indicated a change and this time in k_3 thus correctly estimating the values.

4.7 Chapter Summary and Concluding Remarks

The problem of on-line estimation of structural parameter values from the measured vibration data has been of interest in the area of structural health monitoring. In this chapter, we examine the application of a modified and improved version of the Kalman filter approach using the unscented transform. To use the Kalman filtering to estimate of parameters of a dynamic system such as a structure excited by earthquake induced ground motion, the parameters to be estimated must be a part of the state vector of the system. Systems equations expressed in this form are necessarily nonlinear. One way

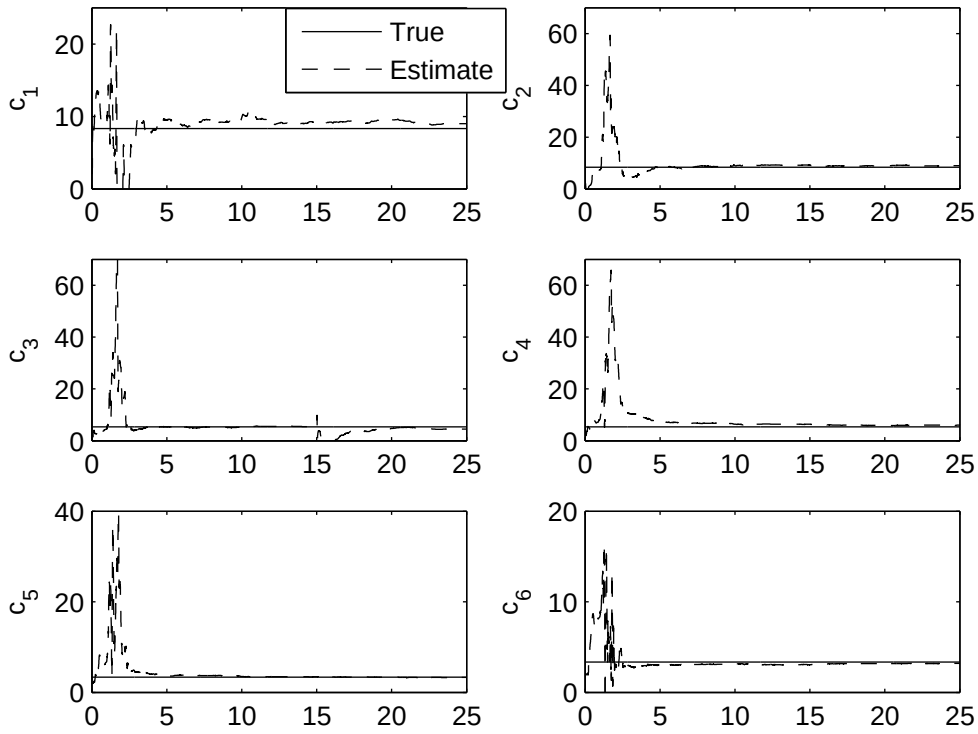

Figure 4.19: Estimated damping for the 6-DOF structure under base excitation when k_1 k_6 and k_3 are reduced by 10% at 9 10 and 15 seconds respectively. 2% noise case.

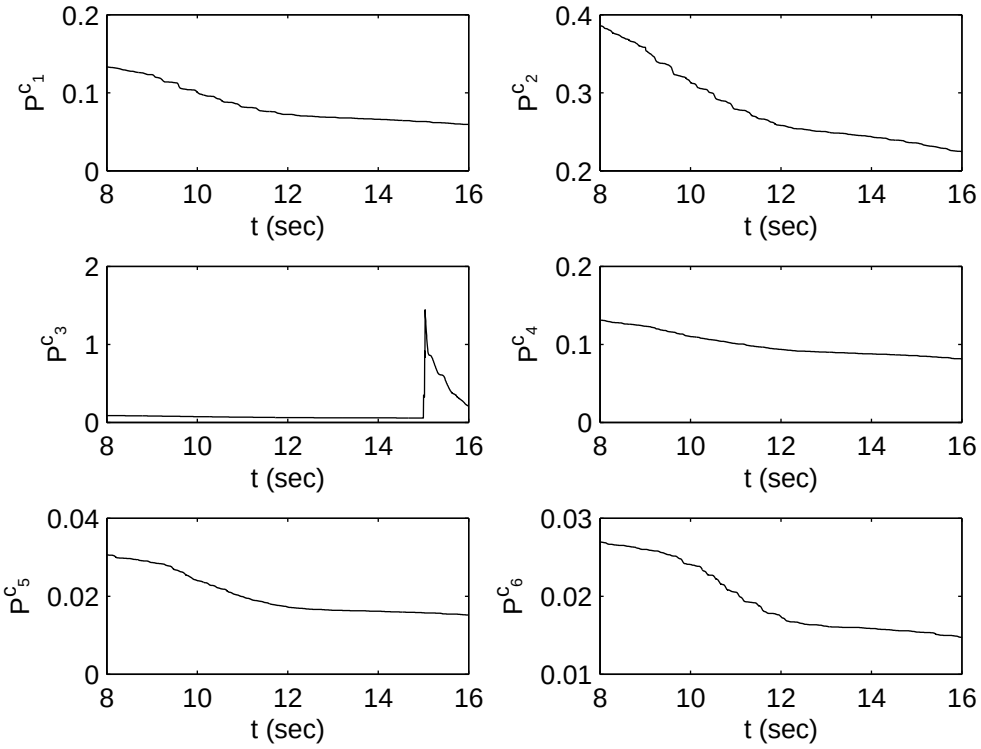

Figure 4.20: Diagonal elements of the covariance matrix corresponding to damping for the 6-DOF structure under base excitation when k_1 k_6 and k_3 are reduced by 10% at 9 10 and 15 seconds respectively. 2% noise case.

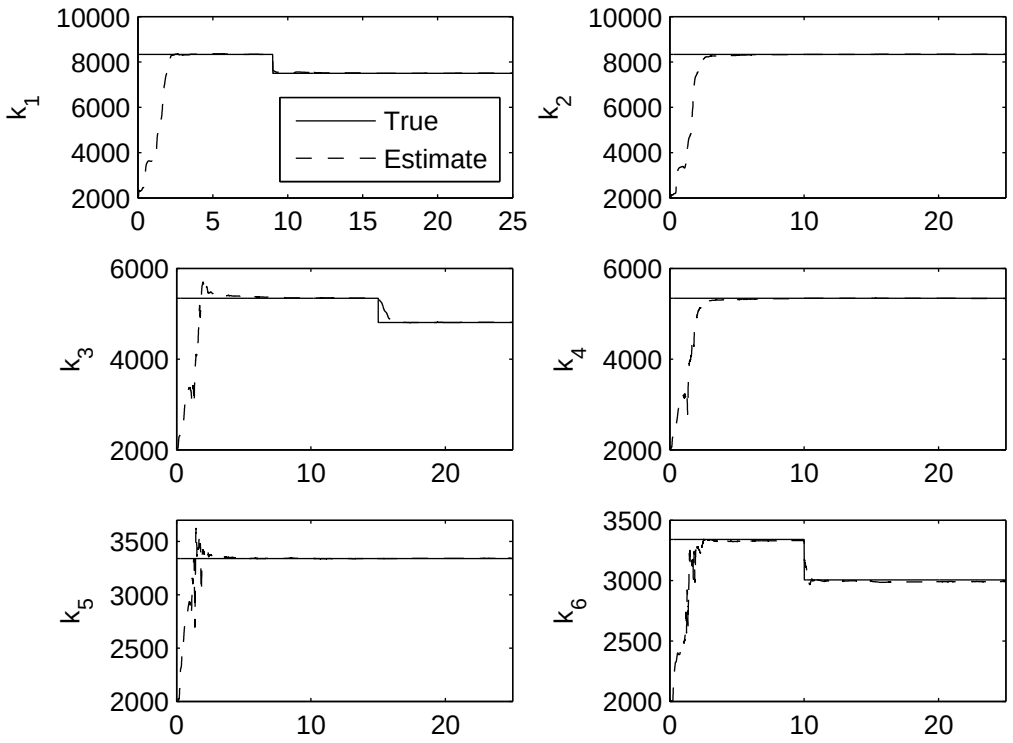

Figure 4.21: Estimated stiffness for the 6-DOF structure under base excitation when k_1 k_6 and k_3 are reduced by 10% at 9 10 and 15 seconds respectively. 2% noise case.

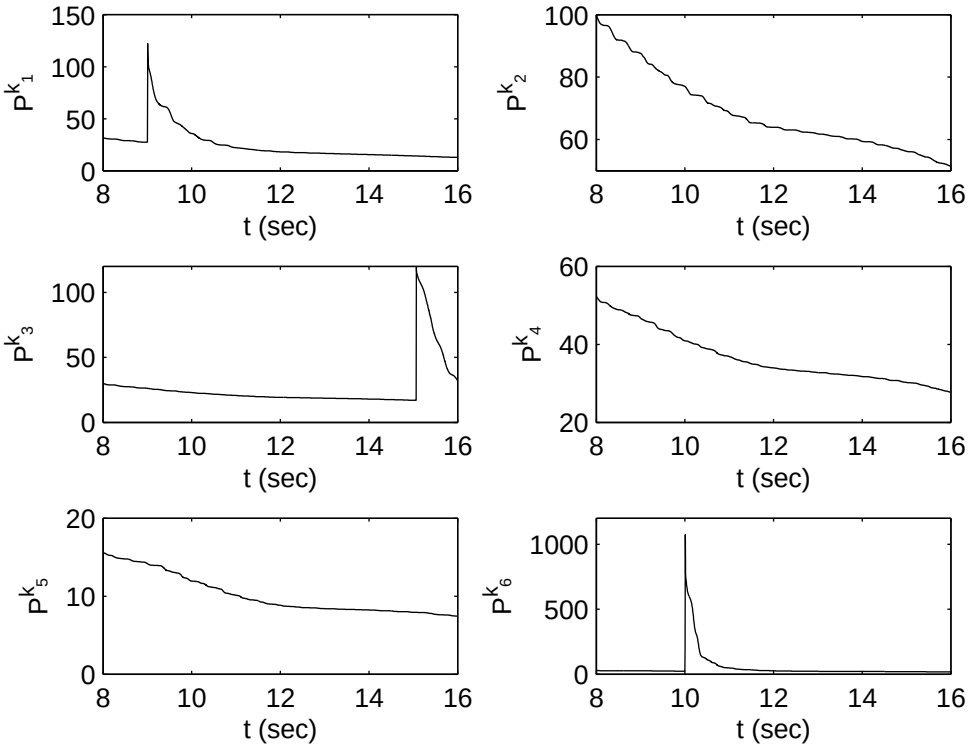

Figure 4.22: Diagonal elements of the covariance matrix corresponding to stiffness for the 6-DOF structure under base excitation when k_1 k_6 and k_3 are reduced by 10% at 9 10 and 15 seconds respectively. 2% noise case.

to such a nonlinear Kalman filter problem is to linearize the equation. Such linearizations, however, introduce errors in the predicted system. Since these nonlinearities are usually of the second order, in this chapter the use of the unscented transform, which is able to provide accurate estimates of the first two moments of the nonlinear terms needed in the implementation of the Kalman filter algorithm, has been explored. This enhanced Kalman filter approach applicable to nonlinear system has been called as unscented Kalman filter (UKF) approach.

However, by itself the UKF cannot track sudden changes in structural parameters. To detect such changes, in this chapter a new scheme is proposed which first detect when a sudden change occurs, and then from that time one it modifies the covariance matrix in such a way that sudden changes in structural parameters can be tracked. This new approach is called as the adaptive UKF (AUKF). The application of the AUKF in tracking changes in stiffness is illustrated through numerical simulations on a smaller two-DOF structure and a larger 6-DOF structure. It is shown that the AUKF is able to track single and multiple changes accurately. As is true with other estimation approaches, the performance of the AUKF also degrades in the presence of measurement noise thus pointing the need for collecting accurate measurements. The AUKF might also give false indication of a change, but such false positives usually disappear as the recursive algorithm advances to the following steps.

Chapter 5

Summary and Concluding Remarks

In the area of structural health monitoring methods are being developed for better and robust identification of damages. This study has been concerned with the vibration data based damage identification methods. The basic idea of such methods is to use the collected vibration response of a structure to identify and quantify damages. Such methods can be broadly classified as either modal parameter based methods or as model identification based methods. In the former, modal parameters are first extracted from vibration data and then subsequently used for damage identification. In the latter, the vibration data is directly used to estimate or update a mathematical model of the structure, and the parameters of this model are used for damage identification. In this study, both the modal parameter based method and model identification method for damage identification were developed. The theory behind these methods was developed in their individual chapters and based on the numerical studies conducted; the main conclusions which can be drawn are summarized below followed by a discussion on possible future studies.

5.1 Summary of Studies and Major Conclusions

Chapter 2 focused on the development of a new flexibility matrix-based damage identification approach. In this approach, the changes in flexibility matrix, called as the damage index matrix, of the system were related to the change in stiffness values of structural elements through the Taylor's series expansion. Knowing the damage index

matrix, an iterative scheme was suggested to solve for the unknown stiffness changes. The method was found to be effective for damage identification when used to detect and quantify various damage scenarios in the analytical benchmark problem. It was found that the performance of the method degraded with the decrease in the number of modes available for the estimation of the flexibility matrix. The numerical studies showed that with less number of modes it might be possible to identify the location of damage but the accuracy of the quantification process degraded. The concept of curvature flexibility is also explored with its application to framed structures where often the inertia-less rotational degrees of freedom are usually condensed out and cannot be measured. It was observed that though this can be used for damage identification including localization in the condensed system, but detecting damage in a specific element of the original expanded system may not be possible unless more element specific response data is collected.

Chapter 3 focused on the detection of time of occurrence of sudden changes in structural stiffness that may occur in a vibrating system exposed to overload. For real time damage identification of such occurrences, several studies have noted that the discrete wavelet transform (DWT) can be used to identify the damage instant corresponding to a sudden change in stiffness. These studies have shown that such damages are indicated by spikes in the plots of the level-1 details obtained using the DWT. Also, it had been observed that these spikes are lost, if the measurement noise level is high, thus making damage identification impossible in the presence of high noise levels. In this chapter, it was formally shown that a sudden change in stiffness introduced a jump discontinuity in the response acceleration. The size of this jump was shown to be proportional to the change in stiffness. Further, using the concept of Gibb's phenomenon it was shown that, if signals consisting of such discontinuities are passed through a high-pass filter, then they produce an output which is the scaled step response of the filter. The scaling factor was shown to be equal to the size of the jump discontinuity. These scaled step responses are what, in the past, have been referred to as spikes.

Following this, the application of high-pass filters, with appropriate cut-off frequency, in identifying sudden change in stiffness was studied. Through numerical

examples, the application of the high-pass filters in identifying sudden changes in stiffness was demonstrated. The effect of measurement noise on the ability to detect such sudden changes in stiffness was also outlined and demonstrated through numerical simulations. It was found that, as long as the contribution of measurement noise to the filter output was small, damage could be identified in the form of spikes. In particular, it was found that, if the measurement noise could be represented as filtered white noise, then damage could be identified even for large noise levels. Though the application of the high-pass filter allowed the identification of damage instant, it was noted that, for damage quantification, the knowledge of displacement values was needed.

Chapter 4 focused on the on-line estimation and tracking of sudden changes in stiffness. Such a problem can be put in the form of a state-estimation problem. One of the most popular methods to solve the state-estimation problem for systems described by linear state and measurement equation is the Kalman filter. However, if structural parameters like damping and stiffness are also treated as unknowns, along with displacement and velocities, then the state and measurement equations describing the system become nonlinear. For state-estimation, instead of using the process of linearization, leading to the extended Kalman filter, the unscented Kalman filter (UKF) was used. This was motivated by the fact that, the process of linearization of non-linear transformations, introduces error in the estimated mean and variance values. Such errors are less if the unscented transform (used in the UKF) is used.

It was shown that the standard application of the UKF was not able to track sudden parameter variations. To use the UKF to track sudden stiffness changes, a two step approach was developed. In the first step the occurrence of such changes was identified when a parameter related to the innovation value (which is the error in the estimated measurement) and its covariance attained a very large value. Next, having identified a change, the covariance matrix was modified in order to allow the UKF to correctly track the sudden change. The algorithm making use of this two step approach along with the traditional UKF was referred to as the adaptive unscented Kalman filter (AUKF). The application of the AUKF in tracking sudden stiffness changes was demonstrated through numerical examples. It was found that the AUKF was able to correctly track

such changes but the performance of the AUKF degraded with an increase in the measurement noise level. In particular, it was shown that the occurrence of damage could not be identified if the measurement noise level was too high.

5.2 Suggested Future studies

The flexibility based damage identification approach developed in this study is an off-line method. In contrast, the application of high-pass filters to detect sudden stiffness changes, and the use of the AUKF in tracking structural parameter values, are on-line methods. The effectiveness of each of these approaches has been demonstrated in this study. However, scope for improvement and further investigation still remains.

In the flexibility based damage identification approach it has been shown, through numerical examples that error in the estimated flexibility matrix, caused due to incomplete modal information, leads to errors in the damage identification procedure. Actual application of this technique for health monitoring of large civil engineering structures thus needs to be tested. In addition, the accuracy in the estimation of the flexibility matrix largely depends on the accuracy of the modal parameters extracted. Thus, robust methods for accurate estimation of modal parameters need to be further explored. The use of other measurement data such as dynamic strain measurements for better localization of the damage in practical applications also needs further exploration.

The damage identification approach based on the high-pass filter and the approach based on the AUKF can be implemented in real time. In the application of the high-pass filter for damage identification, the procedure can be applied at each sensor location where measurements are made, independent of other measurements. However, in the AUKF, acceleration values are needed at all the degrees-of-freedom simultaneously in order to estimate the state vector. Also, the computations would be carried out on some processor. Then all the measurements at different degrees-of-freedom need to be transferred to that processor. In this sense this approach is a centralized approach.

If we consider a structure with a large number of measurements, then in addition to computational costs, the cost of having to transfer all the measurements regularly to one centralized location might be an issue of concern. Therefore it is of interest to investigate if the approach of AUKF can be applied in some decentralized form.

Finally, for practical implementation, the possibility of coupling the two approaches, (the high-pass filters and the AUKF), need to be examined. Instead of having to continuously estimate the values of the state vector, the estimation can be triggered each time a sudden change in stiffness is identified by the high-pass filter technique. This might not be a very efficient technique for tracking sudden changes in stiffness values. Since each time the AUKF is triggered it will take some time to converge to the true set of values. But this can reduce the overall computational burden. Instead of having to run the AUKF continuously (which is computationally more expensive), the high-pass filtering can be continuously applied, and the AUKF can occasionally be used when triggered. The practical feasibility of such a scheme needs to be further investigated.

Appendix A

Extraction of Modal Parameters

In this appendix we briefly describe the approach that we have used for extracting the modal properties from the measured dynamic response for use in the proposed flexibility-based damage identification approach. The methods for extraction of modal properties from the dynamic response depend upon what information is available to extract them. In vibration of civil engineering structures, the responses that can possibly be measured are the accelerations, velocities, displacements, forces, and strains. However, the most common measurement one makes on civil engineering structure is for acceleration response primarily because the acceleration is, perhaps, the most convenient quantity to measure accurately in a vibrating structure. The type of modal identification approach to be used with such measured response also depends on whether or not the input causing the dynamic response is also available. If the input along with the output (acceleration) is available, then the approaches like ARX, stochastic subspace identification, or transfer function and peak picking methods can be use. Quite often, however, the excitation causing the motion may not be available. This happens in the structures that are excited by wind or other immeasurable forces. In such case the most popular methods that have been used are either the stochastic subspace identification (Overschee and De Moor (1996)) or the ERA approach (Juang and Papa (2001)). In the following, we present the very basic steps of the ERA approach as this was used in this study. Since to implement ERA it is necessary to have the free vibration response of the structure, this is usually obtained by the random decrement approach (Cole (1968,1973)) or through natural excitation technique NeXT (James *et*

al. (1993)). In our study we have used NeXT. In the following, we thus present a brief description of the natural excitation technique (NeXT) (James *et al.* (1993)) followed by the basic steps of eigensystem realization algorithm (ERA) used for calculating the modal parameters from the free vibration response.

A.1 Natural Excitation Technique (NeXT)

The NeXT is based on the observation that the displacement (and also the acceleration) correlation sequences satisfy the homogeneous equation of motion (James *et al.* (1993), Beck *et al.* (1994)). Consider the equation of motion of a multi-degree-of-freedom system under stationary excitation written as,

$$\mathbf{M}\ddot{x}(t_1) + \mathbf{C}\dot{x}(t_1) + \mathbf{K}x(t_1) = \mathbf{F}(t_1) \tag{A.1}$$

where **M C** and **K** are the mass damping and stiffness matrices, x is the displacement vector and **F** is the stationary input excitation. Multiplying the above equation by $x(t_2)$ and taking the expectation (denoted by $E[.]$),

$$\mathbf{M}E[\ddot{x}(t_1)x(t_2)] + \mathbf{C}E[\dot{x}(t_1)x(t_2)] + \mathbf{K}E[x(t_1)x(t_2)] = E[\mathbf{F}(t_1)x(t_2)] \tag{A.2}$$

which is equal to,

$$\mathbf{M}R_{\ddot{x}x}(t_1, t_2) + \mathbf{C}R_{\dot{x}x}(t_1, t_2) + \mathbf{K}R_{xx}(t_1, t_2) = R_{Fx}(t_1, t_2) \tag{A.3}$$

where it has been assumed that the mass damping and stiffness matrices are deterministic. Since the input and the response are (atleast) weakly stationary the derivative can be moved to obtain,

$$\mathbf{M}\ddot{R}_{xx}(\tau) + \mathbf{C}\dot{R}_{xx}(\tau) + \mathbf{K}R_{xx}(\tau) = R_{Fx}(\tau) \tag{A.4}$$

where $\tau = t_1 - t_2$ and the derivative of the correlation function is with respect to τ. Since for a causal system the present response is uncorrelated with future input we have,

$$\mathbf{M}\ddot{R}_{xx}(\tau) + \mathbf{C}\dot{R}_{xx}(\tau) + \mathbf{K}R_{xx}(\tau) = 0 \tag{A.5}$$

Therefore the displacement correlation sequences satisfy the homogeneous equation of motion. Beck *et al.* (1994) showed that the acceleration correlation sequence also satisfies the homogeneous differential equation. Therefore, given the measured acceleration response one can use the correlation sequence as the free vibration response.

A.2 Eigensystem Realization Algorithm (ERA)

In this study the ERA (Juang and Pappa (1985)) is used to calculate the matrices **A B C** and **D** used in the state-space representation of a multi-degree of freedom system. The eigenvalues and eigenvectors of the system matrix (**A**) then provide the modal parameters (natural frequencies, damping and mode-shapes). The algorithm requires the knowledge of the Hankel matrix **H** whose elements are the system Markov parameters (which can be estimated from measured acceleration response using the NeXT). The presentation on ERA is included for completeness and is mainly based on the text Juang and Phan (2001).

A.2.1 Markov Parameters for a Mdof System

The state-space model can be written as,

$$\dot{\mathbf{x}}(k+1) = \mathbf{A}\mathbf{x}(k) + \mathbf{B}\mathbf{u}(k)$$

$$\mathbf{y}(k) = \mathbf{C}\mathbf{x}(k) + \mathbf{D}\mathbf{u}(k)$$

where **x y** and **u** are the state measurement and the input vectors and **A B C** and **D** are matrices of appropriate dimension.

For a pulse input ($u(k) = 1$ for k=k, else $u(k) = 0$), and zero initial conditions, the output can be seen to be

$$\begin{aligned}
\mathbf{y}(k) &= \mathbf{Y}_0 = \mathbf{D} \\
\mathbf{y}(k+1) &= \mathbf{Y}_1 = \mathbf{CB} \\
\mathbf{y}(k+2) &= \mathbf{Y}_2 = \mathbf{CAB} \\
&\vdots \\
\mathbf{y}(k+h) &= \mathbf{Y}_h = \mathbf{CA}^{h-1}\mathbf{B}
\end{aligned}$$

The matrices **D**, **CB**, **CAB**, ... $\mathbf{CA}^{h-1}\mathbf{B}$ are commonly referred to as the Markov parameters of the system.

A.2.2 Hankel Matrix

The ERA uses the Hankel matrix,

$$\mathbf{H}(0) = \begin{bmatrix} \mathbf{Y}_1 & \mathbf{Y}_2 & \cdots & \mathbf{Y}_\gamma \\ \mathbf{Y}_2 & \mathbf{Y}_3 & \cdots & \mathbf{Y}_{\gamma+1} \\ \vdots & \vdots & \ddots & \cdots \\ \mathbf{Y}_p & \mathbf{Y}_{p+1} & \cdots & \mathbf{Y}_{p+\gamma-1} \end{bmatrix}$$

and

$$\mathbf{H}(1) = \begin{bmatrix} \mathbf{Y}_2 & \mathbf{Y}_3 & \cdots & \mathbf{Y}_{\gamma+1} \\ \mathbf{Y}_3 & \mathbf{Y}_4 & \cdots & \mathbf{Y}_{\gamma+2} \\ \vdots & \vdots & \ddots & \cdots \\ \mathbf{Y}_{p+1} & \mathbf{Y}_{p+2} & \cdots & \mathbf{Y}_{p+\gamma} \end{bmatrix}$$

In terms of the Markov parameters these can be written as,

$$\mathbf{H}(0) = \begin{bmatrix} \mathbf{CB} & \mathbf{CAB} & \cdots & \mathbf{CA}^{\gamma-1}\mathbf{B} \\ \mathbf{CAB} & \mathbf{CA}^2\mathbf{B} & \cdots & \mathbf{CA}^{\gamma}\mathbf{B} \\ \vdots & \vdots & \ddots & \cdots \\ \mathbf{CA}^{p-1}\mathbf{B} & \mathbf{CA}^{p}\mathbf{B} & \cdots & \mathbf{CA}^{p+\gamma-2}\mathbf{B} \end{bmatrix}$$

and

$$\mathbf{H}(1) = \begin{bmatrix} \mathbf{CAB} & \mathbf{CA}^2\mathbf{B} & \cdots & \mathbf{CA}^{\gamma}\mathbf{B} \\ \mathbf{CA}^2\mathbf{B} & \mathbf{CA}^3\mathbf{B} & \cdots & \mathbf{CA}^{\gamma+1}\mathbf{B} \\ \vdots & \vdots & \ddots & \cdots \\ \mathbf{CA}^{p}\mathbf{B} & \mathbf{CA}^{p+1}\mathbf{B} & \cdots & \mathbf{CA}^{p+\gamma-1}\mathbf{B} \end{bmatrix}$$

It can be seen that

$$\mathbf{H}(0) = \mathbf{P}_p\mathbf{O}_\gamma$$

where

$$\mathbf{P}_p = \begin{bmatrix} \mathbf{C} \\ \mathbf{CA} \\ \mathbf{CA}^2 \\ \vdots \\ \mathbf{CA}^{p-1} \end{bmatrix}$$

and is commonly referred to as the observability matrix and

$$\mathbf{O}_\gamma = \begin{bmatrix} \mathbf{B} & \mathbf{AB} & \mathbf{A}^2\mathbf{B} & \cdots & \mathbf{A}^{\gamma-1}\mathbf{B} \end{bmatrix}$$

is commonly referred to as the controllability matrix. Similarly

$$\mathbf{H}(1) = \mathbf{P}_p\mathbf{A}\mathbf{O}_\gamma$$

A.2.3 Algorithm

1. From the measured responses form the Hankel matrices $\mathbf{H}(0)$ and $\mathbf{H}(1)$.

2. Obtain the singular value decomposition of $\mathbf{H}(0)$.

$$\mathbf{H}(0) = \mathbf{R}\mathbf{\Sigma}\mathbf{S}^T$$

   Since

$$\mathbf{\Sigma} = \begin{bmatrix} \Sigma_n & 0 \\ 0 & 0 \end{bmatrix}$$

$$\mathbf{H}(0) = \mathbf{R}_n\mathbf{\Sigma}_n\mathbf{S}_n^T$$

   where $\mathbf{R}_n$ and $\mathbf{S}_n$ are matrices formed by the first n columns of $\mathbf{R}$ and $\mathbf{S}$ respectively.

3. Form the observability and controllability matrices using

$$\mathbf{H}(0) = [\mathbf{R}_n\mathbf{\Sigma}_n^{\frac{1}{2}}][\mathbf{\Sigma}_n^{\frac{1}{2}}\mathbf{S}_n^T] \cong \mathbf{P}_p\mathbf{O}_\gamma$$

4. Obtain $\mathbf{B}$ and $\mathbf{C}$ from $\mathbf{P}_p$ and $\mathbf{O}_\gamma$.

5. Obtain $\mathbf{A}$ from

$$\mathbf{A} = \mathbf{\Sigma}_n^{-\frac{1}{2}}\mathbf{R}_n^T\mathbf{H}(1)\mathbf{S}_n\mathbf{\Sigma}_n^{-\frac{1}{2}}$$

   this follows from

$$\mathbf{H}(1) = \mathbf{P}_p\mathbf{A}\mathbf{O}_\gamma = [\mathbf{R}_n\mathbf{\Sigma}_n^{\frac{1}{2}}]A[\mathbf{\Sigma}_n^{\frac{1}{2}}\mathbf{S}_n^T]$$

Once the system matrix $\mathbf{A}$ has been estimated its eigenvalues and eigenvectors provide the natural frequencies damping and mode-shapes for the system.

In implementing the ERA certain things need to be noted. The eigenvectors of the system matrix **A** need to be pre-multiplied by the measurement matrix **C** in order to obtain the mode-shape values at the sensor location. When working with data, it is common to end up with several estimated modes which actually are not structural modes. This may be caused due to noise in the measurement data or other numerical errors. Therefore some common checks can be done in order to decide which modes to retain. In this study the mode phase collinearity (MPC) (Pappa and Elliott (1993)) was used. For a classical normal mode all the degrees of freedom attain their extreme locations at the same time. In other words the phase angles of the elements of a complex mode vector are either all in-phase or out-of-phase. The MPC is a measure of how close a mode is to a classical normal mode. The value of the MPC varies between 0 and 100. Where 100 indicates a perfect normal mode characteristic. Again, due to numerical and measurement errors even for a true structural mode the MPC value might not exactly be 100. In this study any mode with a MPC of greater than 90 was accepted to be a structural mode.

Appendix B

Rate of Change of Modal Frequencies and Mode Shapes for Classical Eigenvalue Problem

In this Appendix the expressions for the first and higher order rates of change used in damage identification in this study are listed. The first order rates are available in literature for classical eigenvalue problems (Fox and Kapoor (1968)) and for nonclassically damped systems (Ashtiany and Singh (1982)). These have been used by Zhao and DeWolf (1999) and by Singh and Bisht (2006) in structural health monitoring related studies. For the calculation of the first order rates of change the steps used below parallel those used in Fox and Kapoor (1968) and Zhao and DeWolf (1999) and .

Consider a n degree-of-freedom system. The eigenvalue problem for the undamped system is given by,

$$\left(\mathbf{K} - \omega_r^2 \mathbf{M}\right) \phi_r = \{0\} \tag{B.1}$$

where $r = 1, 2 \ldots n$, $\mathbf{K}$ and $\mathbf{M}$ are the $n \times n$ stiffness and mass matrices, ω_r and ϕ_r are the r^{th} natural frequency and mode shape and $\{0\}$ is a zero vector of size $n \times 1$. It is assumed that the mass matrix is independent of the stiffness terms k_i. Also, the mode shapes are assumed to be mass normalized i.e.

$$\phi_p^T \mathbf{M} \phi_q = \delta_{pq} \tag{B.2}$$

where $\delta_{pq} = 1$ if $p = q$ else $\delta_{pq} = 0$.

B.1 Rates of Change of Modal Frequencies

Taking the partial derivative of Eq. B.1 with respect to k_i (the i^{th} stiffness element) we obtain,

$$\left[\frac{\partial \mathbf{K}}{\partial k_i} - 2\omega_w \frac{\partial \omega_r}{\partial k_i}\mathbf{M} - \omega_r^2 \frac{\partial \mathbf{M}}{\partial k_i} + \right] \phi_r + \left(\mathbf{K} - \omega_r^2 \mathbf{M}\right) \frac{\partial \phi_r}{\partial k_i}$$

Premultiplying the above equation with ϕ_r^T and using Eqs. B.1 and B.2,

$$\frac{\partial \omega_r}{\partial k_i} = \frac{1}{2\omega_r} \phi_r^T \frac{\partial \mathbf{K}}{\partial k_i} \phi_r \tag{B.3}$$

Taking the partial derivative of the above equation with respect to k_j we obtain,

$$\frac{\partial^2 \omega_r}{\partial k_j \partial k_i} = -\frac{1}{2\omega_r^2} \frac{\partial \omega_r}{\partial k_j} \phi_r^T \frac{\partial \mathbf{K}}{\partial k_i} \phi_r + \frac{1}{2\omega_r} \frac{\partial \phi_r^T}{\partial k_j} \frac{\partial \mathbf{K}}{\partial k_i} \phi_r + \frac{1}{2\omega_r} \phi_r^T \frac{\partial^2 \mathbf{K}}{\partial k_j \partial k_i} \phi_r + \frac{1}{2\omega_r} \phi_r^T \frac{\partial \mathbf{K}}{\partial k_i} \frac{\partial \phi_r}{\partial k_j}$$

or

$$\frac{\partial^2 \omega_r}{\partial k_j \partial k_i} = -\frac{1}{\omega_r} \frac{\partial \omega_r}{\partial k_j} \frac{\partial \omega_r}{\partial k_i} + \frac{1}{2\omega_r} \left\{ \frac{\partial \phi_r^T}{\partial k_j} \frac{\partial \mathbf{K}}{\partial k_i} \phi_r + \phi_r^T \frac{\partial^2 \mathbf{K}}{\partial k_j \partial k_i} \phi_r + \phi_r^T \frac{\partial \mathbf{K}}{\partial k_i} \frac{\partial \phi_r}{\partial k_j} \right\} \tag{B.4}$$

Taking the partial derivative of the above equation with respect to k_q we obtain,

$$\begin{aligned} \frac{\partial^3 \omega_r}{\partial k_q \partial k_j \partial k_i} = &-\frac{1}{\omega_r} \frac{\partial \omega_r}{\partial k_q} \frac{\partial^2 \omega_r}{\partial k_j \partial k_i} + \frac{1}{2\omega_r} \left\{ \frac{\partial^2 \phi_r^T}{\partial k_q \partial k_j} \frac{\partial \mathbf{K}}{\partial k_i} \phi_r + \frac{\partial \phi_r^T}{\partial k_j} \frac{\partial^2 \mathbf{K}}{\partial k_q \partial k_i} \phi_r + \frac{\partial \phi_r^T}{\partial k_j} \frac{\partial \mathbf{K}}{\partial k_i} \frac{\partial \phi_r}{\partial k_q} \right. \\ &\frac{\partial \phi_r^T}{\partial k_q} \frac{\partial^2 \mathbf{K}}{\partial k_j \partial k_i} \phi_r + \phi_r^T \frac{\partial^3 \mathbf{K}}{\partial k_q \partial k_j \partial k_i} \phi_r + \phi_r^T \frac{\partial^2 \mathbf{K}}{\partial k_j \partial k_i} \frac{\partial \phi_r}{\partial k_q} + \\ &\left. \frac{\partial \phi_r^T}{\partial k_q} \frac{\partial \mathbf{K}}{\partial k_i} \frac{\partial \phi_r}{\partial k_j} + \phi_r^T \frac{\partial^2 \mathbf{K}}{\partial k_q \partial k_i} \frac{\partial \phi_r}{\partial k_j} + \phi_r^T \frac{\partial \mathbf{K}}{\partial k_i} \frac{\partial^2 \phi_r}{\partial k_q \partial k_j} \right\} \end{aligned} \tag{B.5}$$

Eqs. B.3, B.4 and B.5 provide the expressions for the first, second and third order rates of change of modal frequencies respectively. The rates of change of mode shapes needed in these equations are given in the next section.

B.2 Rates of Change of Mode Shapes

Following the steps outlined in Fox and Kapoor (1968) the first order rate of change of mode shapes can be written as,

$$\frac{\partial \phi_r}{\partial k_i} = \sum_{s=1}^{n} \alpha_s \phi_s \tag{B.6}$$

where

$$\alpha_s = \begin{cases} \frac{1}{\omega_r^2 - \omega_s^2} \phi_s^T \frac{\partial \mathbf{K}}{\partial k_i} \phi_r & s \neq r \\ 0 & s = r \end{cases} \tag{B.7}$$

Taking the partial derivative with respect to k_j for the expression of α_s for the case when $s \neq r$ we obtain,

$$\frac{\partial \alpha_s}{\partial k_j} = -\frac{1}{(\omega_r^2 - \omega_s^2)^2} 2\omega_r \frac{\partial \omega_r}{\partial k_j} \phi_s^T \frac{\partial \mathbf{K}}{\partial k_i} \phi_r + \frac{1}{(\omega_r^2 - \omega_s^2)^2} 2\omega_s \frac{\partial \omega_s}{\partial k_j} \phi_s^T \frac{\partial \mathbf{K}}{\partial k_i} \phi_r$$

$$+ \frac{1}{\omega_r^2 - \omega_s^2} \frac{\partial \phi_s^T}{\partial k_j} \frac{\partial \mathbf{K}}{\partial k_i} \phi_r + \frac{1}{\omega_r^2 - \omega_s^2} \phi_s^T \frac{\partial^2 \mathbf{K}}{\partial k_j \partial k_i} \phi_r + \frac{1}{\omega_r^2 - \omega_s^2} \phi_s^T \frac{\partial \mathbf{K}}{\partial k_i} \frac{\partial \phi_r}{\partial k_j}$$

or

$$\frac{\partial \alpha_s}{\partial k_j} = \frac{2}{\omega_r^2 - \omega_s^2} \alpha_s \left\{ -\omega_r \frac{\partial \omega_r}{\partial k_j} + \omega_s \frac{\partial \omega_s}{\partial k_j} \right\}$$

$$+ \frac{1}{\omega_r^2 - \omega_s^2} \left\{ \frac{\partial \phi_s^T}{\partial k_j} \frac{\partial \mathbf{K}}{\partial k_i} \phi_r + \phi_s^T \frac{\partial^2 \mathbf{K}}{\partial k_j \partial k_i} \phi_r + \phi_s^T \frac{\partial \mathbf{K}}{\partial k_i} \frac{\partial \phi_r}{\partial k_j} \right\} \tag{B.8}$$

Taking the partial derivative of Eq. B.6 with respect to k_j the second order rate of change of mode shape can be written as

$$\frac{\partial^2 \phi_r}{\partial k_j \partial k_i} = \sum_{s=1}^{n} \left\{ \frac{\partial \alpha_s}{\partial k_j} \phi_s + \alpha_s \frac{\partial \phi_s}{\partial k_j} \right\} \tag{B.9}$$

where the partial derivatives on the right hand side can be calculated using Eqs. B.6, B.7 and B.8. Taking the partial derivative of Eq. B.8 with respect to k_q we obtain,

$$\frac{\partial^2 \alpha_s}{\partial k_q \partial k_j} = T_1 + T_2 + T + 3 \tag{B.10}$$

where,

$$T_1 = 2 \left\{ -\omega_r \frac{\partial \omega_r}{\partial k_q} + \omega_s \frac{\partial \omega_s}{\partial k_q} \right\} \frac{\partial \alpha_s}{\partial k_j}$$

$$T_2 = \frac{1}{\omega_r^2 - \omega_s^2} \left\{ 2 \frac{\partial \alpha_s}{\partial k_q} \left(-\omega_r \frac{\partial \omega_r}{\partial k_j} + \omega_s \frac{\partial \omega_s}{\partial k_j} \right) \right.$$

$$\left. + 2\alpha_s \left(-\frac{\partial \omega_r}{\partial k_q} \frac{\partial \omega_r}{\partial k_j} + -\omega_r \frac{\partial^2 \omega_r}{\partial k_q \partial k_j} + \frac{\partial \omega_s}{\partial k_q} \frac{\partial \omega_s}{\partial k_j} + \omega_s \frac{\partial^2 \omega_s}{\partial k_q \partial k_j} \right) \right\}$$

and

$$T_3 = \frac{1}{\omega_r^2 - \omega_s^2} \left\{ \frac{\partial^2 \phi_s^T}{\partial k_q \partial k_j} \frac{\partial \mathbf{K}}{\partial k_i} \phi_r + \frac{\partial \phi_s^T}{\partial k_j} \frac{\partial^2 \mathbf{K}}{\partial k_q \partial k_i} \phi_r + \frac{\partial \phi_s^T}{\partial k_j} \frac{\partial \mathbf{K}}{\partial k_i} \frac{\partial \phi_r}{\partial k_q} \right.$$

$$\left. + \frac{\partial \phi_s^T}{\partial k_q} \frac{\partial^2 \mathbf{K}}{\partial k_j \partial k_i} \phi_r + \phi_s^T \frac{\partial^3 \mathbf{K}}{\partial k_q \partial k_j \partial k_i} \phi_r + \phi_s^T \frac{\partial^2 \mathbf{K}}{\partial k_j \partial k_i} \frac{\partial \phi_r}{\partial k_q} \right.$$

$$\frac{\partial \phi_s^T}{\partial k_q}\frac{\partial \mathbf{K}}{\partial k_i}\frac{\partial \phi_r}{\partial k_j} + \phi_s^T\frac{\partial^2 \mathbf{K}}{\partial k_q \partial k_i}\frac{\partial \phi_r}{\partial k_j} + \phi_s^T\frac{\partial \mathbf{K}}{\partial k_i}\frac{\partial^2 \phi_r}{\partial k_q \partial k_j}\Bigg\}$$

Taking the partial derivative of Eq. B.9 The third order rate of change of mode shape can be written as

$$\frac{\partial^3 \phi_r}{\partial k_q \partial k_j \partial k_i} = \sum_{s=1}^{n}\left\{\frac{\partial^2 \alpha_s}{\partial k_q \partial k_j}\phi_s + \frac{\partial \alpha_s}{\partial k_j}\frac{\partial \phi_s}{\partial k_q} + \frac{\partial \alpha_s}{\partial k_q}\frac{\partial \phi_s}{\partial k_j} + \alpha_s\frac{\partial^2 \phi_s}{\partial k_q \partial k_j}\right\} \tag{B.11}$$

where the required partial derivatives of α are given by Eqs. B.8 and B.10 and those of the mode shape are given by Eqs. B.6 and B.9. Note that for $s = r$ α_s and all its partial derivatives are zero.

Appendix C

State and Measurement Equations for the 6-DOF Example

In this appendix the expressions for the state and measurement equations for the 6-DOF shear beam model considered in the AUKF study are given.

The equation of motion for this system can be written as,

$$\mathbf{M}\ddot{\mathbf{q}} + \mathbf{C}\dot{\mathbf{q}} + \mathbf{K}\mathbf{q} = -\mathbf{M}\gamma u \tag{C.1}$$

where $\mathbf{M}$, $\mathbf{C}$, and $\mathbf{K}$ are the mass damping and stiffness matrices, $\mathbf{q}$ is the displacement vector, γ is the influence vector and u is the input excitation. These matrices and vectors are given by:

$$\mathbf{M} = \begin{bmatrix} m_1 & 0 & 0 & 0 & 0 & 0 \\ 0 & m_2 & 0 & 0 & 0 & 0 \\ 0 & 0 & m_3 & 0 & 0 & 0 \\ 0 & 0 & 0 & m_4 & 0 & 0 \\ 0 & 0 & 0 & 0 & m_5 & 0 \\ 0 & 0 & 0 & 0 & 0 & m_6 \end{bmatrix}$$

$$\mathbf{C} = \begin{bmatrix} c_1 + c_2 & -c_2 & 0 & 0 & 0 & 0 \\ -c_2 & c_2 + c_3 & -c_3 & 0 & 0 & 0 \\ 0 & -c_3 & c_3 + c_4 & -c_4 & 0 & 0 \\ 0 & 0 & -c_4 & c_4 + c_5 & -c_5 & 0 \\ 0 & 0 & 0 & -c_5 & c_5 + c_6 & -c_6 \\ 0 & 0 & 0 & 0 & -c_6 & c_6 \end{bmatrix}$$

$$\mathbf{K} = \begin{bmatrix} k_1 + k_2 & -k_2 & 0 & 0 & 0 & 0 \\ -k_2 & k_2 + k_3 & -k_3 & 0 & 0 & 0 \\ 0 & -k_3 & k_3 + k_4 & -k_4 & 0 & 0 \\ 0 & 0 & -k_4 & k_4 + k_5 & -k_5 & 0 \\ 0 & 0 & 0 & -k_5 & k_5 + k_6 & -k_6 \\ 0 & 0 & 0 & 0 & -k_6 & k_6 \end{bmatrix}$$

$$\mathbf{q} = \begin{Bmatrix} q_1 \\ q_2 \\ q_3 \\ q_4 \\ q_5 \\ q_6 \end{Bmatrix} \quad \gamma = \begin{Bmatrix} 1 \\ 1 \\ 1 \\ 1 \\ 1 \\ 1 \end{Bmatrix}$$

in which m_i, c_i and k_i (for $i = 1 \ldots 6$) are the i^{th} story mass damping and stiffness coefficients. Considering the displacements velocities dampings and stiffnesses as unknowns to be estimated, the state vector is defined as,

$$x = \left\{ \begin{array}{c} x_1 \\ x_2 \\ x_3 \\ x_4 \\ x_5 \\ x_6 \\ x_7 \\ x_8 \\ x_9 \\ x_{10} \\ x_{11} \\ x_{12} \\ x_{13} \\ x_{14} \\ x_{15} \\ x_{16} \\ x_{17} \\ x_{18} \\ x_{19} \\ x_{20} \\ x_{21} \\ x_{22} \\ x_{23} \\ x_{24} \end{array} \right\} = \left\{ \begin{array}{c} q_1 \\ q_2 \\ q_3 \\ q_4 \\ q_5 \\ q_6 \\ \dot{q_1} \\ \dot{q_2} \\ \dot{q_3} \\ \dot{q_4} \\ \dot{q_5} \\ \dot{q_6} \\ c_1 \\ c_2 \\ c_3 \\ c_4 \\ c_5 \\ c_6 \\ k_1 \\ k_2 \\ k_3 \\ k_4 \\ k_5 \\ k_6 \end{array} \right\}$$

The length of the state vector in this case is 24 (6 displacements velocities damping and stiffness coefficients). Using this state vector and the equation of motion for the

6-DOF system, the state equation can be written as,

$$\dot{x} = \begin{Bmatrix} \dot{x_1} \\ \dot{x_2} \\ \dot{x_3} \\ \dot{x_4} \\ \dot{x_5} \\ \dot{x_6} \\ \dot{x_7} \\ \dot{x_8} \\ \dot{x_9} \\ \dot{x_{10}} \\ \dot{x_{11}} \\ \dot{x_{12}} \\ \dot{x_{13}} \\ \dot{x_{14}} \\ \dot{x_{15}} \\ \dot{x_{16}} \\ \dot{x_{17}} \\ \dot{x_{18}} \\ \dot{x_{19}} \\ \dot{x_{20}} \\ \dot{x_{21}} \\ \dot{x_{22}} \\ \dot{x_{23}} \\ \dot{x_{24}} \end{Bmatrix} = \begin{Bmatrix} x_7 \\ x_8 \\ x_9 \\ x_{10} \\ x_{11} \\ x_{12} \\ \frac{1}{m_1}((x_{13}+x_{14})x_7 + x_{14}x_8 - (x_{19}+x_{20})x_1 + x_{20}x_2) - m_1u) \\ \frac{1}{m_2}(x_{14}x_7 - (x_{14}+x_{15})x_8 + x_{15}x_9 + x_{20}x_1 - (x_{20}+x_{21})x_2 + x_{21}x_3) - m_2u) \\ \frac{1}{m_3}(x_{15}x_8 - (x_{15}+x_{16})x_9 + x_{16}x_{10} + x_{21}x_2 - (x_{21}+x_{22})x_3 + x_{22}x_4) - m_3u) \\ \frac{1}{m_4}(x_{16}x_9 - (x_{16}+x_{17})x_{10} + x_{17}x_{11} + x_{22}x_3 - (x_{22}+x_{23})x_4 + x_{23}x_5) - m_4u) \\ \frac{1}{m_5}(x_{17}x_{10} - (x_{17}+x_{18})x_{11} + x_{18}x_{12} + x_{23}x_4 - (x_{23}+x_{24})x_5 + x_{24}x_6) - m_5u) \\ \frac{1}{m_6}(x_{18}x_{11} - x_{18}x_{12} + x_{24}x_5 - x_{24}x_6) - m_6u) \\ 0 \\ 0 \\ 0 \\ 0 \\ 0 \\ 0 \\ 0 \\ 0 \\ 0 \\ 0 \\ 0 \\ 0 \end{Bmatrix}$$

With the absolute acceleration as the available measurements, the measurement equa-

tion is given by,

$$y = \begin{Bmatrix} y_1 \\ y_2 \\ y_3 \\ y_4 \\ y_5 \\ y_6 \end{Bmatrix} = \begin{Bmatrix} \ddot{q_1} + u \\ \ddot{q_2} + u \\ \ddot{q_3} + u \\ \ddot{q_4} + u \\ \ddot{q_5} + u \\ \ddot{q_6} + u \end{Bmatrix} =$$

$$\begin{Bmatrix} \frac{1}{m_1}((x_{13} + x_{14})x_7 + x_{14}x_8 - (x_{19} + x_{20})x_1 + x_{20}x_2)) \\ \frac{1}{m_2}(x_{14}x_7 - (x_{14} + x_{15})x_8 + x_{15}x_9 + x_{20}x_1 - (x_{20} + x_{21})x_2 + x_{21}x_3)) \\ \frac{1}{m_3}(x_{15}x_8 - (x_{15} + x_{16})x_9 + x_{16}x_{10} + x_{21}x_2 - (x_{21} + x_{22})x_3 + x_{22}x_4)) \\ \frac{1}{m_4}(x_{16}x_9 - (x_{16} + x_{17})x_{10} + x_{17}x_{11} + x_{22}x_3 - (x_{22} + x_{23})x_4 + x_{23}x_5)) \\ \frac{1}{m_5}(x_{17}x_{10} - (x_{17} + x_{18})x_{11} + x_{18}x_{12} + x_{23}x_4 - (x_{23} + x_{24})x_5 + x_{24}x_6)) \\ \frac{1}{m_6}(x_{18}x_{11} - x_{18}x_{12} + x_{24}x_5 - x_{24}x_6)) \end{Bmatrix}$$

Bibliography

[Adams *et al.* (1978)] Adams, R. D., Cawley P., Pye C. J. and Stone, B. J. (1978) "Vibration Technique for non-destructively assessing the integrity of structures", *Journal of Mechanical Engineering Science*, 20, 93-100.

[Alampalli *et al.* (2005)] Alampalli, S., Ettouney, M. M. and Agarwal, A. K. (2005) "Structural health monitoring for bridge maintenance", *Bridge Structures*, 1, 3, 345-354.

[Allemang (2002)] Allemang R. J. (2002) "The modal assurance criterion (MAC): twenty years of use and abuse", *Proceedings of 20th International Modal Analysis Conference*, Los Angeles, CA, USA, 397-405.

[Amaravadi *et al.* (2001)] Amaravadi V., Rao V. and Koval L. R. (2001) "Structural health monitoring using wavelet transforms", *Proceedings of SPIE - Smart Structures and Materials*, 4327, 258-269.

[Ashtiany and Singh (1982)] Ashtiany, M. G. and Singh, M. P. (1982) "Seismic response of structural system with random parameter", *Technical report No. PFR-8023978*, Virginia Polytechnic Institute and State University, Blacksburg, VA, USA.

[Atalla and Orisamolu (2001)] Atalla, M. J. and Orisamolu, I. R. (2001) "Framework for remote inspection and health management of engineered systems", *Proceedings of the* 3rd *International Workshop on Structural Health Monitoring*, Stanford, CA, USA, 713-722.

[Basu *et al.* (2008)] Basu B, Nagarajaiah S, Chakraborty A. Online identification of linear time varying stiffness of structural systems by wavelet analysis *Structural Health Monitoring* 2008; **7**(1):21-36.

[Bayissa *et al.* (2008)] Bayissa W. L., Haritos N. and Thelandersson S. (2008) "Vibration based structural damage identification using wavelet transform", *Mechanical Signal and Signal Processing*, 22, 1194-1215.

[Beck *et al.* (1994)] Beck, J. L., Vanik, M. W., and Katafygiotis, L. S. (1994) "Determination of model parameters from ambient vibration data for structural health monitoring." Proc., 1st World Conf. on Structural Control, Pasadena, Calif., 3-12.

[Bernal (2002)] Bernal, D. (2002) "Load vectors for damage localization", *Journal of Engineering Mechanics*, 128, 1, 7-14.

[Bernal (2006)] Bernal, D. (2006) "Flexibility-based damage localization for stochastic realization results", *Journal of Engineering Mechanics*, 132, 6, 651-658.

[Bernal and Gunes (2004)] Bernal, D. and Gunes B. (2004) "Flexibility based approach for damage characterization: Benchmark application," *Journal of Engineering Mechanics*, 130, 1, 61-70.

[Bisht and Singh (2006a)] Bisht, S. S. and Singh, M. P. (2006a) "Damage detection and quantification in shear beam buildings", 4^{th} *International Conference on Earthquake Engineering*, Taipei, Taiwan.

[Bisht and Singh (2006b)] Bisht, S. S. and Singh, M. P. (2006b) "Damage detection and quantification using damage indices: comparison of flexibility and rotational flexibility", *US-Taiwan Workshop on Smart Structural Technology for Seismic Hazard Mitigation*, Taipei, Taiwan.

[Carden and Fanning (2004)] Carden E. P. and Fanning P. (2004) "Vibration based condition monitoring: A review", *Structural Health Monitoring*, 3, 4, 355-377.

[Chang *et al.* (2003)] Chang, P. C., Flatau, A. and Liu S. C. (2003) "Review paper: Health monitoring of civil infrastructure", *Structural Health Monitoring*, 2, 3, 257-267.

[Chang and Chen (2003)] Chang C. C and Chen L-W. (2003) "Vibration damage detection of a Timoshenko beam by spatial wavelet based approach", *Applied Acoustics*, 64, 1217-1240.

[Chang and Chen (2004)] Chang C. C and Chen L-W. (2004) "Damage detection of a rectangular plate by spatial wavelet based approach", *Applied Acoustics*, 65, 8, 819-832.

[Chang and Liu, 2003] Chang, P. C. and Liu, S. C. (2003) "Recent research in nondestructive evaluation of civil infrastructures", *Journal of Materials in Civil Engineering*, 15, 3, 298-304.

[Chase *et al.* (2005a)] Chase, J. G., Hwang, K. L., Barroso, L. R. and Mander, J. B. (2005a) "A simple LMS based approach to the structural health monitoring benchmark problem", *Earthquake Engineering and Structural Dynamics*, 34, 575-594.

[Chase *et al.* (2005b)] Chase, J. G., Begoc, V. and Barroso, L. R. (2005b) "Efficient structural health monitoring for a benchmark structure using adaptive RLS filters" *Computers and Structures*, 83, 639-647.

[Chatzi and Smyth (2009)] Chatzi, E. N. and Smyth, A. W. (2009) "The unscented Kalman filter and particle filter methods for nonlinear structural system identification with non-collocated heterogeneous sensing", *Structural Control and Health Monitoring*, 16, 99-123.

[Chen *et al.* (2007)] Chen H. G., Yan Y. J., Chen W. H., Jiang J. S., Yu L. and Wu Z. Y. (2007) "Early damage detection in composite wingbox structures using Hilbert-Huang transform and genetic algorithm", *Structural Health Monitoring*, 6, 4, 281-297.

[Choy *et al.* (1995)] Choy F. K., Liang R., and Xu P. (1995) "Fault identification of beams on elastic foundation", *Computers and Geotechnics*, 17, 157-176.

[Cole (1968)] Cole H. A. (1968) "On-the-line analysis of random vibrations", *AIAA*, 68-288.

[Cole (1973)] Cole, H. A. (1973) "On line failure detection and damping measurement of aerospace structures by random decrement signature", *NASA CR-2205*.

[Demetriou and Hou (2003)] Demetriou M. A. and Hou Z. (2003) "On-line fault/damage detection schemes for mechanical and structural systems", *Journal of Structural Control*, 10, 1-23.

[Doebling *et al.*, 1996] Doebling, S. W., Farrar, C. R., Prime, M. B., and Shevitz, D. W. (1996) "Damage identification and health monitoring of structural and mechanical systems from changes in their vibration characteristics: A literature review", *Los Alamos National Laboratory Report*, LA-13070-MS.

[Duan *et al.* (2004)] Duan, Z., Yan, G., and Ou, J. (2004) "Structural damage localization based on rotational flexibility", *Proceedings of the* 3^{rd} *International Conference on Earthquake Engineering*, 846-850.

[Duan *et al.* (2005a)] Duan, Z., Li, X. R., Han, C. and Zhu H. (2005) "Sequential unscented Kalman filter for radar target tracking with range rate measurements", 7^{th} *International Conference on Information Fusion*, 130-137.

[Duan *et al.* (2005b)] Duan, Z., Yan, G., Ou, J., and Spencer, B. F. (2005) "Damage localization in ambient vibration by constructing proportional flexibility matrix", *Journal of Sound and Vibration*, 284, 455-466.

[Fortescue *et al.* (1981)] Fortescue, T. R., Kershenbaum, L. S., and Ydstie, B. E. (1981) "Implementation of self-tuning regulator with variable forgetting factor", *Automatica*, 17, 6, 831-835.

[Fox and Kapoor (1968)] Fox, R. L. and Kapoor, M. P. (1968) "Rate of change of eigenvalues and eigenvectors", *AIAA Journal*, 6, 12.

[Gao *et al.* (2007)] Gao, Y., Spencer, B. F., and Bernal, D. (2007) "Experimental verification of the flexibility-based damage locating vector method", *Journal of Engineering Mechanics*, 133, 10, 1043-1049.

[Gao and Spencer (2002)] Gao, Y., and Spencer, B. F., Jr., (2002) "Damage localization under ambient vibration using changes in flexibility", *Journal of Earthquake Engineering and Engineering Vibration*, 1, 1, 136-144.

[Hagglud, 1984] Hagglud, T. (1984) "Adaptive control of systems subject to large parameter changes", *International Federation of Automatic Control 9th Triennial World Conference*, Budapest, Hungary, 993-998.

[Hearn and Testa (1991)] Hearn, G. and Testa, R. B. (1991) "Modal analysis for damage detection in structures", *Journal of Structural Engineering*, 117, 10, 3042-3063.

[Hera and Hou (2004)] Hera A. and Hou Z. (2004) "Application of wavelet approach for ASCE structural health monitoring benchmark studies", *Journal of Engineering Mechanics*, 130, 1, 96-104.

[Hong *et al.* (2002)] Hong J. C., Kim Y. Y., Lee H. C. and Lee Y. W. (2002) "Damage detection using the Lipschitz exponent estimated by the wavelet transform: applications to vibration modes of a beam" *International Journal of Solids and Structures*, 39, 7, 1803-1816.

[Hou *et al.* (2000)] Hou Z., Noori M., Amand, RSt. (2000) "Wavelet-based approach for structural damage detection", *Journal of Engineering Mechanics*, 126, 7, 677-683.

[Huang *et al.* (1998)] Huang NE, Shen Z, Long SR, Wu MC, Shih HH, Zheng Q, Yen NC, Tung CC, Liu HH. The empirical model decomposition and the Hilbert spectrum for nonlinear and non-stationary time series analysis. *Proc. R. Soc. Lond. A* 1998; 454: 903-995.

[Ioannou and Sun (1996)] Ioannou, P. A. and Sun, J. (1996) "Robust Adaptive Control", Prentice-Hall, Upper Saddle River NJ.

[James *et al.* (1993)] James, G. H., Carne, T. G., and Lauffer, J. P. (1993) "The natural excitation technique for modal parameter extraction from operating wind turbines" Rep. No. SAND92-1666, UC-261, Sandia National Laboratories, Sandia, N.M.

[Johnson *et al.* (2004)] Johnson, E. A., Lam, H. F., Katafygiotis, L. S. and Beck, J. L. (2004) "Phase I IASC-ASCE structural health monitoring benchmark problem using simulated data", *Journal of Engineering Mechanics*, 130, 1, 3-15.

[Juang and Pappa (1985)] Juang, J. N., and Pappa, R. S. (1985) "An eigensystem realization algorithm for modal parameter identification and model reduction" *Journal of Guidance Control and Dynamics*, 8, 620-627.

[Juang and Phan (2001)] Juang, J. N. and Phan, M. Q. (2001) *Identification and Control of Mechanical systems* , Cambridge University Press.

[Julier (2002)] Julier, S. J. (2002) "The scaled unscented transform", *Proceedings of the American Control Conference*, 4555-4559.

[Julier (2003)] Julier, S. J. (2003) "The spherical simplex unscented transform", *Proceedings of the American Control Conference*, 2430-2434.

[Julier *et al.* (1995)] Julier, S. J., Uhlmann, J. K. and Durrant-Whyte, H. F. (1995) "A new approach for filtering nonlinear systems", *American Control Conference*, 1628-1632.

[Julier *et al.* (2000)] Julier, S., Uhlmann, J. and Durrant-Whyte, H. F. (2000) "A new method for the nonlinear transformation of means and covariances in filters and estimators", *IEEE Transactions on Automatic Control*, 45, 3, 477-482.

[Julier and Uhlmann (2002)] Julier, S. J. and Uhlmann, J. K. (2002) "Reduced sigma point filters for the propagation of means and covariances through nonlinear transformations", *Proceedings of the American Control Conference*, 887-892.

[Julier and Uhlmann (2004)] Julier, S. J. and Uhlmann, J. K. (2004) "Unscented filtering and nonlinear estimation ", *Proceedings of the IEEE*, 92, 3, 401-422.

[Kam and Lee (1992)] Kam, T. Y. and Lee, T. Y. (1992) "Detection of cracks in structures using modal test data", *Engineering Fracture Mechanics*, 42, 2, 381-387.

[Kang *et al.* (2005)] Kang, J. S., Park, S-K., Shin, S. and Lee, H. S. (2005) "Structural system identification in time domain using measured acceleration", *Journal of Sound and Vibration*, 288, 215-234.

[Khairnar *et al.* (2007)] Khairnar, D.G., Nandakumar, S., Merchant, S.N. and Desai, U.B. (2007) "Nonlinear target identification and tracking using UKF", *IEEE International Conference on Granular Computing, GRC*, 761 - 764.

[Kim and Melhem (2004)] Kim H. and Melhem H. (2004) "Damage detection of structures by wavelet analysis" *Engineering Structures*, 26, 347-362.

[Landau *et al.* (1998)] Landau, I. D., Lozano, R. and M'Saad M. (1998) *Adaptive control*, Springer.

[Lei *et al.* (2003)] Lei, Y., Kiremidjian, A. S., Nair, K. K., Lynch, J. P. and Law, K. H. (2003) "An enhanced statistical damage detection algorithm using time series analysis", *Proceedings of the* 4^{th} *International Workshop on Structural Health Monitoring*, Stanford, CA, USA.

[Leven and Lanterman (2009)] Leven, W.F. and Lanterman, A. D. (2009) "Unscented Kalman filters for multiple target tracking with symmetric measurement equations", *IEEE Transactions on Automatic Control*, 54, 2, 370-375.

[Li *et al.* (2006)] Li, H., Yang, H. and Hu, S.-L. J. (2006) "Modal strain energy decomposition method for damage localization in 3D frame structures", *Journal of Engineering Mechanics*, 132, 9, 941-951.

[Lin (1990)] Lin, C. S. (1990) "Location of modeling errors using modal test data", *AIAA Journal*, 28, 9, 1650-1654.

[Lin *et al.* (2001)] Lin, J.W., Betti, R., Smyth, A. W. and Longman, R. W. (2001) "On-line identification of non-linear structural systems using a variable trace approach", *Earthquake Engineering and Structural Dynamics*, 30, 1279-1303.

[Ljung (1999)] Ljung, L. (1999) *System Identification: Theory for the User*, Prentics Hall.

[Ljung and Soderstrom (1993)] Ljung, L. and Soderstrom, T. (1983) "Theory and Practice of Recursive Identification", The MIT Press.

[Maeck (2003)] Maeck, J. (2003) "Damage assessment of civil engineering structures by vibration monitoring", Ph.D. dissertation, Structural Mechanics, Civil Engineering Department , K.U.Leuven, Belgium.

[Maybeck, 1979] Maybeck, P. S. (1979) *Stochastic models estimation and control*, Vol. 1 and 2, Academic Press.

[Melhem and Kim (2003)] Melhem H. and Kim H. (2003) "Damage detection in concrete by Fourier and wavelet analysis" *Journal of Engineering Mechanics*, 29, 5, 571-577.

[Messina *et al.* (1998)] Messina A., Williams E. J. and Contursi T. (1998) "Structural damage detection by a sensitivity and statistical based method", *Journal of Sound and Vibration*, 216, 5, 791-808.

[Meuter *et al.* (2008)] Meuter, M., Iurgel, U., Park, S.-B., and Kummert, A. (2008) "The unscented Kalman filter for pedestrian tracking from a moving host", *IEEE Intelligent Vehicles Symposium*, Eindhoven, Netherlands, 37 - 42.

[Morassi (2001)] Morassi A., (2001) "Identification of a crack in a rod based on changes in a pair of natural frequencies", *Journal of Sound and Vibration*, 242, 4, 577-596.

[Nagarajaiah and Basu (2009)] Nagarajaiah S. and Basu B. (2009) "Output only modal identification and structural damage detection using time frequency and wavelet techniques", *Earthquake Engineering and Engineering Vibration* 8, 583-605.

[Nair *et al.* (2006)] Nair, K. K., Kiremidjian, A. S. and Law, K. H. (2006) "Time series based damage detection and localization algorithm with application to the ASCE benchmark structure", *Journal of Sound and Vibration*, 291, 349-368.

[Nair and Kiremidjian (2007)] Nair, K. K. and Kiremidjian, A. S. (2007) "Time series based structural damage detection algorithm using Gaussian mixtures modeling", *Journal of Dynamic Systems, Measurement, and Control*, 129, 285-293.

[Narkis (1994)] Narkis, Y. (1994) "Identification of crack location in vibrating simply supported beams", *Journal of Sound and Vibration*, 172, 4, 549-558.

[Okafor and Dutta (2000)] Okafor A. C. and Dutta, A. (2000) "Structural damage detection in beams by wavelet transform" *Smart Materials and Structures*, 9, 906-917.

[Overschee and DeMoor (1996)] Van Overschee, P. and De Moor, B. (1996) "Subspace Identification for Linear Systems. Theory Implementation Applications", Kluwer Academic Publishers.

[Pandey *et al.* (1991)] Pandey A. K., Biswas M., and Samman M. M. (1991) "Damage detection from changes in curvature mode shapes", *Journal of Sound and Vibration*, 145, 2, 321-332.

[Pandey and Biswas (1994)] Pandey A. K. and Biswas M. (1994) "Damage detection in structures using changes in flexibility", *Journal of Sound and Vibration*, 169, 1, 3-17.

[Pandey and Biswas (1995)] Pandey, A. K., and Biswas, M. (1995) "Experimental verification of flexibility difference method for locating damage in structures", *Journal of Sound and Vibration*, 184, 2, 311-328.

[Papoulis (1962)] Papoulis A. *The Fourier integral and its applications*. McGraw Hill Book and Company, 1962.

[Pappa and Elliott (1993)] Pappa, R. S. and Elliott, K. B. (1993) "Consistent-mode indicator for the Eigensystem realization algorithm", *Journal of Guidance Control and Dynamics*, 16, 5, 852-858.

[Peng *et al.* (2007)] Peng Z. K., Chu F. L. and Tse W. P. (2007) "Singularity analysis of the vibration signals by means of wavelet modulus maximal method", *Mechanical Systems and Signal Processing* 21, 780-794.

[Pi and Mickleborough (1989)] Pi, Y. L. and Mickleborough, N. C. (1989), "Modal identification of vibrating structures using ARMA model", *Journal of Engineering Mechanics*, 115, 10, 2232-2249.

[Pines and Aktan, 2002] Pines D. and Aktan A. E. (2002) "Status of structural health monitoring of long-span bridges in the United States", *Progress in Structural Engineering and Materials*, 4, 372-380.

[Rao and Babu (2008)] Rao, S. K. and Babu, V.S. (2008) "Unscented Kalman filter with application to bearings-only passive manoeuvring target tracking", *International Conference on Signal Processing, Communications and Networking, ICSCN*, Chennai, India, 219 - 224.

[Ren and Sun (2008)] Ren W-X. and Sun Z-S. (2008) "Structural damage identification by wavelet entropy", *Engineering Structures*, 30, 2840-2849.

[Robertson *et al.* (2003)] Robertson A. N., Farrar C. R. and Sohn H. (2003) "Singularity detection for structural health monitoring using Holder exponents", *Mechanical Systems and Signal Processing*, 17, 6, 1163-1184.

[Sadeghi and Moshiri (2007)] Sadeghi, B. and Moshiri, B. (2007) "Second-order EKF and unscented Kalman filter fusion for tracking maneuvering targets", *IEEE International Conference on Information Reuse and Integration, IRI*, 514 - 519.

[Singh and Bisht (2006)] Singh, M. P. and Bisht, S. S. (2006) "Vibration data-based damage detection", *Proc. of 3rd Annual workshop of Asian-Pacific Network of Centers for Research in Smart Structure Technology*, Lake Tahoe, USA.

[Smyth *et al.* (1999)] Smyth, A. W., Masri, S. F., Chassiakos, A. G., and Caughey, T. K. (1999) "On-line parametric identification of MDOF nonlinear hysteretic systems", *Journal of Engineering Mechanics*, 125, 2, 133-142.

[Smyth and Wu (2007)] Smyth, A. and Wu, M. (2007) "Multi-rate Kalman filtering for the data fusion of displacement and acceleration response measurements in dynamic system monitoring", *Mechanical Systems and Signal Processing*, 21, 707-723.

[Sohn *et al.*, 2003] Sohn, H., Farrar, C. R., Hemez, F. M., Shunk, D. D., Stinemates, D. W. and Nadler B. R. (2003) "A review of structural health monitoring literature: 1996-2001", *Los Alamos National Laboratory Report*, LA-13976-MS.

[Stubbs *et al.* (1990)] Stubbs, N., Broome T. H. and Osegueda, R. (1990) "Nondestructive construction error detection in large space structures", *AIAA Journal*, 28, 1, 146-152.

[Stubbs and Osegueda (1990a)] Stubbs, N. and Osegueda, R. (1990) "Global nondestructive damage evaluation in solids" *Modal Analysis: The International Journal of Analytical and Experimental Modal Analysis*, 5, 2, 67-79.

[Stubbs and Osegueda (1990b)] Stubbs, N. and Osegueda, R. (1990) "Global damage detection in solids-experimental verification", *Modal Analysis: The International Journal of Analytical and Experimental Modal Analysis*, 5, 2, 81-97.

[Sun and Chang (2002)] Sun Z. and Chang C. C. (2002) "Structural damage assessment based on wavelet packet transform", *Journal of Structural Engineering*, 128, 10, 1354-1361.

[Sun and Chang (2004)] Sun Z. and Chang C. C. (2004) "Statistical wavelet based method for structural health monitoring", *Journal of Structural Engineering*, 130, 7, 1055-1062.

[Taha *et al.* (2006)] Taha M. M. R., Noureldin A., Lucero J. L. and Baca T. J. (2006) "Wavelet transform for structural health monitoring: A compendium of uses and features", *Structural Health Monitoring*, 5, 3, 267-295.

[Tenne and Singh (2003)] Tenne, D. and Singh, T. (2003) "The higher order unscented filter", *Proceedings of the American Control Conference*, 2441-2446.

[USDoC, 2002] U.S. Department of Commerce, "2002 Economic census - business expenses: Construction", EC02-23SG-1.

[Van der Merwe and Wan (2001)] Van der Merwe, R. and Wan E. A. (2001) " The square-root unscented Kalman filter for state and parameter estimation", 3461-3464.

[Wang and Deng (1999)] Wang Q. and Deng X. (1999) "Damage detection with spatial wavelets", *International Journal of Solids and Structures*, 36, 3443-3468.

[Wang and Haldar (1994)] Wang, D. and Haldar, A. (1994) "Element level system identification with unknown input", *Journal of Engineering Mechanics*, 121, 1, 159-176.

[Wang and Haldar (1997)] Wang, D. and Haldar, A. (1997) "System identification with limited observations without inputs", *Journal of Engineering Mechanics*, 123, 5, 504-511.

[Wang and Zhang (1987)] Wang, W. and Zhang, A. (1987) "Sensitivity analysis in fault vibration diagnosis of structures," *Proceedings of* 5^{th} *International Modal Analysis Conference*, 496-501.

[Wu and Law (2004)] Wu, D. and Law, S.S. (2004) "Damage localization in plate structures from flexibility and its derivatives", *Proceedings of SPIE*, 5391, 449-460.

[Wu and Smyth (2007)] Wu, M. and Smyth A. W. (2007) "Application of the unscented Kalman filter for real-time nonlinear structural system identification", *Structural Control and Health Monitoring*, 14, 971-990.

[Xu and Chen (2004)] Xu Y. L. and Chen J. (2004) "Structural damage detection using empirical mode decomposition: experimental investigation", *Journal of Engineering Mechanics*, 130, 11, 1279-1288.

[Yang *et al.* (2004)] Yang J. N., Lei Y., Lin S. and Huang N. (2004) "Hilbert-Huang based approach for structural damage detection", *Journal of Engineering Mechanics*, 130, 1, 85-95.

[Yang *et al.* (2006a)] Yang, J. N., Huang, H. and Lin, S. (2006) "Sequential non-linear least-square estimation for damage indentification of structures", *International Journal of Non-Linear Mechanics*, 41, 124-140.

[Yang *et al.* (2006b)] Yang, J. N., Lin, S., Huang, H. and Zhou, L. (2006) "An adaptive extended Kalman filter for structural damage identification", *Structural Control and Health Monitoring*, 13, 849-867.

[Yang *et al.* (2007)] Yang, J. N., Pan, S. and Lin, S. (2007) "Least-squares estimation with unknown excitations for damage identificaion of structers", *Journal of Engineering Mechanics*, 133, 1, 12-21.

[Yang and Lin (2004)] Yang, J. N. and Lin, S. (2004) "On-line identification of nonlinear hysteretic structures using an adaptive tracking technique", *International Journal of Non-Linear Mechanics*, 39, 1481-1491.

[Yang and Lin (2005)] Yang, J. N. and Lin, S. (2005) "Identification of parametric variations of structures based on least squares estimation and adaptive tracking technique", *Journal of Engineering Mechanics*, 131, 3, 290-298.

[Zhan and Wan (2007)] Zhan, R. and Wan, J. (2007) "Iterated unscented Kalman filter for passive target tracking", *IEEE Transactions on Aerospace and Electronic Systems*, 43, 3, 1155 - 1163.

[Zhang *et al.* (2006)] Zhang, S-S., Hu, G-D., and Liu, S-H. (2006) "Target tracking for maneuvering reentry vehicles with reduced sigma points unscented Kalman filter", 1^{st} *International Symposium on Systems and Control in Aerospace and Astronautics*, 199-202.

[Zhang and Hu (2006)] Zhang, S-S. and Hu G-Da. (2006) "Variations of unscented Kalman filter with their applications in target tracking on re-entry", *Chinese Control Conference, CCC*, 407 - 412.

[Zhao and DeWolf (1999)] Zhao, J. and DeWolf, J. T. (1999) "Sensitivity study for vibration parameters used in damage detection", *Journal of Structural Engineering*, 125, 4, 410-416.

[Zhong and Oyadiji (2007)] Zhong S, and Oyadiji S. O. (2007) "Crack detection in simply supported beams without baseline modal parameters by stationary wavelet transform", *Mechanical Signal and Signal Processing*, 21, 1853-1884.

[Zhu *et al.* (2008)] Zhu B., Leung, A. Y. T., Wong C. K. and Lu, W. Z. (2008) "Online health monitoring and damage detection of structures based on the wavelet transform" *International Journal of Structural Stability and Dynamics*, 8, 3, 367-387.